OPTIMIZATION OF A PARABOLIC REFLECTOR FOR USE IN A TWO-STAGE SOLAR CONCENTRATOR

by

Garrett Dooley

Submitted in partial fulfillment of the requirements
for the degree of Master of Applied Science

at

Dalhousie University
Halifax, Nova Scotia
May 2014

TABLE OF CONTENTS

LIST OF TABLES

LIST OF FIGURES

ABSTRACT

A background of concentrated solar power, and finite element analysis are provided, along with further technical details on the physics of parabolic light concentration and classical plate theory. The concept of optical efficiency is outlined, including the 5 contributing factors: the cosine effect, mirror reflectivity, blocking and shadowing, atmospheric attenuation, and surface irregularities. Surface irregularities are identified as the least predictable factor of optical efficiency, making them the subject of the experimental section. Physical and computational experimentation is conducted to determine a desirable selection for material of reflector substrate, thickness of reflector substrate, holding method of reflector, and aspect ratio of reflector. Physical and computational results are compared with one another to add validity to both sets of results. Recommendations are made for each design criteria selection, however it is found that in many cases the selection of reflector properties falls to an economic decision.

ACKNOWLEDGMENTS

I would like to thank my academic supervisor Dr. George Jarjoura for his patience, giving me the opportunity to pursue my masters, and giving me the guidance I required to complete it.

Further, a thanks to Dr. Darrel Doman for his guidance and insight into finite element methods, and to Dr. Dominic Groulx for initially introducing me to the Prometheus Project and laying much of the groundwork upon which my research has been built.

I also wish to thank Peter Kinley for his flexibility in allowing me to complete this degree while working at Lunenburg Industrial Foundry & Engineering, and everyone else at LIFE who has helped with the Prometheus Project, in particular Mark Charlton, Ricky Hodder, Michael MacNeil, and Lance Rowley.

Finally, a huge thanks to my family and friends for their support during the entirety of my studies.

Chapter 1: INTRODUCTION

1.1 OBJECTIVE

The objective of this work is to explore the results of different design selections pertaining to parabolic reflective substrate plates used in a two stage solar concentrator. Upon discovery of the effect of the different design selections, recommendations will be made to optimize the concentrative ability of the design of the reflective surfaces within a realm of reasonability, which includes the effect these selections will have on the overall viability of the resulting two-stage concentrator.

The design selection criteria that will be considered are:

- Material of plate.
- Thickness of plate.
- Holding method of plate.
- Aspect ratio of plate.

1.2 CONCENTRATED SOLAR POWER

Concentrated solar power (CSP) is a relatively simple technology that uses reflectors to concentrate solar light, producing extreme temperatures. This heat is then used for a variety of applications, most commonly electricity generation by either producing steam to run a steam turbine, or by powering a Stirling engine. The heat produced by CSP devices can also be used directly for materials or chemical processing or, on a much smaller scale, solar cooking. There are three main commercially established CSP technologies: parabolic troughs, towers, and parabolic dishes. These different CSP technologies are all fundamentally similar in that they use reflectors to concentrate solar

light. Where these three methods differ is the orientation of the reflectors. A summary of the following section is provided in Table 1-1.

1.2.1 Parabolic Trough Collector

The most commonly used CSP model is the parabolic trough collector, as seen in Figure 1-1. Trough systems consist of rows of semi-curved parabolic mirrors that focus the solar energy on an absorber tube through which a heat transfer fluid flows. The mirrors feature a single axis tracking system, which follows the sun's path throughout each day. By concentrating solar energy over a small area, the heat transfer fluid is raised to temperatures of roughly 400 °C. This fluid is then used to create steam, which powers a turbine and produces electricity. This system requires large fields of concentrators to generate enough energy to run a turbine at a high efficiency, and does not lend itself well to thermal applications, as the achieved temperatures are relatively low compared to other reflectors. It is however; the most popular form of CSP for electricity production as the capital costs for a trough collection system is lower than parabolic dish systems or central tower systems.

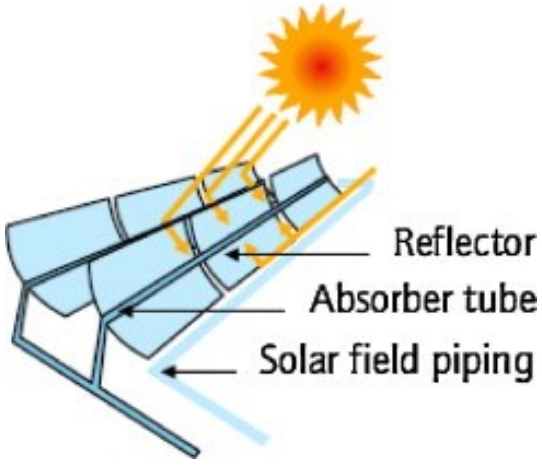

Figure 1-1. Parabolic trough collector. [1]

1.2.2 Parabolic Dish Collector

Parabolic dish collectors operate in a similar manner to trough collectors, but instead of focusing the sunlight along one axis, the parabolic dish focuses an area of sunlight into a single point, yielding temperatures in excess of 750 °C, as shown in Figure 1-2. Unlike the parabolic trough concentrator which tracks over a single axis, the parabolic dish collector tracks the sun's movement using a dual-axis tracking system, which increases its accuracy and overall efficiency. Another fundamental difference between these two solar concentrators is that with the parabolic dish, the energy is used directly at the focal point (predominantly in the form of a Stirling engine) instead of transferred to a central location to run a turbine. This type of system has the advantage of being scalable. It is not required to have a large farm of these receivers to operate at a high efficiency, making parabolic dish concentrators a more desirable choice for small scale electrical production, but less attractive than parabolic troughs for utility sized electricity production due to the increased costs associated with constructing two dimensional curved surfaces, and due to requiring separate engines at each dish. A drawback of the parabolic dish collector from a thermal application standpoint is that due to the parabolic dish's requirement of pointing directly at the sun, the focal point is usually high above ground level, well above working level. Any sort of infrastructure built to operate at the focal point would reduce the power of the concentrator by casting shadows over the reflective surface, and would also require a large degree of mechanical sophistication to deal with the changing focal location.

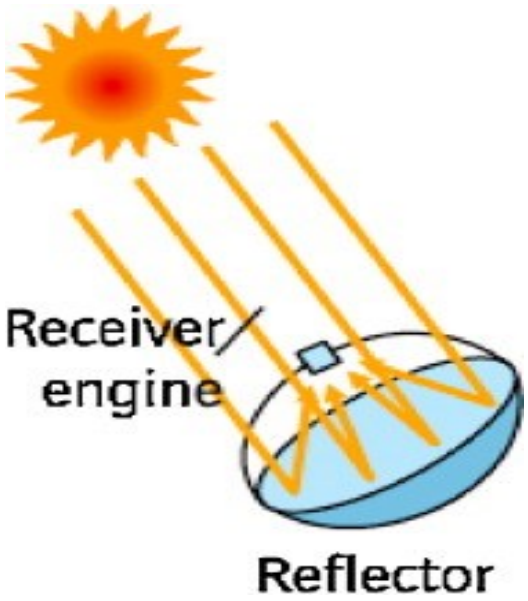

Figure 1-2. Parabolic dish collector. [1]

1.2.3 Central Tower Receiver

The third common type of CSP is the central tower receiver (Figure 1-3), which can be described as a combination of the solar trough technology and parabolic dish technology. Solar towers consist of a large field of flat reflectors called heliostats, surrounding a centrally located tower. These heliostats track the sun and reflect the sunlight to a single point located high above ground, called the central receiver. A heat transfer medium is contained within this central tower and is heated by the concentrated light to temperatures in excess of 700 °C. Like the parabolic trough systems, this set-up is only effective when dealing with utility scale power production, and like the parabolic dish collectors, due to the focus being located well above ground, it isn't very feasible for use with any direct thermal processing.

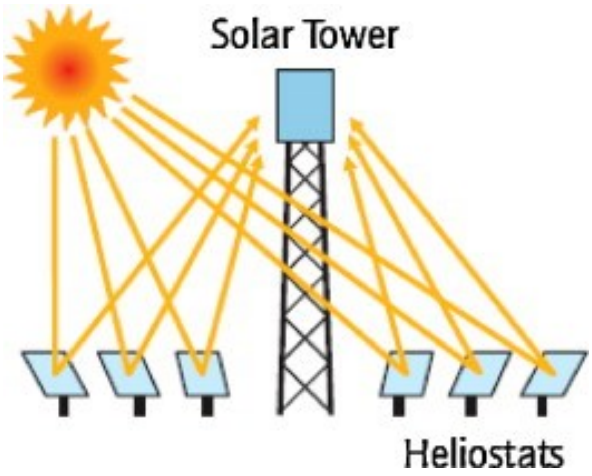

Figure 1-3. Central tower receiver. [1]

Table 1-1. Characteristics of main CSP electricity generation techniques. [2]

Method	Output range	Advantages	Disadvantages
Parabolic dish	3-50 kW	• Modular units • Very high solar to electricity conversion efficiencies exceeding 30% • Simple operational procedure • No water cooling requirements	• Earlier stage of technology • Thermal storage possible only via battery • No hybridization to date • Precise tracking of sun required
Solar tower	30-160 MW, increasing to 200 MW by 2030	• High solar to electricity conversion efficiency around 23% • Operating temperatures potentially up to 1000 C, increasing electricity conversion efficiency • Hybridization with oil or gas • Modular Components • Simple operation procedure • Cogeneration of heat and electricity possible	• High stability required for heliostats • Water needed for cooling and cleaning • Investment and operational costs at commercial scale not yet proven

Method	Output range	Advantages	Disadvantages
Parabolic trough	30-150 MW, increasing to 320 MW by 2030	• Well-established technology • Hybridization with oil or gas • Modular components • Cogeneration of heat and electricity possible	• Relatively low (14-20%) solar to electricity conversion efficiency • Maximum heat retention fluid operating temperature of 400 C • High stability required for heliostats • Water needed for cooling and cleaning

1.2.4 Two-stage Concentrator

Lunenburg Industrial Foundry & Engineering (LIFE) has developed and patented a unique two-stage solar concentrator. Developed under the project name Prometheus Project, this technology uses two orthogonally arranged parabolic mirrors to produce a point focus. As shown in Figure 1-4, a primary reflector is shaped as an off axis parabola around the horizontal axis of symmetry. Rays of sunlight are reflected off of this mirror and onto a secondary reflector, which is shaped as a symmetrical parabola around the horizontal axis of symmetry. The rays are then reflected off of the secondary reflector and on to a receiver positioned so that both mirrors achieve their line focus at the same distance, resulting in a combined point focus. Spacing between these two mirrors is critical to achieve a maximum temperature, however the ability to spread the primary and secondary mirror provides some interesting options with regards to generating a focus of different shapes that could be desirable for different applications. The orientation of the

two reflectors remains fixed to one another and the focus, while the entire assembly rotates both horizontally and vertically to follow the path of the sun.

The two-stage concentrator combines the relatively simple single axis curvature of the parabolic trough concentrator with the tracking accuracy, focusing power, and scalability of the parabolic dish concentrator. Significant manufacturing costs should be gained through the ability to form a point focus while only manufacturing single axis curves, which are much simpler to manufacture than their two axis counterparts. Another inherent value to the two-stage concentrator system is that the focal point can be brought down to a reasonable working height, unlike the parabolic dish system, which reflects sunlight back towards the sun. A lower focus means that an infrastructure can be built more easily to make use of the incredibly hot focal point, and that any such infrastructure will not be located in between the sun and primary reflector, or the primary and secondary reflectors which would block incoming light rays, and reduce the efficiency of the solar concentrator.

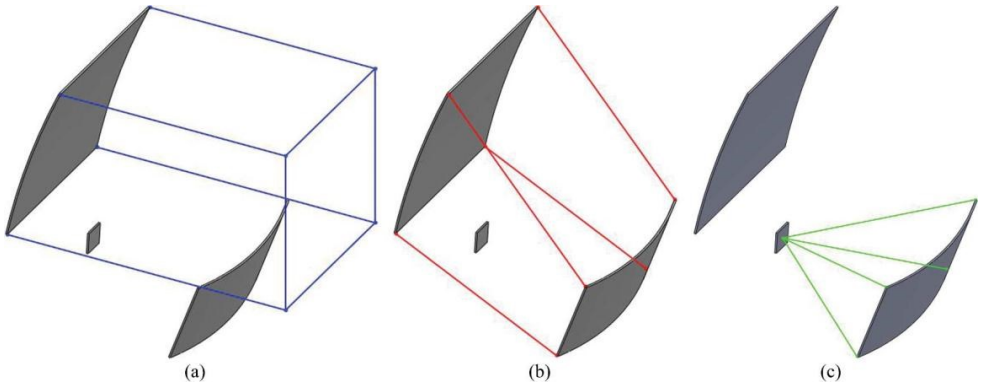

Figure 1-4. Reflection path of two-stage concentrator. [3]

1.3 SOLAR FURNACE

A solar furnace is a structure that uses CSP to produce high temperatures, usually for an industrial application. To achieve adequately high temperatures for such applications, solar furnaces generally are required to produce a point focus. As such, solar furnaces can either use heliostats, parabolic mirrors, or a combination of both.

The world's largest solar furnace (Figure 1-5), located in Odeillo, France was opened in 1970. This arrangement consists of a field of heliostats that reflect light towards a parabolic dish, which concentrates light towards a single point, the size of a cooking pot and generates temperatures in excess of 3,500 °C. Because of the two-stage reflections, the focal point structure is located in a manageable location and does not block any incoming light. By employing different numbers of heliostats, the temperature generated using the Odeillo solar furnace can be altered to meet the needs of a given application, for example:

- 1,000 °C for metallic receivers producing hot air for the next generation solar towers as it will be tested at the Themis plant with the Pegase project [4].
- 1,400 °C to produce hydrogen by cracking methane molecules [5].
- up to 2,500 °C to test materials for extreme environment such as nuclear reactors or space vehicle atmospheric reentry.
- up to 3,500 °C to produce nanomaterials by solar induced sublimation and controlled cooling, such as carbon nanotubes [6] or zinc nanoparticles [7].

Figure 1-5. Odeillo Solar Furnace

The LIFE two-stage solar concentrator represents an opportunity to achieve many of the same benefits present with the Odeillo solar furnace, but with a completely scalable and portable design. Originally designed for use in their foundry, the LIFE two-stage solar concentrator prototypes have been used for both scientific experiments, and also in ordinary production of small castings. By boiling small Iron samples, the LIFE solar furnace has shown that it can achieve temperatures in excess of 2850 °C. This extremely high temperature, coupled with a relatively low construction cost when compared to a solar furnace as seen in Figure 1-5 indicate that the LIFE two-stage concentrator system may be the optimal platform for both scientific testing and industrial solar furnace use.

It is generally accepted that for use of a solar furnace, the focus must be relatively small, and the temperature will be relatively high when compared to using CSP for electricity generation. This difference in temperature requirement and focal size can be attributed to the fact that electricity generation doesn't require as high a temperature (in the range of 400 °C) as the aforementioned solar furnace applications. Therefore, the accuracy and

quality of both the tracking accuracy, and focal quality of a solar furnace must be greater than that of an industrial scale CSP electricity generation facility. To this end, it is very important to understand all of the mechanisms contributing to the focal quality of a solar furnace, to better design a system that will maximize the amount of sunlight energy that is transferred to the desired target.

1.4 FINITE ELEMENT MODELING, FEA

The finite element method (FEM) is a numerical technique for calculating approximate solutions to boundary value problems. FEM incorporates all of the methods for approximating a complex equation over a large domain by connecting many simple element equations over many small subdomains, named finite elements. That is to say, a complex shape will be replaced with a summation of many simple shapes that are combined to correctly model the original shape. By considering all of the relatively simple resulting equations, an accurate approximation of the very complex original domain is achieved. Due to its natural benefits over other techniques, the finite element method has become the most useful numerical analysis tool for engineers and applied mathematicians [8]. The main advantages of the finite element method over other numerical approaches are:

- FEM can be applied to any shape and any number of directions.
- The shape on to which the FEM is applied can be made out of any number of materials.
- The material properties of the shape being analyzed can be non-homogeneous and/or anisotropic.

- A finer mesh can be used at regions of interest to generate more accurate results locally.

When used for a practical application, FEM is often referred to as finite element analysis (FEA). FEA can be used for a specific field of analysis, such as stress analysis, thermal analysis, or vibration analysis, to provide a detailed understanding of a complex system. FEA includes the use of mesh generation techniques to divide a complex system into manageable simple elements, and the use of a FEM algorithm to solve the entire field of equations. In many cases, various fields of FEA study are related. An example of such an inter-field relation between FEA studies would be the distributions of non-uniform temperatures inducing loading conditions on structural members. In this scenario, the output of a thermal FEA analysis could yield temperature results that would become an input for a subsequent stress FEA analysis [8].

The origins of modern FEA can be credited to a 1950 publication by Turner et al [9]. In 1960, Clough [10] was the first to use the common term "finite element method" when describing the technique. This work in matrix methods for stress analysis was further advanced by Argyris [11]. During the following decade and a half, the work of Babuska and Ariz [12], Strang and Fix [13], and Oden and Reddy [14] greatly developed and promoted the mathematical theory of finite elements. The development of the finite element technique for practical applied applications has been led by Zienkiwicz and Taylor [15].

Since the initial development of the finite element method, the plate-bending problem has been of particular interest for this field of research, being one of the first areas where FEA was applied. The work of Holand [16], Ashwell and Gallagher [17], Parisch [18], Batoz et al [19], Hrabok and Hrudey [20] and Ortiz and Morris [21], represents a good sampling of the effort that has devoted to developing efficient and accurate bending elements.

FEA can be incorporated into 3D modeling software such as SolidWorks or AutoDesk Inventor to allow designers to quickly determine intermediate stresses and displacements of components they're designing when the components are subjected to different loadings. However for more accurate results of more complex systems, a dedicated FEA program such as the HyperWorks package should be used. A dedicated FEA program can allow for much more control over a model by offering additional options with regards to meshing, input forces, constraints and material properties. A dedicated FEA program also gives the operator full numerical results of the system, providing greater ability to analyze the results instead of relying on a simple graphical solution that would be provided from a built in CAD FEA system.

It is important to understand the limitations of FEA and not assume all outputs are correct without subjecting them to proper scrutiny. Error is inherent in FEA methods. This error, originates from arbitrary assumptions that are required to represent the stress distribution within elements [22]. The magnitude of error is determined by how well the FEA model approximates the real stress distribution.

The fundamental equation of FEA is:

$$[F] = [K] * [d] \tag{1.1}$$

where [F] is the known matrix of nodal loads, [K] is the known stiffness matrix, and [d] is the unknown vector of nodal displacements. The known stiffness matrix depends on the geometry of the model, material properties and restraints applied on the model.

If it is assumed that the analyzed model retains whatever stiffness it possessed in its undeformed shape prior to loading, that is to say the [K] matrix is unchanged, then corresponding analysis is relatively simple and is called a linear analysis. Conversely, nonlinear analysis abandons the assumption of constant stiffness, and the nonlinear solver runs through an iterative solution operation throughout which the stiffness matrix must be updated to reflect a continuously changing stiffness [23]. An increased number of iterations increases the accuracy of the results, but also increases the computing power and computing time required to solve the system [23].

Several rules of thumb are used to indicate when a nonlinear analysis might be necessary to acquire accurate results:

- Large deformation. If the deformations are larger than 5% of the part's largest dimension, nonlinear analysis should be conducted [23].
- Membrane effects. Small amounts of deformation can also call for nonlinear analysis. When a membrane is curved, it gains additional stiffness when compared to an equivalent flat membrane. If the deformation due to the applied

loading causes the membranes to curve, the deformed membrane exhibits stiffness additional to the original bending stiffness [23].

- Nonlinear material. If the loads are high enough to cause permanent deformations, or if the strains are over 50%, nonlinear analysis should be conducted [23].
- Contact stresses and nonlinear supports. If support conditions change during the application of operating loads, nonlinear analysis is needed [23].
- Buckling. Linear analysis can be used to calculate the load under which a model will buckle, however nonlinear analysis should be conducted to explain post-buckling behavior [23].

Mesh size also contributes to the accuracy of a FEA model. A model with a very fine mesh size, that is to say many small elements, will likely yield a more accurate result than a model with a more coarse mesh size. However, an increase in computing time acts as a trade off to the increase in accuracy. It is also possible to experience the occurrence of numerical anomalies if a very fine mesh size is selected. It is therefore responsible for the FEA operator to conduct a convergence analysis to determine the appropriate element size, and estimate the error in the results. A traditional convergence analysis, or so-called h-convergence, consists of changing the element size without changing the element order [9]. By comparing and plotting the results of using different mesh sizes, the operator can make an educated selection regarding how large the mesh elements should be without sacrificing accuracy in the model's results. Automated convergence analysis, also known as adaptive finite element method, represents an alternative to refining mesh convergence

analysis. In an automated convergence analysis, element sizes remain the same but element orders change while an algorithm compares results from the last two iterations and upgrades element order where required to meet user specified accuracy [22]. Iterations continue without user intervention until the convergence error becomes lower than a user-defined value or until calculations hit the highest possible element order [22].

The type of mesh element used will have an impact on the computational results of an FEA model. For a 2D analysis, mesh elements can be chosen to be quadrilateral or triangular shaped. For a 3D analysis, mesh elements can be chosen as hexahedral, tetrahedral or prism shaped. A first order mesh element contains nodes at each of its corners, while a second order mesh element contains nodes at the corners, but also intermediate nodes at the midway point of each edge. Second order elements should be used with caution because in addition to increasing accuracy, the memory and computational requirements are also increased [24].

When modeling plate and membrane bending behavior of thin, three-dimensional structures shell elements are useful. A given FEA solution algorithm will have its own shell card, into which the user will input his own parameters. It is important to understand the difference between the modeling of thin and thick shells.
The main difference between thin and thick shell formulation is the inclusion of transverse shear deformation. Thick plate formulation follows the Mindlin-Reissner theory of plates, which accounts for transverse shear deformations. Thin plate

formulation follows a Kirchhoff application which neglects shear deformation through the thickness of the plate.

Whenever possible, it is desirable to compare model results with a real world experiment for validation of the FEA model. This validation is of particular importance when a user would like to confirm the validity of certain assumptions he has made when converting a real world model to a computerized representation.

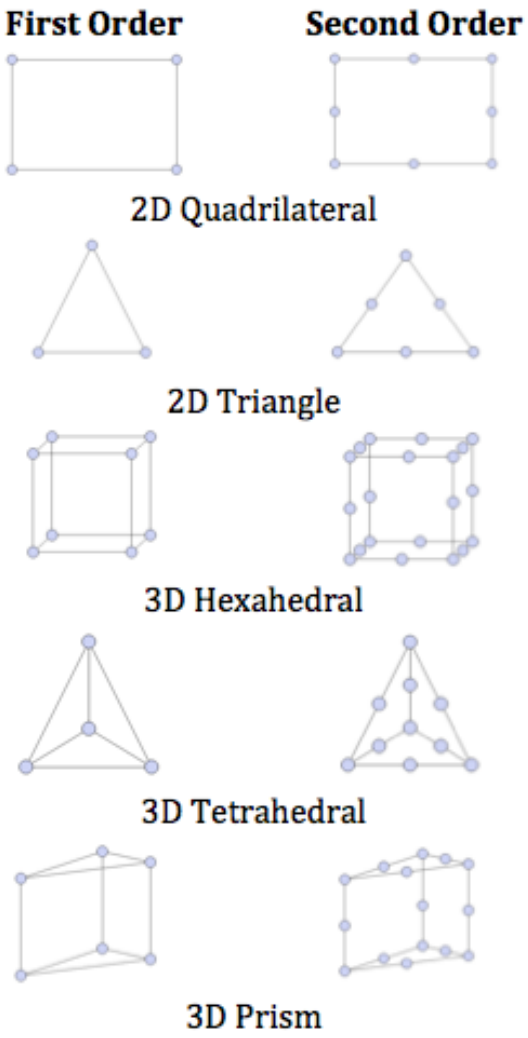

Figure 1-6. Graphical representation of different FEA mesh types.

1.5 HISTORY OF PLATE THEORY

The earliest statement of plate theory was developed by Euler [25], when he performed a free vibrations analysis of drums in 1776. Euler's work was then expanded on in 1789 by Bernoulli [26], presenting a plate system that would be known as the Euler-Bernoulli beam theory. Bernoulli's system represented a plate as a system of mutually perpendicular strips at right angles to one another, each acting as a beam. Work by Germain [27] and Lagrange [28] improved upon the Euler-Bernoulli theory, developing a governing differential equation, the Germain-Langrange plate equation, which was the first properly formulated general plate equation. An 1829 publication by Poisson [26] expanded on the Germain-Lagrange plate equation to the solution of a static loaded plate with a constant term plate flexural rigidity. Through his work in elasticity, Navier [30] developed a theory of plate bending which considers the thickness of the plate as a function of its rigidity.

The Kirchhoff-Love thin plate theory, also known as the classical plate theory, was developed by Love [31] using assumptions proposed by Kirchhoff [32], which are now referred to as "Kirchhoff's hypotheses". The Kirchhoff-Love theory assumes that straight lines normal to the mid-surface of the plate remain straight and normal to the mid-surface after deformation, and that the thickness of the plate does not change during deformation.

Timoshenko [33] provided further development to the theory of plate bending analysis by developing a collection of solutions to many different plate-bending problems, most

notably problems considering large deflections in circular plates, and the development of elastic stability problems.

Mindlin [34] developed an extension of the Kirchhoff-Love plate theory that takes into account shear deformations through the thickness of a plate. Mindlin's theory, also known as the first-order shear plate theory, assumes a linear variation of displacement through the thickness of the plate, and that the thickness of the plate does not change during deformation. Additionally, the Mindlin plate theory assumes the plane stress condition, that the normal stress through the thickness is ignored.

Membranes, which are similar to thin plates but having thinner thicknesses with respect to their other dimensions, can be considered a simplified plate, and therefore the theory of membrane mechanics was developed alongside that of thin plate theory. Foppl [35] derived equilibrium equations for a membrane plate, which were essentially classical plate bending equations with a bending rigidity set to zero. Hencky [36] also used the assumption of no flexural stiffness in the thin plate equations to investigate the problem of a membrane with circular boundary conditions inflated by a uniform pressure.

Chapter 2: THEORETICAL CONSIDERATIONS

Technical background information, which is important in understanding the research presented in this work, is provided in this section. A brief background on the concepts of solar concentration is provided, followed by an explanation of optical efficiency and finally an explanation of plate bending equations.

2.1. REFLECTORS

While the types of CSP systems outlined in section 1.1 have very different geometries, one commonality between all of these systems is that they use reflectors to control the path of solar light. This section gives a technical background regarding reflection, concentration, and how reflectors are used to direct the path of light rays.

2.1.1. Concentration Ratio

Concentration ratio is a means of defining the amount of light energy concentration achieved by a solar concentrator. There are two different definitions of concentration ratio in general use.

Optical Concentration Ratio (CR_O) is the averaged irradiance (I_r) integrated over the receiver area (A_r), divided by the insolation incident on the collector aperture [37].

$$CR_O = \frac{\frac{1}{A_r}\int I_r dA_r}{I_a} \tag{2.1}$$

Geometric Concentration Ratio (CR_g) is the area of the collector aperture A_a divided by the surface area of the receiver A_r [37].

$$CR_g = \frac{A_a}{A_r} \tag{2.2}$$

While the geometric concentration ratio is only a function of the size and shape of the reflector and receiver, the optical concentration ratio is directly dependent on the quality of the reflector. It should also be noted that in many systems, the concentrated solar image is smaller than the receiver, and therefore both concentration ratio definitions offer information on the concentration ratio of the entire system, not of the concentrator in particular.

2.1.2. Parabolic Geometry

A parabola is the locus of a point that moves so that its distance from a fixed line and a fixed point are equal [37]. This is shown on Figure 2-1, where the fixed line is called the directrix and the fixed point *F*, the focus. The length *FR* equals the length *RD*, and would for any *R* locations chosen along the parabolic curve. The axis of the parabola is the line perpendicular to the directrix and passing through the focus *F* [37]. The parabola intersects its axis at a point *V* called the vertex, which is exactly midway between the focus and the directrix [37]. The distance between the vertex and the focus is known as the focal length *f*.

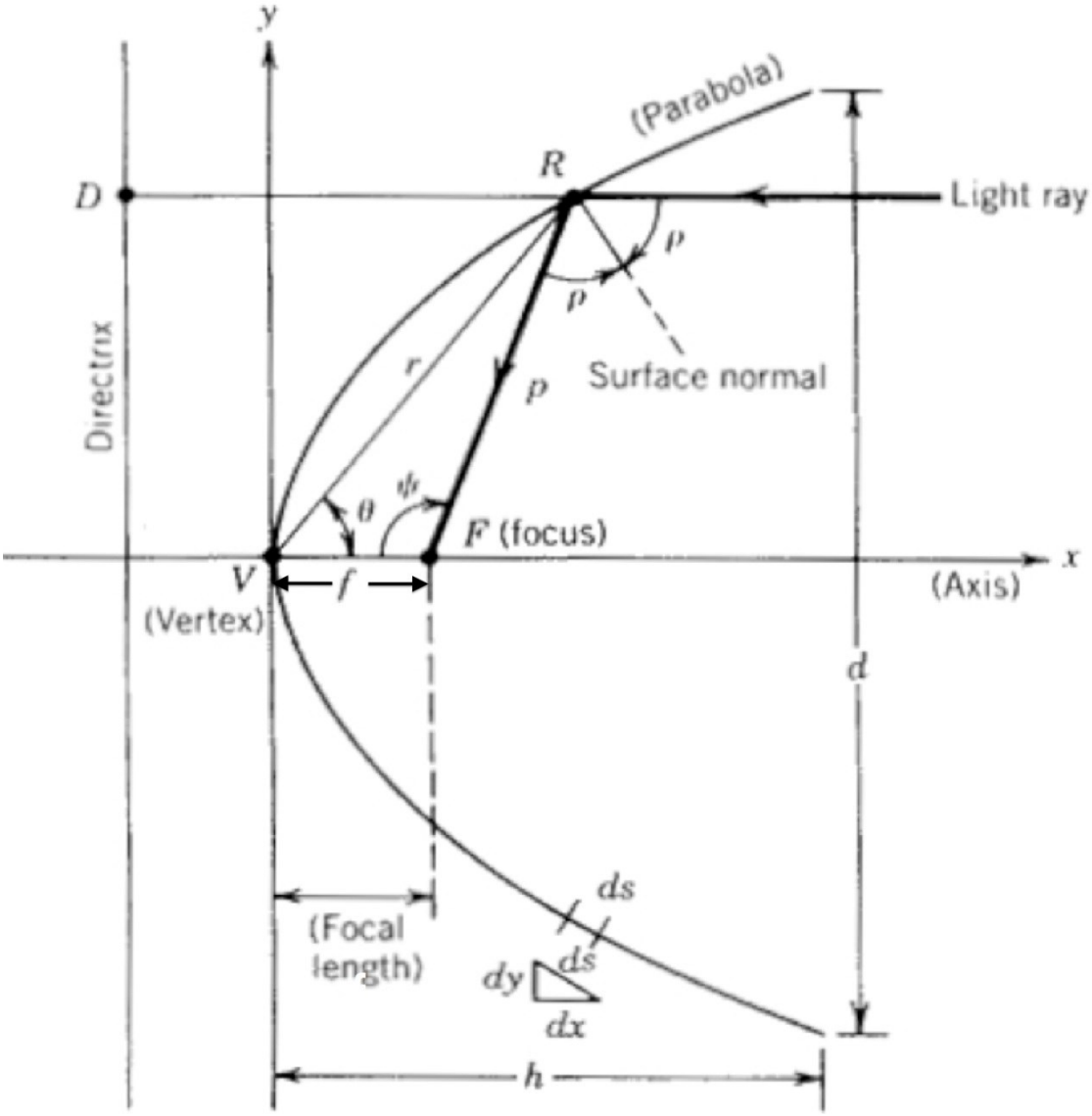

Figure 2-1. Graphical definition of a parabola. [37]

Due to the property that, for any line parallel to the axis of the parabola, the angle between it and the surface normal is equal to the angle between the normal and a line to the focal point, the parabolic shape is widely used as the reflecting surface for concentrating solar collectors [37]. Since solar radiation arrives at the earth in

essentially parallel rays, all radiation parallel to the axis of the parabola will be reflected to a single point, which is the focus [37].

If the origin is taken at the vertex and the y-axis is defined along the axis of the parabola, a parabola, on a two dimensional plane can be defined with relation to its focal length as:

$$y = \frac{x^2}{4f} \tag{2.3}$$

It is valuable to be able to relate the slope of a parabola to its focal length, as this is the value that indicates where the absorber must be located with respect to the surface location of a parabolic reflector.

The arc length of a parabola *s* following the above equation *f*(x) can be calculated by formula 2.4:

$$s = \int_a^b \sqrt{1 + \left(\frac{dy}{dx}\right)^2}\, dx \tag{2.4}$$

This is of particular value when calculating the amount of material required for a solar reflector of a given parabolic curve, or conversely, to determine the maximum and/or minimum coordinates of a parabolic curve of a known focal length given specific material dimensions. When using a parabolic material to build a solar concentrator, the arc length of the parabolic curve is used to define the surface area of reflector A_s. How the arc length relates to material requirements is explained on a case-by-case basis for each type of parabolic concentrator.

2.1.3. Principles of Reflection and Refraction

The fundamental process that takes place when light waves encounter the surface of a material is shown in Figure 2-2. A portion of an incident (incoming) light ray may be reflected from the surface, and a portion of the incoming light ray may pass through the surface and enter the material. In doing so, the direction of the light is refracted in accordance with Snell's law, equation 2.5 [37]:

$$n_1 sin\theta_1 = n_2 sin\theta_2 \tag{2.5}$$

where angles are determined normal to the surface, and n is a property of a medium called the index of refraction, which relates to the speed of light *v* in the material by equation 2.6 [37]:

$$n = \frac{c}{v} \tag{2.6}$$

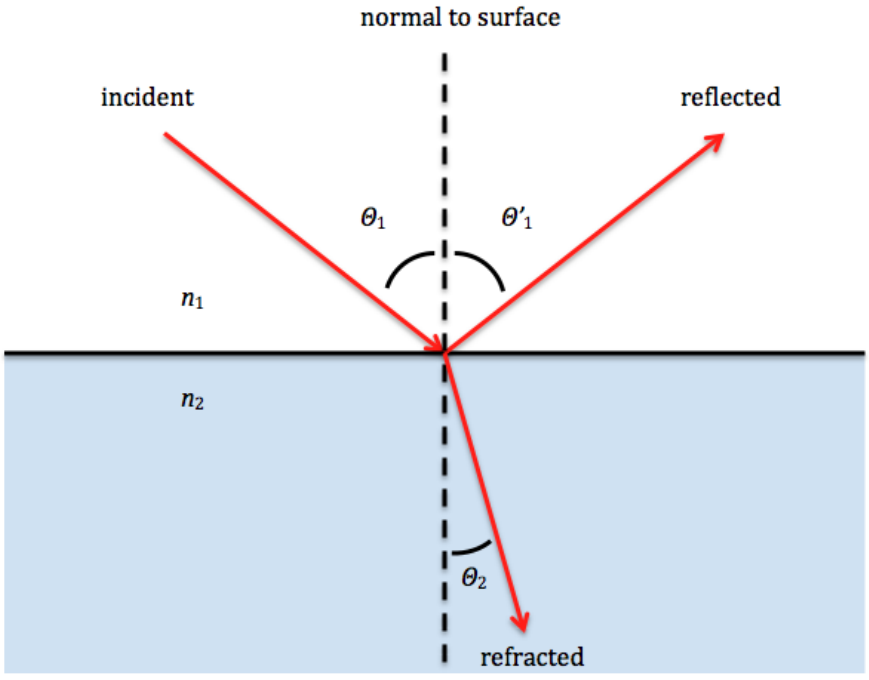

Figure 2-2. Graphical representation of Snell's law.

The percentage of incident light that is reflected off of a given material is known as the reflectivity of the material, and is of great significance in the design of a concentrated solar power system.

The reflected light ray is of particular interest because it is responsible for the concentration of CSP systems, and is governed by the law of reflection, which states that the direction of the incident ray and the direction of the reflected ray make the same angle with respect to the normal surface, as seen in Figure 2-2. Therefore, if the direction of the incoming solar radiation is known, as would be if the location of the sun at a given moment is known, a smooth reflective surface can be placed in the path of the incoming light at a known angle to reflect the incoming light rays to a predetermined location [37].

2.1.4. Parabolic Trough Concentrator

The surface of a parabolic trough concentrator consists of a portion of a parabolic cylinder. Moving a parabola along the axis normal to its plane forms a parabolic cylinder. For a parabolic cylinder having a length l and having the cross-sectional dimensions of Figure 2-1, the collector aperture area is given by equation 2.7 [37]:

$$A_a = ld \tag{2.7}$$

while the reflective surface area is found by using equation 2.4 to give:

$$A_s = ls \tag{2.8}$$

2.1.5. Solar Dish

The surface of a parabolic dish concentrator is formed by rotating a parabolic curve about its axis, creating a shape called a paraboloid of revolution [37]. The equation for a paraboloid of revolution with the z-axis as the axis of symmetry is given by equation 2.9 [37]:

$$x^2 + y^2 = 4fz \tag{2.9}$$

For a paraboloid of revolution of aperture diameter *d*, the collector aperture area is simply the circular area defined by the aperture diameter, and is given by equation 2.10 [37]:

$$A_a = \frac{\pi d^2}{4} \tag{2.10}$$

The surface area of a paraboloid of revolution, useful for determining the amount of reflective material required for the construction of a parabolic dish solar concentrator, as defined by its focal length and aperture diameter is given by equation 2.11 [37]:

$$A_s = \frac{8\pi f^2}{3}\left\{\left[\left(\frac{d}{4f}\right)^2 + 1\right]^{3/2} - 1\right\} \tag{2.11}$$

2.1.6. Solar Tower

The optics of a solar tower concentrator is much simpler than that of a parabolic trough, or solar dish concentrator in that it is simply composed of many flat plate mirrors. While the reflective surface area is simply defined as the sum of the square area of each heliostat, the collector aperture area is much more complicated, as it changes continuously due to the rotation of the earth relative to the sun.

To operate effectively, each heliostat must be pointing midway between the sun at its present location, and the central tower. The collector aperture area is therefore reduced on each heliostat by the cosine effect, which is explained in detail in section 2.2.1. Figure 2-3 displays how two heliostats in the same central tower system can experience different effective heliostat areas at the same instant. θ_i is defined as the angle between the incident ray, and the surface normal to a given heliostat, or half the angle between the incident ray and reflected ray, so that the reflection will hit the receiver tower. It can be seen that the smaller for smaller values of θ_i, a greater effective reflective area is achieved.

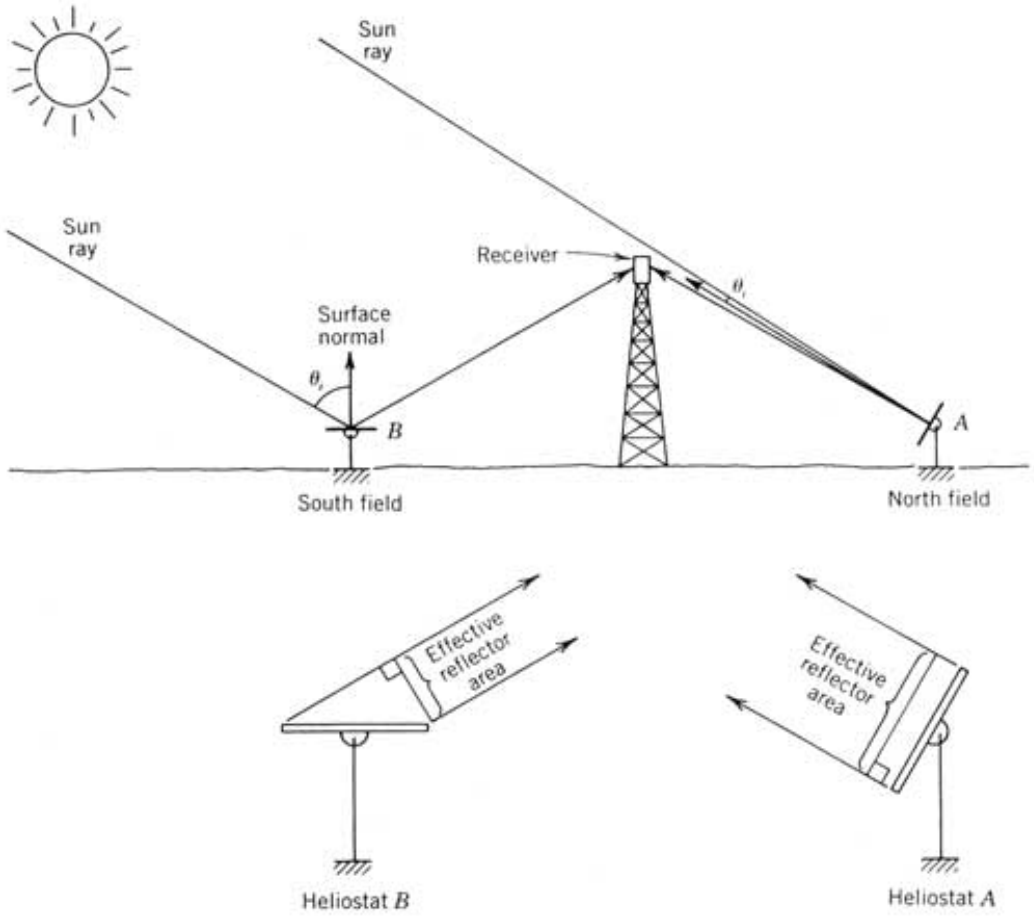

Figure 2-3. Effective reflector area of flat plate heliostat. [37]

2.1.7. Two-Stage Concentrator

The two stage concentrator is composed of two reflector sets, both having parabolic properties as described in section 2.1.4. In the case of the two stage concentrator, the two parabolas will have different focal lengths, and be spaced in such a manner that both parabolas converge at the same location (or slightly different locations if a full temperature focus is not desired). The primary reflector is typically designed to have square dimensions, that is to say the width of the primary reflector is equal to the arc length of the parabolic curve by which it is shaped. The secondary reflector is typically designed to have the same width as the primary reflector, and half the height of the primary reflector. The matching width is a requirement as the primary reflector provides no concentration about its own vertical axis. The height of the secondary reflector however, could be modified based on the spacing between the two reflectors. The further away the secondary reflector is from the primary reflector, the smaller the secondary reflector's height dimension can be, as at this point the primary reflector has accomplished more concentration of light rays about its horizontal axis.

Given that the primary reflector is the only reflector capturing initial incident sunlight rays, the collector aperture area is defined as:

$$A_a = ld \tag{2.12}$$

where l is the width of the primary reflector, and d is the linear distance from bottom to top of the parabolic curve.

The reflective surface area encompasses both the primary and secondary reflectors. For the common case where the secondary reflector has a height of half the primary reflector's width, the reflective surface area would be defined as:

$$A_r = A_{r1} + A_{r2} \tag{2.13}$$

where A_{r1} and A_{r2} are the primary and secondary reflector areas respectively, and are defined as:

$$A_{r1} = s_1 l \tag{2.14}$$

$$A_{r2} = \frac{s_1 s_2}{2} \tag{2.15}$$

where s_1 and s_2 are determined using the equations from section 2.1.2, and s_2 is selected so that it equals l.

Therefore, for this case, the reflective surface area of the entire two stage solar concentrator is defined by equation 2.16 as:

$$A_r = \frac{3\, s_1 l}{2} \tag{2.16}$$

2.2. OPTICAL EFFICIENCY

Optical efficiency is measured as the ratio of captured sunlight to the available incident sunlight [32]. There are many factors that contribute to the degradation of overall optical efficiency of a CSP system, the main ones being:

- The cosine effect
- Mirror reflectivity
- Blocking and shadowing

- Atmospheric attenuation
- Surface irregularities

Each of these factors, which will be explored in further depth in the following sections, represent a different obstacle that must be minimized to fully maximize the overall efficiency of a CSP system. The experimental and theoretical research that follows in chapters 3 and 4 will focus on understanding the cause of naturally occurring surface irregularities for a reflector in a two stage solar concentrator, and exploring different methods to minimize these irregularities.

2.2.1. The Cosine Effect

The cosine effect is a manner to represent the difference between the amount of energy falling on a surface pointing parallel at the sun, and a surface parallel to the earth [37]. The angle between these two vectors is known as the angle of incidence, and is of the utmost importance to a solar designer, as the maximum amount of solar radiation energy available to the collector is reduced by the cosine of the angle of incidence [37].

The effect of the cosine effect on a CSP system's optical efficiency is inherent to the configuration and tracking system used. The parabolic trough collector, which uses single-axis tracking, and therefore has a larger cosine effect, suffers from large variations in optical efficiency between summer and winter, especially at high latitudes [38].

Once the cosine effect and angle of incidence have been defined, attention turns to the method for determining the angle of incidence for different CSP systems. A CSP system using dual axis tracking, such as a dish system or a system using heliostats will experience minimal optical efficiency degradation due to the cosine effect. However, for

a single axis tracking system, such as a parabolic trough system, losses due to the cosine effect must be considered [37].

Figure 2-4 shows how rotation of a collector about a tracking axis r brings the central ray unit vector S into the plane formed by the normal vector (*N*) and the axis of tracking [37]. The tracking angle (*p*) measures rotation about the tracking axis (*r*), with p=0 when N is vertical. The angle of incidence (θ_I) is shown as the angle between the *S* and *N* vectors [37].

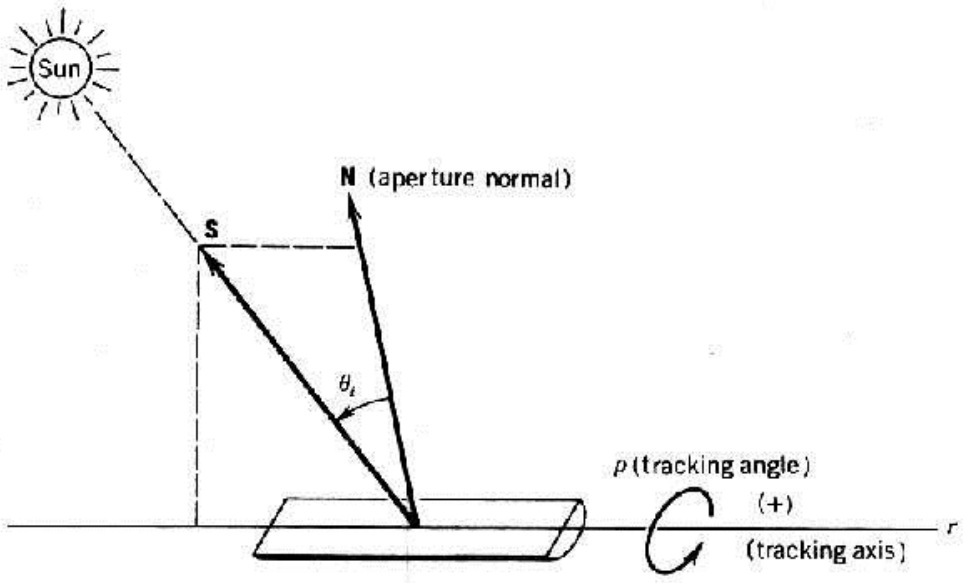

Figure 2-4. Parabolic trough angle of incidence. [37]

This system is further developed by placing it on a three dimensional coordinate system whereby *r* is the tracking axis, *b* is an axis that always remains parallel to the earth's surface, and u is the third orthogonal axis [37]. The coordinates remain fixed as the concentrator normal vector *N* rotates in the *u*-*b* plane [37].

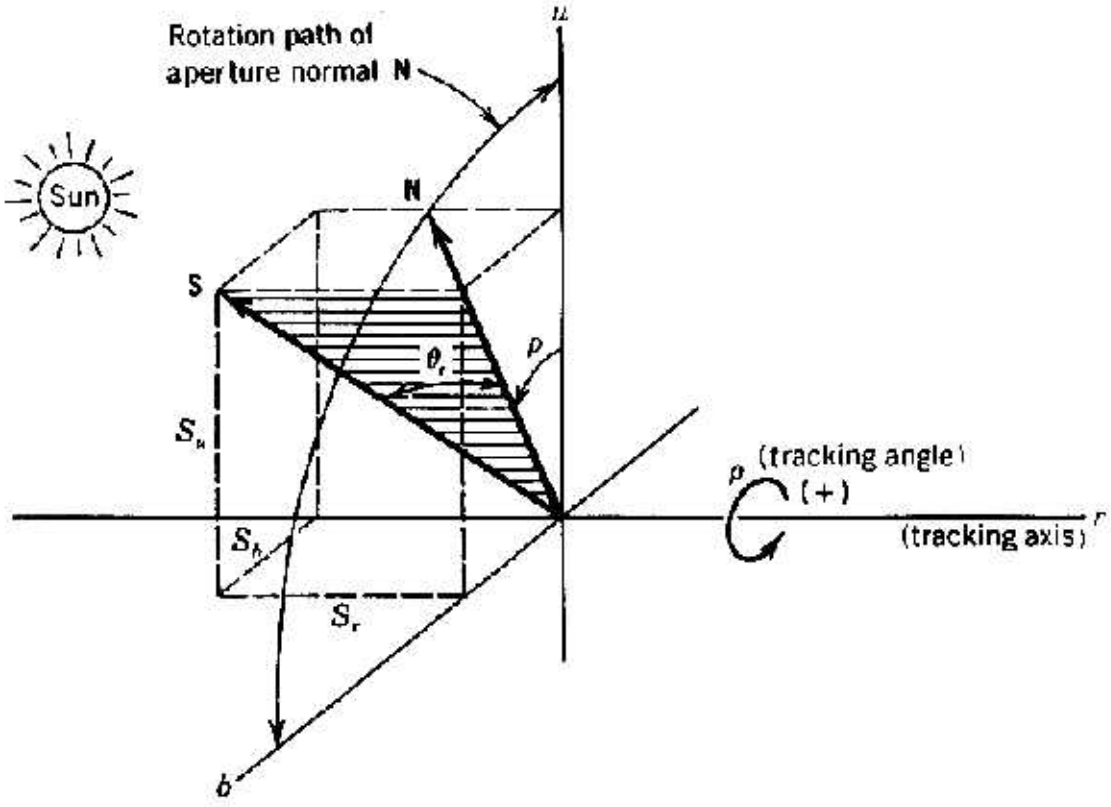

Figure 2-5. Single axis tracking in 3D coordinate system. [37]

From Figure 2-5 it can be deduced that both p and θ_l can be defined in terms of the direction cosines of the central ray unit vector S along the u, b and r axes, denoted as Su, Sb and Sr respectively. In this case, the tracking angle is then:

$$\tan p = \frac{S_b}{S_u} \tag{2.17}$$

And since S is a unit vector, the cosine of the angle of incidence is:

$$\cos \theta_1 = \sqrt{S_b^2 + S_a^2} \tag{2.18}$$

One final consideration must be made when dealing with the cosine effect. Even if a CSP concentrator is designed to track the sun over both axis at all times, depending on the type of concentrator, there is still often an offset angle. This offset angle allows for the reflected light to be transmitted in a direction other than directly back towards the

sunlight. While this is of no value for solar dishes or troughs, which are content to point towards the sun at all times, it is a consideration for heliostat CSP systems, as they desire to point direct the sun at a central location.

Figure 2-6 demonstrates the offset angle (μ) of a heliostat directing sunlight at a normal angle N lower than the sun vector. In the event of an offset angle, the angle of incidence is simply the offset angle, as it would have been calculated above, plus or minus the offset angle depending on the orientation of the system [37].

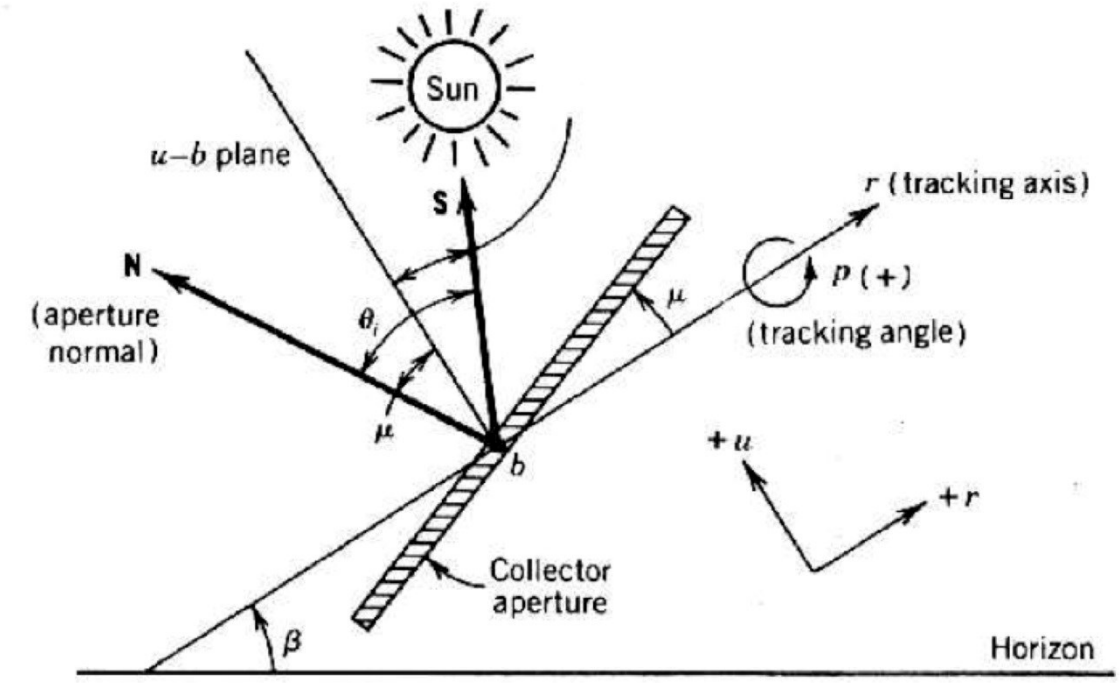

Figure 2-6. Offset angle. [37]

In summary:

- The maximum amount of solar irradiation available to a CSP system is equal to the local solar irradiance multiplied by the cosine of the angle of incidence.

- For a parabolic trough collector the angle of incidence is determined using equation 2.18.
- For a heliostat collector, the angle of incidence is equal to the offset angle.
- For a parabolic dish collector, the angle of incidence is 0.

2.2.2. Mirror Reflectivity

The reflectivity of the material chosen for concentrating purposes has a very large impact on the overall optical efficiency of a CSP system.

Real surfaces are not perfect specular reflectors. Reflectivity is measured as the fraction of incident radiation reflected by a surface [39]. The important feature for concentrators is the distribution of outgoing rays near an outgoing central ray, which lies in the plane of incidence with respect to the "average" surface [39]. Thus a specular reflectance can be defined as the fraction of incoming energy with a particular incidence angle that leaves centered about a leaving ray relative to the "average" surface.

Common types of reflectors used for concentrated solar power systems are glass, polished metals, or metallic films. Table 2-1 summarizes the specular reflectance for different common reflector materials. It is seen that reflectivity ratings range from 84% to 98% depending on the material chosen, however for economic purposes, it does not always make sense to choose the most reflective. Mirror reflectivity can be optimized considering the economical trade-off between increased reflectivity and greater mirror cost [38]. Glass is a very economical choice given its high reflectivity rating and

relatively low cost, however extra design considerations are required due to the brittle nature of glass, and the dangers associated with potential fracturing [40].

Table 2-1. Reflectivity of various materials [39]

Material	Specular Reflectance
Laminated glass – Carolina Mirror Co.	0.93
Laminated glass – Gardner Mirror Co.	0.90
Corning microsheet (Vacuum Chuck)	0.95
3M Scotchcal 5400	0.85
3M FEK-163	0.85
Sheldahl Aluminized Teflon	0.87
Polished aluminum Alcoa Alzak	0.85
Polished aluminum Kingston Ind. Kinglux	0.85
Metalic Fabrications Bright Aluminum	0.84
ReflecTech Mirror Film	0.94
Anolux MIRO-SILVER	0.98

Further reflectivity concern must be given to the long-term reflectivity of a selected reflective surface. Weathering can have dramatically negative effects on the specular reflectance of any surface. Exposure to the elements and cleaning operations can cause changes to any particular surface [39]. Light accumulations of dust and dirt decrease the performance of concentrating collectors more than they would for flat place collectors, since such accumulations often seem to cause scattering more than absorption of incident radiation. Washing can restore this latter property if the surface is hard enough to withstand the abrasion associated with washing [39].

Long time exposure to the elements can cause corrosion or discoloration, in turn reducing the reflectivity of the surface [39]. Figure 2-7 shows the effects of weathering on a sheet of polished aluminum after being exposed to 28 months of Arizona's environment. A loss of about 4% from the original solar weighted value of 0.82 is shown for this material in this environment.

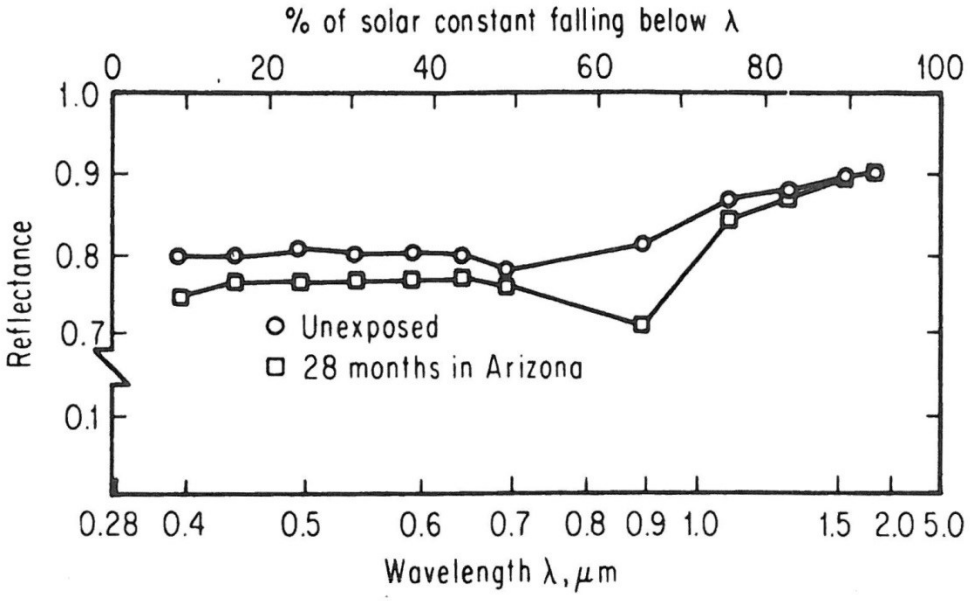

Figure 2-7. Weathering effects on reflective surface [39]

A similar experiment conducted on aluminized fiberglass with a protective coating showed 22% degradation over a 69 week period [39]. The same experiment showed 0% degradation to an aluminized glass reflector over a 63-week period in Arizona [39]. Similarly, ReflecTechSolar promise no reflectivity degradation on their products over a 25-year period. What can be concluded from these experiments is that different materials experience different reflectivity degradation due to weathering effects, much like different materials exhibit different reflectivity values to start with.

In summary:

- Reflectors of different materials demonstrate different initial reflectivity ratings, and also different abilities to withstand the effects of long-term weathering.
- The maximum available energy available at the focus of a concentrating solar device is equal to the input energy multiplied by the reflectivity value of the system's reflectors.

2.2.3. Blocking and Shadowing

The terms blocking and shadowing refer to when part of a CSP system casts a shadow over another portion of the system, lowering the amount of energy concentrated per unit area of reflecting surface [41].

When dealing with a single heliostat, trough or dish, blocking and shadowing are not much of an issue. However when dealing with multiple collectors tied together in a larger system, shadowing is unavoidable. Studies have concluded that solar plant and power plant scale-up provides the largest cost reduction opportunities, meaning that dealing with blocking and shadowing in the best manner possible is of great concern for solar engineers [41].

The angle of the sun with respect to the horizon of the earth changes from 0 degrees at sunrise, to a maximum of 90 degrees throughout the day. If concentrators are placed tightly with one another, then large amounts of blocking will be experienced during the sunrise and sunset portions of the day. If the concentrators are spaced out a large distance from one another, then less blocking and shadowing is experienced during the

early and late portions of the day, but less solar energy is being collected per unit area land during the middle portion of the day [35]. This analysis is not trivial, and has led to the development of complex computer models to determine the optimal distance to space solar concentrators. For simplicity, this thesis will focus on the case of heliostats used for a central tower solar system, however the principles could be applied to a solar farm using trough or dish collectors [42].

A computer model developed by Francisco J Collado can be described as a combination of two analytical tools, namely an analytical flux density function of the energy reflected by a heliostat, and a continuous function of the mirror density per unit square meter of plain ground [42]. It has been found that the model is able to acceptably reproduce the results of discrete evaluations, which were based on actual distributions of thousands of heliostats. Therefore the model can be used to appropriately determine preliminary estimations and primary optimizations, which should be refined later for a specific CSP system [42].

This model defines blocking factor f_b i.e. the fraction of the heliostat area free of blocking as:

$$f_b = 1 - \left[\frac{\Delta R}{LH}\left(\frac{\cos\varepsilon_\tau + \tan\beta \sin\varepsilon_\tau}{\cos S}\right)\right] * \left[\frac{2wr - (\sqrt{1+wr^2} + ds)}{wr}\right] \quad (2.19)$$

where ΔR is the radial increment between consecutive and staggered rows, LH is the height of the heliostat, ε_τ is the elevation angle (origin the zenith) of the tower unit vector pointing from the center of the heliostat surface to the receiver, S is the incidence angle of

the sunrays onto the heliostat surface, *wr* is the width-height ratio of the heliostats, β is the ground slope, and *ds* x *LH* is any additional security distance between adjacent heliostats in the same row [42].

The effect of blocking and shadowing on optical efficiency at any discrete point in time is average of the blocking factor of each individual heliostat. This number would then be multiplied by the available input energy to give an accurate field energy value. To determine the annual effect of blocking and shadowing, an entire year should be modeled giving a final annual blocking factor that can be factored into larger calculations. Figure 2-8 shows an example of an output provided by this model, using the case of spring equinox. 884 heliostats are placed in a circle of diameter = 750 m, and at a blocking factor of 0.95, a value that corresponds with the optimum values found by University of Houston for shading and blocking factor [41]. The colors of each heliostat are associated with the efficiency of that specific heliostat, and the overall efficiency of the system, which accounts for other losses explained elsewhere in this thesis, is stated in the top left corner, 75.77%

The model output of Figure 2-8 is then contrasted with a similar model, seen in Figure 2-9, but for a blocking factor of 0.99. In this case 900 heliostats of the same size are placed in a slightly larger circle, and yield an overall field efficiency of 78.37%. It is shown as one would expect, that with a larger blocking factor, and all other factors being held constant, a higher overall field efficiency is found. This however must be measured

against the cost to build a CSP system using a larger landmass, and spacing collectors at a larger distance.

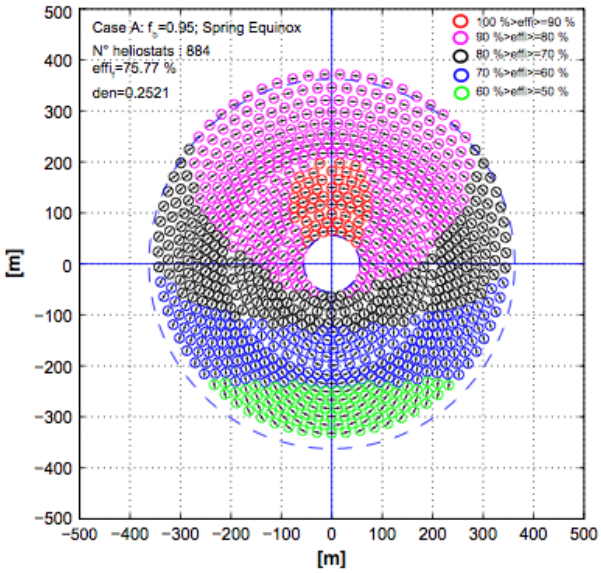

Figure 2-8. Example output of packing factor model fb=0.95. [42]

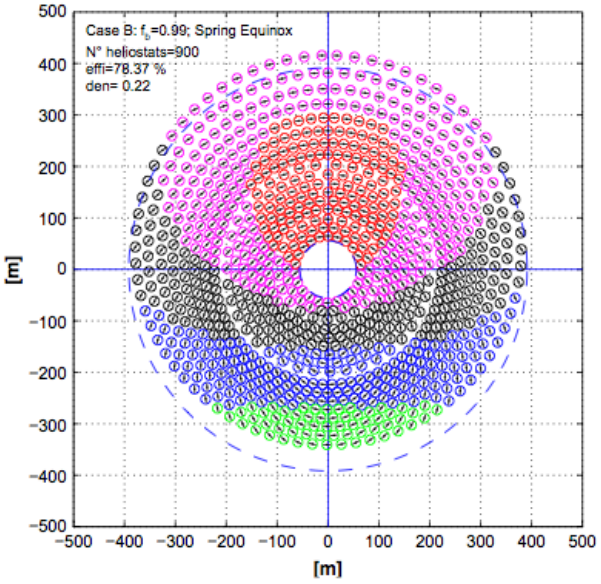

Figure 2-9. Example output of packing factor model fb=0.99. [42]

In summary:

- Blocking factor is a useful value to help determine the optimal distance collectors should be placed from one another in a large-scale CSP system.
- An economic assessment must be done on a case by case basis to determine if a greater blocking factor is indeed worth the larger capital cost associated with such a plant.

2.2.4. Atmospheric Attenuation

The effect of atmospheric attenuation is of less importance than the three factors previously discussed, but still worthy of consideration. Atmospheric attenuation can be defined as 'a process in which the flux density of a parallel beam of energy decreases with increasing distance from the source as a result of absorption or scattering by the atmosphere' [39]. Because this factor is directly related to the distance over which a beam travels, the only way to possibly reduce the amount of atmospheric attenuation, aside from changing atmospheric conditions, is to reduce the distance between the solar concentrator and target point [39].

The exact effects of atmospheric attenuation differ depending on a given atmospheric condition, which not only changes by location but also on a daily basis [39]. To accurately estimate the effect of atmospheric attenuation, an experiment would be required that would measure the output energy of similar concentrators operating at different focal lengths. It is unlikely that this experiment would be conducted for low focal length concentrators such as troughs or dishes, but it is a very useful procedure for central tower heliostat systems as the throughput of remote heliostats suffers from

atmospheric scattering and absorption, which increase exponentially with distance [38]. A value for $f_{at,}$ which depends on distance traveled after reflection, can then be determined for a given situation and used as a factor in a final field optical efficiency calculation.

2.2.5. Surface Irregularities

Of the five factors of optical efficiency discussed in this thesis, surface irregularities are the most difficult to quantify. Surface irregularities can be broken down into two categories, small-scale irregularities, and large-scale irregularities. Small-scale irregularities are caused at a microscopic level, and are accounted for when calculating a material's reflectance [39]. Large-scale surface imperfections can be extremely critical for collectors' efficiency. These are deviations of the average surface from its intended shape, usually parabolic [39]. For the most part, these imperfections are readily apparent to the unaided eye in the form of the distortions they cause in reflected imagery [39]. The spillage factor f_s of a system can be determined experimentally by measuring the portion of light reaching the desired target compared to the amount of light reflecting off of the mirrored surface. Figure 2-10 demonstrates the problem caused by true surface tangents being different from ideal. Instead of the central ray from the sun being directed to the center of the absorber, it is misdirected along another plane. It should be noted that the angle error δ in the mirror slope causes an error of 2δ in the departing ray [39].

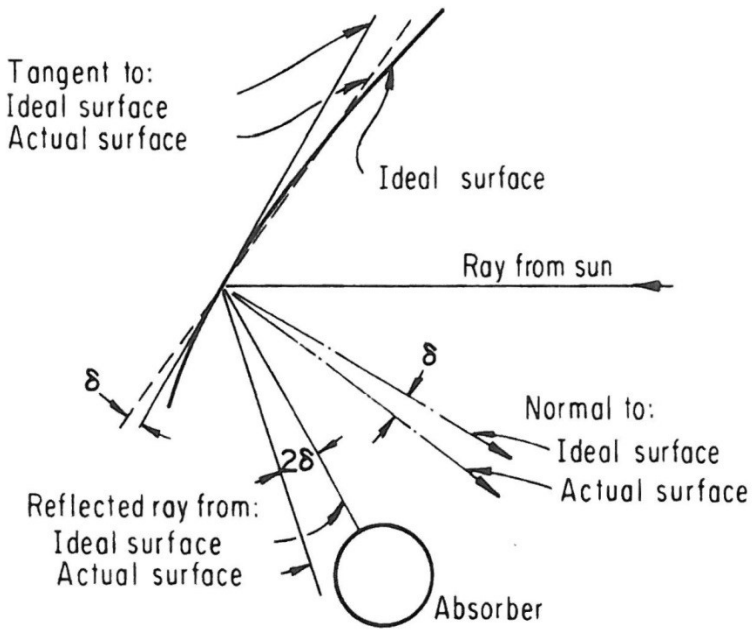

Figure 2-10. Surface slope errors caused by surface imperfections. [39]

Studies to assess manufacturing techniques and projected costs of concentrators have concluded that surface accuracies of 0.1° are readily achievable [39]. Image spread at the optical focus can be minimized by reducing the distance between the concentrator and absorber [39]. This is demonstrated in Figure 2-11, which shows various rim-angle trough concentrators, all having a common focal point. The axis on the left indicates the relative length of the curve, while the axis on the right indicates the angle of the parabola at its edge [39]. While the 90° rim angle parabola has the smallest maximum distance from concentrator to focus, it can be shown that a rim angle of 120° has the shortest average distance between concentrator surface and focal point [39]. However, this does not necessarily mean that 120° is the ideal rim angle, as there are other considerations, primarily cost. The material added at large rim angles is inefficiently used, and might be better added as an extension of the length of a trough or as an additional collector [39].

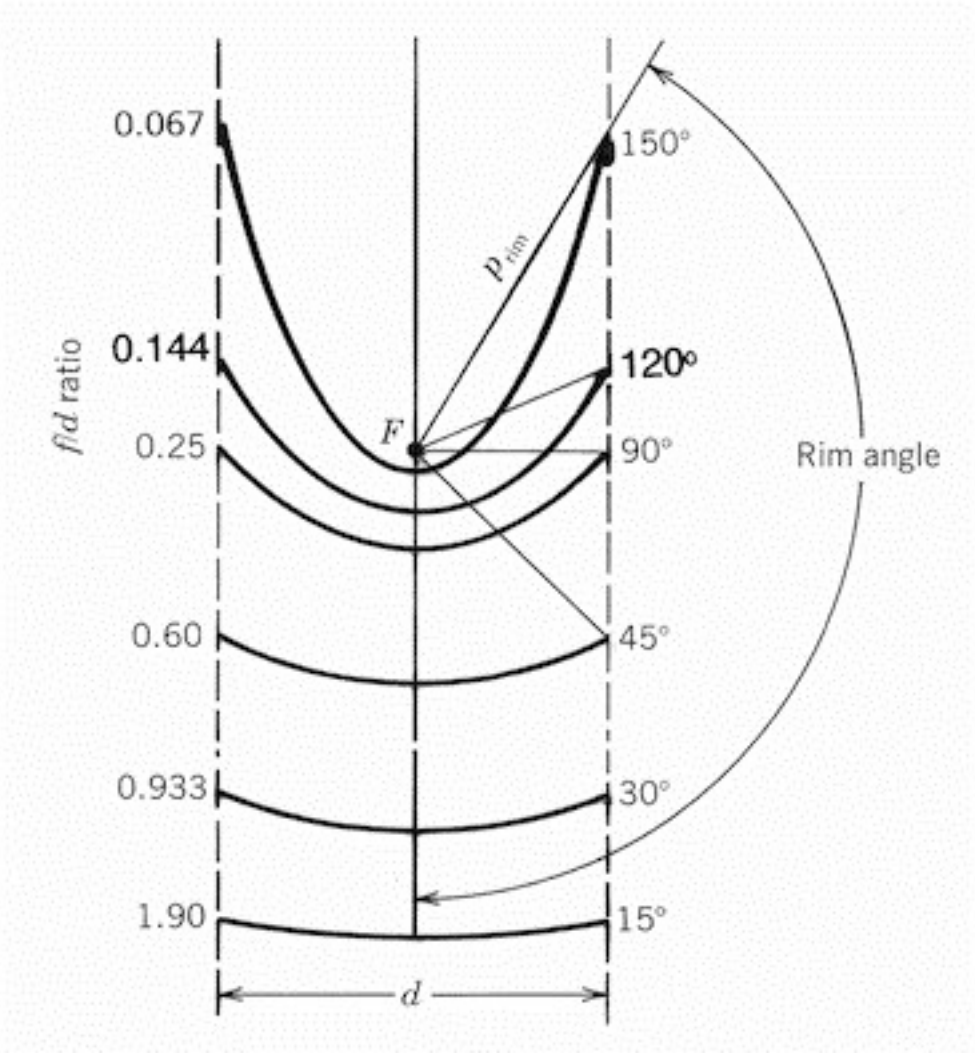

Figure 2-11. Equal aperture area parabolas of various rim angles. [41]

Much like the other optical efficiency aspects considered in this thesis, the minimization of large-scale imperfections becomes an economic study. By ensuring that a reflector is forced to an appropriate curve, and by adequately supporting it over its entire area, slope error can be minimized. Furthermore, by minimizing the distance between reflector and target, the effect of the slope error is further minimized.

2.3. PLATE BENDING FORMULATION

Plates are typically split into three broad classifications according to the thickness ratio a/h, where a is a typical dimension of a plate in a plane and h is the thickness of the plate [43]:

1. Thick Plates – Plates having ratios $a/h \leq 8$. These plates are treated as solid bodies and can be solved using the general equations of three-dimensional elasticity for components of stresses, strains and displacements. Mindlin plate equations can be used to solve thick plates [43].
2. Membranes – Plates having ratios $a/h \geq 80$. Membranes are very thin plates that are devoid of flexural rigidity. Membranes carry loads by axial tensile forces, known as membrane forces, acting in the middle surface of the plate. Membrane forces balance a lateral load applied to the membrane by producing projection on a vertical axis [43]. To be considered a true membrane, a structure must satisfy the following conditions [43]:
    - The boundaries are free from transverse shear forces and moments. Loads applied to the boundaries must lie in planes tangent to the middle surface.
    - The normal displacements and rotations at the edges are unconstrained.
    - A membrane must have a smoothly varying, continuous surface.
3. Thin Plates – Plates having ratios $8 \leq a/h \leq 80$. Depending on the ratio of the maximum deflection, w, of the plate to its thickness, h, the effect of flexural and

membrane forces may be different. Thin plates are therefore subdivided into Stiff Thin Plates and Flexible Thin Plates [43].

a. Stiff Thin Plates – Thin plates where $w/h \leq 0.2$ are considered flexural rigid. These plates carry loads two dimensionally, mostly by internal bending and twisting and by transverse shear forces. Deformation of the middle plane and membrane forces are likely to be negligible when dealing with stiff thin plates. Unless specified otherwise, thin plates are assumed to be stiff thin plates [43].
b. Flexible Thin Plates – Thin plates where $w/h \geq 0.3$ require additional consideration for the stretching of the middle surface. These plates can be considered as a combination of stiff thin plates and membranes, and carry external loads via a combination of internal moments, shear forces and membrane forces. When the magnitude of the maximum deflection is considerably greater than the plate thickness, on the order of $w/h > 5$, flexural stresses can likely be neglected compared with membrane stresses [43].

To analytically solve for the deformation of thin plates using classic plate theory, it is convenient to make the following assumptions, which are known as the Kirchhoff hypotheses [43]:

1. "The plate material is elastic and follows Hooke's law."
2. "The plate material is homogeneous and isotropic. Its elastic deformation is characterized by Young's modulus and Poisson's ratio."

3. “The thickness of the plate is small compared to its lateral dimensions. The normal stress in the transverse direction can be neglected compared to the normal stresses in the plane of the plate.”
4. “Points that lie on a line perpendicular to the center plane of the plate remain on a straight line perpendicular to the center plane after deformation.”
5. “The deflection of the plate is small compared to the plate thickness. The curvature of the plate after deformation can then be approximated by the second derivative of the deflection.”
6. “The center plane of the plate is stress free.”
7. “Loads are applied in a direction perpendicular to the center plane of the plate. “

Consider the representative plate geometry shown in Figure 2-12. This geometry shows the midplane, or middle surface of the plate, and typical Cartesian coordinate axes, upon which we can relate the governing equation of thin plate bending.

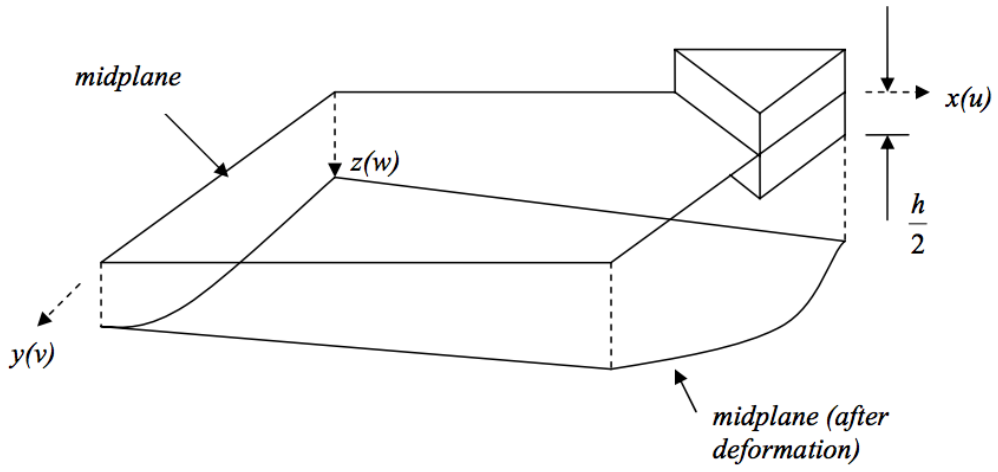

Figure 2-12 – Representative plate geometry. [44]

Under Kirchhoff's hypotheses, the governing equation of motion can be derived for small deflections in thin plates as:

$$D\left[\frac{\partial^4 w(x,y,t)}{\partial x^4} + 2\frac{\partial^4 w(x,y,t)}{\partial x^2 \partial x^2} + \frac{\partial^4 w(x,y,t)}{\partial y^4}\right] = \rho h \frac{\partial^2 w(x,y,t)}{\partial t^2} \tag{2.20}$$

where w(x,y,t) is the deflection of the plate, ρ is the density, h is the thickness of the plate, and D is the flexural rigidity of the plate.

Furthermore the stress-strain relations can be expressed as:

$$\begin{bmatrix}\sigma_{11}\\ \sigma_{22}\\ \sigma_{12}\end{bmatrix} = \frac{E}{1-v^2}\begin{bmatrix}1 & v & 0\\ v & 1 & 0\\ 0 & 0 & 1-v\end{bmatrix}\begin{bmatrix}\varepsilon_{11}\\ \varepsilon_{22}\\ \varepsilon_{12}\end{bmatrix} \tag{2.21}$$

While the moments corresponding to these stresses can be expressed as:

$$\begin{bmatrix}M_{11}\\ M_{22}\\ M_{12}\end{bmatrix} = \frac{2h^3 E}{3(1-v^2)}\begin{bmatrix}1 & v & 0\\ v & 1 & 0\\ 0 & 0 & 1-v\end{bmatrix}\begin{bmatrix}\omega_{11}^0\\ \omega_{22}^0\\ \omega_{12}^0\end{bmatrix} \tag{2.22}$$

Unfortunately, while these systems of equations represent an accurate solution for the deflections of thin plates under certain conditions, the curvature inherent in parabolic reflectors means that classic plate solutions don't apply, as both Kirchhoff hypothesis #7 and membrane requirements can't apply to a curved surface under gravitational loading. Furthermore, the governing equations of classic plate theory are intended to be used on plates that are initially flat, and are then subjected to different loadings.

To this end, in order to study the deflections and deformations of a solar reflector under gravitational loading, computational methods are preferable over analytical solutions.

Chapter 3: METHODOLOGY

The experiments in the present work are broken into two categories: Experimental, which deals with experiments and experienced gained while working hands on with the Prometheus two-stage solar concentrator prototypes, and FEM, which consists of using finite element software to simulate reflector plates under different conditions, onto which a highly reflective film would be laminated.

3.1. EXPERIMENTAL

While operating Prometheus style two-stage solar concentrators aberrations in the resulting focus have been observed. It has been observed that a single reflector, which is expected to produce a line focus, produces a focus that contains a high intensity central line and also rounded areas of focal spilling referred to as “hamburger buns”. At the point in time of these observations, the reflectors were made of 4’x8’ polished stainless steel sheets constrained only along their 8’ lengths. Initial hypothesis was that these aberrations are caused by end conditions existing at the uncontrolled 4’ ends of the reflective surface. An experiment was conducted to isolate the effects of the end conditions, and the cause of the “hamburger bun” phenomenon. The reflection caused by a single 4’x8’ parabolic mirror, with a 5’ focal length is seen in Figure 3-1. There exists a high intensity strip down the center of the focal area, which is bracketed by lower intensity areas to the right and left of the central strip.

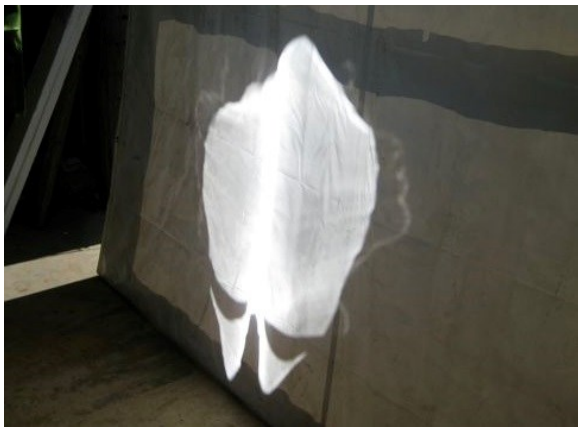

Figure 3-1. Focus image resulting from single 4'x8' reflector of 5' focal length constrained about its 8' edges, showing "hamburger buns" effect.

To check the hypothesis that the bracketing light areas were caused by the free end conditions, the outermost 12.5% of the reflector was covered with a non-reflective material. The resulting focus of this identical reflector having no input from the uncontrolled ends is show in Figure 3-2. It should be noted that only the central strip region is present when eliminating the edges and that there are no signs of the "hamburger bun" bracketing area.

Figure 3-2. Focus image resulting from single 4'x8' reflector of 5' focal length constrained about its 8' edges with outermost 12.5% of reflector covered, showing much improved line focus.

When the end conditions of both the primary, and secondary reflector are compounded, the resulting focus has a 'cross' effect, where there is an area of light spillage along the horizontal axis that is cause by the end conditions of the secondary reflector, and an area of light spillage along the vertical axis that is caused by the end conditions of the primary reflector. An example of the combined focus cross effect is seen in Figure 3-3, which has been photographed through a lens to allow for visual distinction between the very high intensity focus area, and the lower intensity areas which surround it. The highest light intensity is still observed at the central location where it is desired, but its intensity would be greater if all exterior light were focused properly.

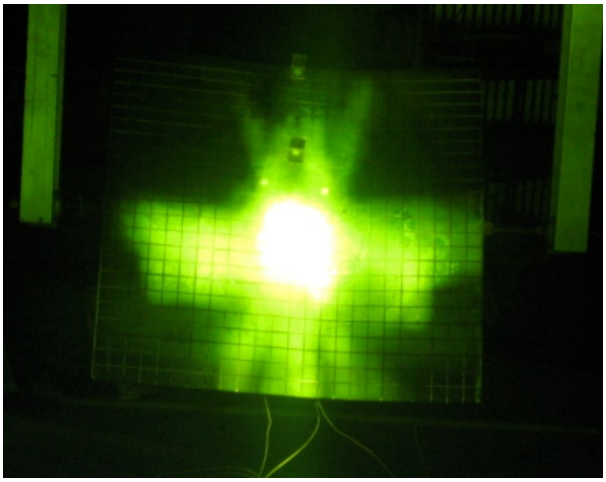

Figure 3-3. Example of combined focus cross effect, resulting from end conditions on primary and secondary reflectors.

3.1.1. Effect of Material and Thickness

Throughout a testing period from spring 2009 to fall 2012, many different materials were used as reflectors by LIFE on two-stage concentrator prototypes. These materials include:

- 430 mirror finish stainless steel with PVC coating
- Glass mirrors
- Plexiglass mirrors – clear mirror acrylic
- Anomet reflective aluminum sheets, Anolux MIRO-SILVER
- Reflectec aluminum reflective film

430 mirror polished stainless steel was the first material used due to being readily available and durable. The stainless steel provided acceptable initial reflectance, but very quickly the polished surface began to tarnish, even while being stored indoors protected from wind and rain, and the brightness and temperature of the resulting focused image decreased.

Regular household glass mirrors were then installed into modified reflector frames, as it was thought that they would provide better long-term reflectance. Mirror thicknesses of 3mm, 5mm and 7mm were installed into the primary reflector frames of the Prometheus Beta-Gamma prototype, which had a focal length of 15'. It was found that the 7mm glass mirror could not bend sufficiently to take the required curve shape, and it shattered while being installed. Likewise, none of the glass mirrors were capable of flexing to take the shape of the 5' focal length secondary reflector curve of the Prometheus Beta-Gamma Prototype.

The 3mm and 5mm glass mirrors were installed in separate primary reflector frames and tested directly against one another. For both mirror thicknesses, the reflectors were used

to generate a line focus on a white board held at an appropriate distance (15') from the reflector. An example of the line focus generated can be seen in Figure 3-4. Using a type K thermocouple, a temperature reading was then taken in the concentrated line, and the upper and lower spillage regions. There was a measurable difference in temperature between the 3mm and 5mm glass mirrors with the 3mm achieving a peak focus temperature of 157.2 °C while the 5mm glass achieved a peak focus temperature of 122.5 °C. While these results suggest that the 3mm mirror holds a better surface profile than the 5mm mirror and therefore more accurately reflects light rays, it is important to note that the reflective surface of these mirrors is located behind the glass, unlike a reflective foil laminated to the front face of a substrate plate, and therefore will refract light rays through a glass area before reflecting it back. It should be noted that the two tests were not conducted simultaneously, and therefore the difference in temperatures achieved could be a result of different atmospheric conditions rather than a difference in performance between the two mirror thicknesses.

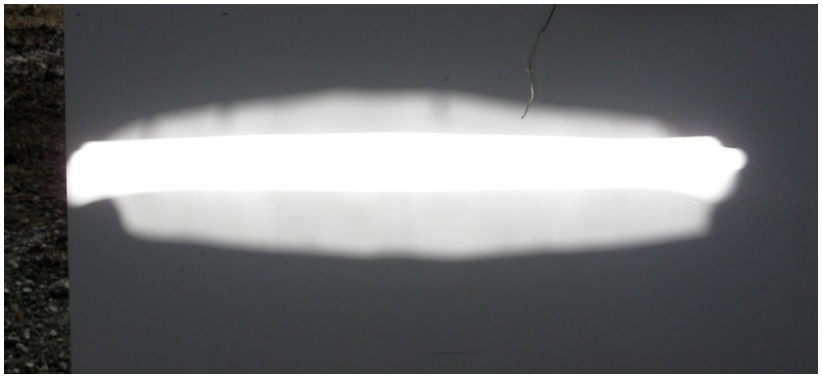

Figure 3-4. Example of line focus generated from material thickness experiment.

With the 3mm performing slightly better, and being a lighter mirror, it was chosen to be installed into the primary mirror frames of the Prometheus Beta-Gamma prototype, and both the primary and secondary reflector frames of the Prometheus Gamma II prototypes,

which have 30’ and 10’ focal lengths respectively. As glass could not be installed into the secondary mirror frames of the Beta Gamma prototype, a more malleable acrylic Plexiglas reflector was installed in its place.

While the performance of the glass mirrors was quite good during fluid heating based thermal efficiency experiments, and material melting experiments, it was not seen as a permanent solution due to the lack of durability with glass products. A material as brittle as glass was deemed both a safety and performance hazard when being left in operation largely unmonitored and exposed to the elements for a continuous and prolonged length of time. The acrylic secondary reflector satisfied the durability requirements under which the glass reflectors fell short, but did not achieve a high enough level of concentration performance.

A purpose designed product was therefore sourced that would achieve and maintain a very high reflectivity value, while being durable enough for continuous access to most weather conditions. Anolux MIRO-SILVER, a solid reflective material with 98% total light reflectivity seemed like an optimal choice due to its high reflectance and ability to withstand corrosion and high temperatures. However, due to the very thin dimensions of the MIRO-SILVER sheets, the sheets did not properly conform to the desired curve profile, and very large end conditions were produced, much worse than those documented during initial observations of the “hamburger bun” effect. An effort was made to increase the rigidity of the MIRO-SILVER product by attaching it to a substrate sheet of 1/8” thick 6061 aluminum to produce a stiffer reflector, however issues arose with any

glues used to attach the MIRO-SILVER to the substrate sheet. Using a vacuum bag technique to provide consistent and equal pressure between the reflective product and substrate plate, lighter spray on adhesives were found to provide a smooth, flat surface reflective surface free of many surface irregularities, however it was discovered that these adhesives did not provide sufficient bonding strength, especially when the reflector was subjected to a parabolic curvature. Thicker adhesives, 3M 2216 B/A and 3M 4323, were then used in the same vacuum bag system to hold the MIRO-SILVER product to the substrate sheet and succeeded in bonding the two sheets together, however this caused pronounced surface irregularities between the two surfaces, negating the benefits of the very high reflectivity promised by Anolux. A process was also developed to bond the MIRO-SILVER product to the substrate plate in a pre-curved manner so as to not stress the adhesive after hardening, however this made no change to the amount of ripples and surface irregularities on the resulting reflective face.

Knowing that a lamination process was likely to be required if a purpose built reflective material was to be used, a different product was tested that was specifically designed to be laminated to a substrate sheet. Reflectec aluminum reflective film was selected due to the fact that it contains a self-adhesive coating on its reverse side. After several failed attempts of performing the lamination manually in house, LIFE outsource the lamination of the Reflectec aluminum foil to a manufacturer that specializes in lamination, and the resulting product far exceeded anything that had been previously tested in both terms of performance and projected durability. To this end, it was concluded that the Reflectec foil, laminated to some sort of substrate plate would be the preferred composition of the

two-stage concentrator reflectors moving forward, however the specifics of the plate on which to laminate the reflective foil would need to be determined, and represent a large portion of the work to be done in the FEM sections of this report.

3.1.2. Effect of Holding Method

Several methods for holding mirrors have been put into experimental practice on the Prometheus style two-stage concentrators. They include:

- Mating male and female curve strips: These 8' arc length aluminum strips are cut to the correct parabolic curve using CNC milling methods. The bottom (female) strips are mounted rigidly to a solid mirror box. The reflector plate is placed over these strips so that it takes the same shape as the curve strips. The upper (male) curve strip contains slotted holes that allow for it to be pressed down on to the reflective surface and be tightened to the same mirror box as the female strips. This results in the full constraint of the two 8' ends of the mirror but has free ends along the 4' ends of the reflector. An additional drawback to this method is that it calls for a ¼" region of each 8' length to be covered by the curve strip, effectively reducing the power of each reflector by 1.04%.
- Mating male and female curve strips with end stiffeners: The same mating curve strip installation is employed to control the curvature of the 8' length of the reflector, however additional stiffeners are added to the 4' ends of the reflector to reduce the effect of the free end condition focal aberration. Two types of stiffeners are typically employed. One type of stiffener, which sees most usage with glass mirrors and is shown in detail in Figure 3-5, consists of a piece of aluminum angle epoxied to a piece of mirror hardware that is specifically designed to hold glass mirrors while

using a rubber gasket. The other form of edge stiffener used is a 2”x2” block of aluminum along which a ½” deep slot is machined of a thickness to match the reflector with which it will be used, and that is inserted over the 4’ end of the reflector. In both cases, additional reflective area is covered.

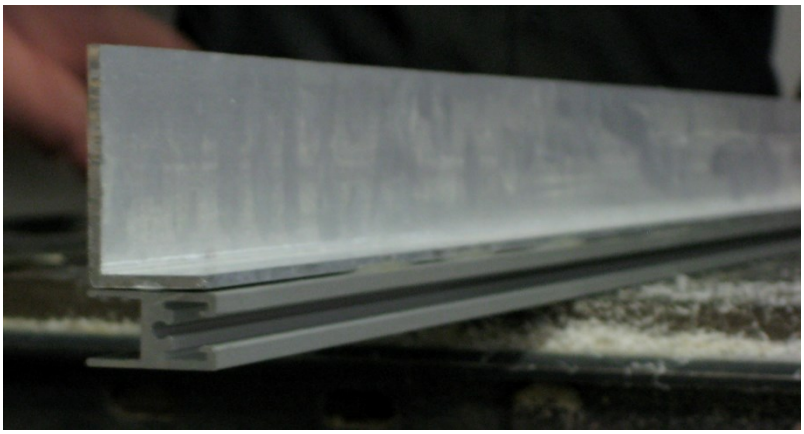

Figure 3-5. Common glass mirror end stiffener.

- Drilled and tapped female curve strips: To allow for the addition of a central curve strip, and thus reduce the distance between areas of control from 4’ to 2’, a method for screwing the mirrors directly into the female curve strip was developed. Small holes were drilled and tapped at approximately 12” intervals into CNC cut aluminum female curve strips in a manner that matched small holes drilled in an aluminum reflector. The mirror is then placed on the reflector strips (which are spaced appropriately by using threaded rods and nuts) and machine screws are used to hold the mirror in place. The ends of the curve strips are cut away to allow for a 4’ length of 1”x1”x1/8” aluminum angle to be placed along the 4 foot end of the reflector, allowing for the reflector to be fixed at 12” intervals along each of its 4 ends. While the screw’s heads do cover some reflective area of the reflector, this is significantly less than having entire ¼” edges of the reflector being covered by a male curve strip.

This method is quite labour intensive to prepare and install compared to the mating curve strip method, as it must be ensured that all of the holes in the mirror and strip/angle frame line up closely.

- Full support structure: Small scale experimentation has been conducted on using a full support system behind reflectors. A scale model of a Prometheus style two-stage solar concentrator has been developed for the purpose of testing different methods of solar tracking. For this model, high density Styrofoam was prepared to contain concave parabolic curves of appropriate focal lengths using a hot wire cutting system. As expected, this model did not experience any end conditions, as there are no real 'ends' in the sense that there are on the full-scale reflectors. The entire area is completely supported and therefore no sagging can take place so long as the Styrofoam remains structurally sound. Scaling up a full support structure to an 8'x8', 16'x16' or larger as planned by LIFE seems impractical due to the quantity and cost associated with procuring so much high density Styrofoam, cutting it to the proper profile, and installing it in place within a working device.

An experiment has been conducted using the Prometheus Gamma II prototype to qualitatively measure the difference of a resulting focus when different stiffeners were added to glass reflectors being held in place by the mating curve strip method. An initial testing took place on the apparatus before an improved slotted stiffener was added to the end of one of the glass secondary mirrors. Styrofoam was used to strategically cover the ends of the mirrors, and observations were made to relate what portion of the reflectors

was responsible for different components of the resulting focus. The test apparatus with the final 1' of each reflector covered by non-reflective Styrofoam is seen in Figure 3-6.

Figure 3-6. Gamma II prototype with final 1' of each secondary reflector covered in non-reflective Styrofoam.

With all 8 reflector ends covered, as seen in Figure 3-6, the focus (Figure 3-7) contained very little horizontal spillage, although it still contained vertical spillage due to the end conditions of the primary reflectors. It is important to understand that for the purpose of this experiment; only horizontal spillage should be considered. By systematically removing different amounts of the non-reflective material, more and more of the horizontal spillage became apparent in the focus, eventually producing the focus seen in Figure 3-3.

From this experiment, the following was concluded:

- The end conditions of the mirrors are responsible for the 'cross' effect on the light focus.
- The focus is relatively tight when the ends of the mirrors are not considered.
- The outside end conditions have more of an effect on the focus dispersion than the interior end conditions.
- The end conditions on one side of the mirror cause a cross on both sides of the focus. Left side is not just responsible for the left side of the cross, for example.
- The end conditions of the two sides "stack" on the focus. Not necessarily making the cross longer, but making the light in the cross more intense.

Figure 3-7. Gamma II focus image with all secondary reflector ends covered.

The next phase of this experiment was to add a slotted stiffener to one of the reflector ends, and compare how this mirror focuses in comparison with an epoxied on stiffener. A slotted stiffener, which makes a very tight connection to the glass mirror and provides a more rigid connection than the original stiffeners, that contain a rubber gasket around the mirror and therefore allow for some flex, was added to the outside edge of the bottom right secondary reflector. Unlike the previous phase of this experiment, where the end conditions were covered and the focus of the central portion of the reflectors was explored, in this phase of the experiment every region except for the ends to be studied were covered, as seen in Figure 3-8, allowing for isolated observation of the areas in question.

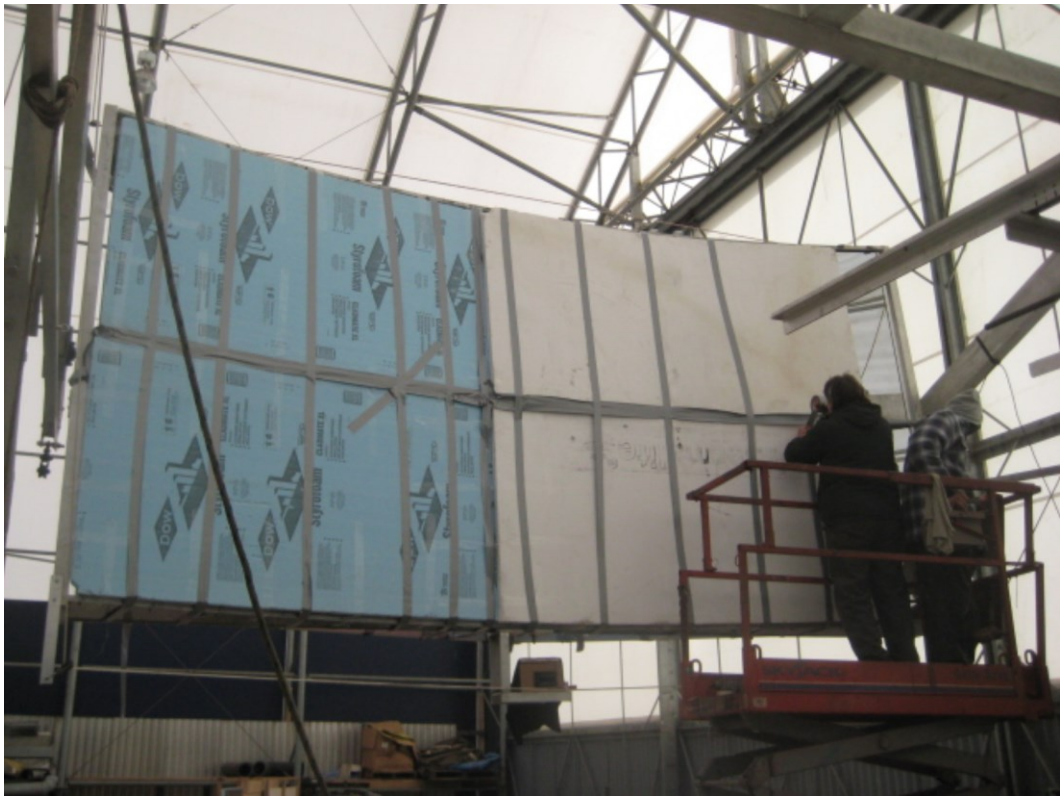

Figure 3-8. Gamma II prototype with all secondary reflectors covered in non-reflective Styrofoam except for final 1' of secondary reflectors #2, and #4 revealed, allowing for isolated observation and comparison of different stiffeners.

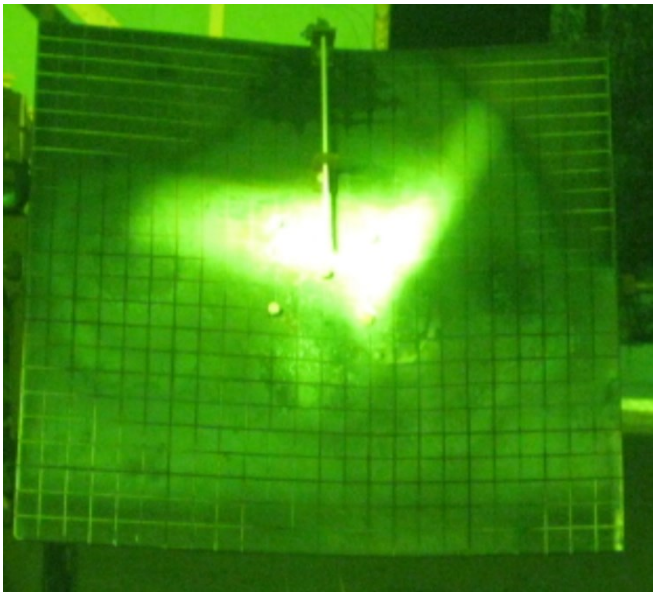

Figure 3-9. Focus image with all secondary reflectors covered except for outside 1' of secondary reflectors #2 and #4, as seen in Figure 3-8.

By comparing Figure 3-10 with Figure 3-11, the difference of focus with the notched stiffener is seen. It is quite clear from these images that the new stiffener produces a more controlled focus than its predecessor.

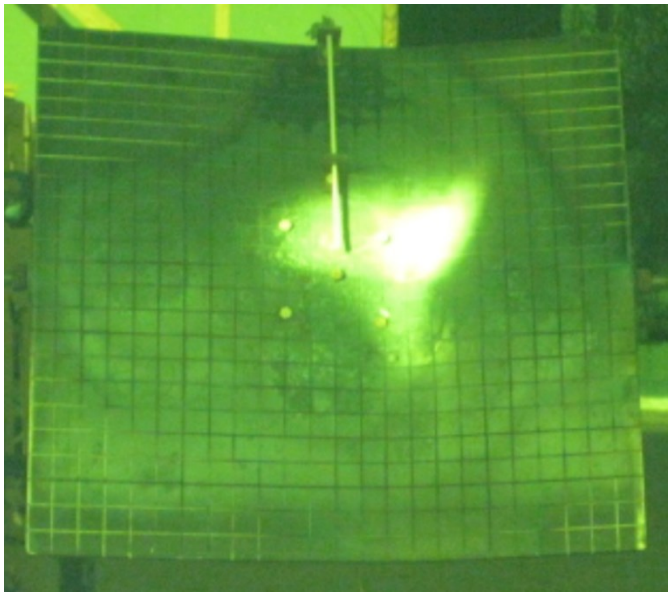

Figure 3-10. Focus image with all secondary reflectors covered except for outside 1' of secondary reflector #4, which is stiffened by machined block stiffener.

The conclusions from comparing different vertical positions of each mirror's end condition (not shown here) were less convincing. The resulting observations suggest that using the older stiffener the top and bottom portions of the end condition scramble the focus more than the center two feet of the mirror. However, the bottom mirror, with the stiffer straightened doesn't agree with the upper observation and showed that the uppermost quadrant produces the most focus deterioration, while the other three quadrants are relatively similar.

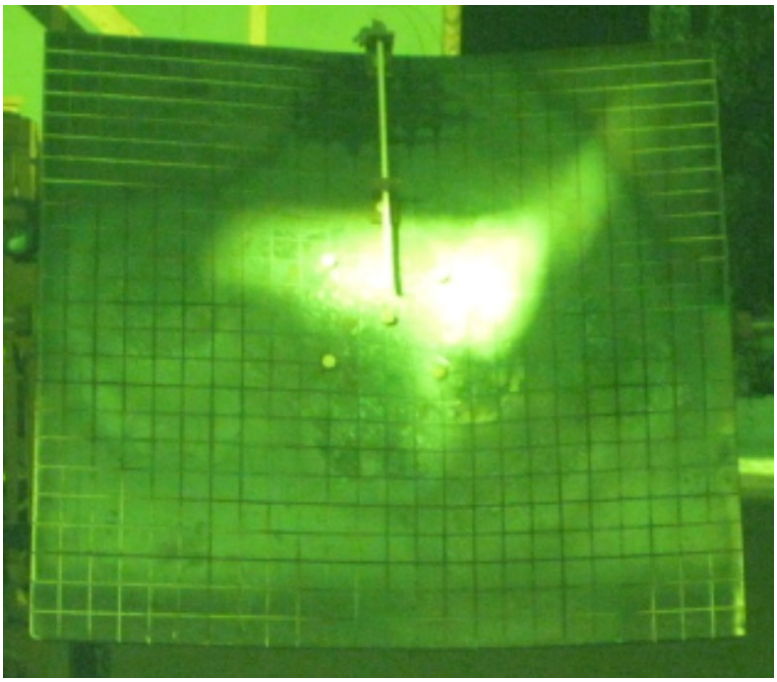

Figure 3-11. Focus image with all secondary reflectors covered except for outside 1' of secondary reflector #4, which is stiffened by common glass stiffener.

This experiment was then modified so a 6" region of mirror was left exposed instead of a 1' region. It was found that when leaving a 6" region at the edge exposed; a much less

desirable focus was achieved compared to leaving the 6” inside of that region exposed, as shown in Figure 3-12 and Figure 3-13.

This procedure was then taken a step further, and the foam cover was slid across to identify at which point the tail portion of the focus started to appear. It was found that with the new stiffener, the final 2” of mirror are responsible for the end condition deterioration. With the older stiffener, the final 4” of mirror are responsible for end condition focus scatter.

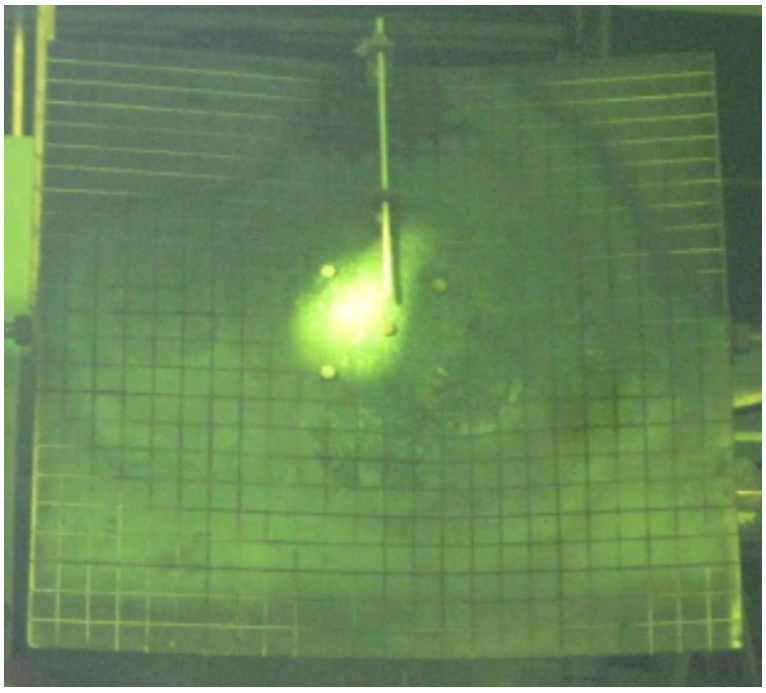

Figure 3-12. Focus image with all secondary reflectors covered except for a region spanning from 6” to 12” from the outside edge of secondary reflector #4.

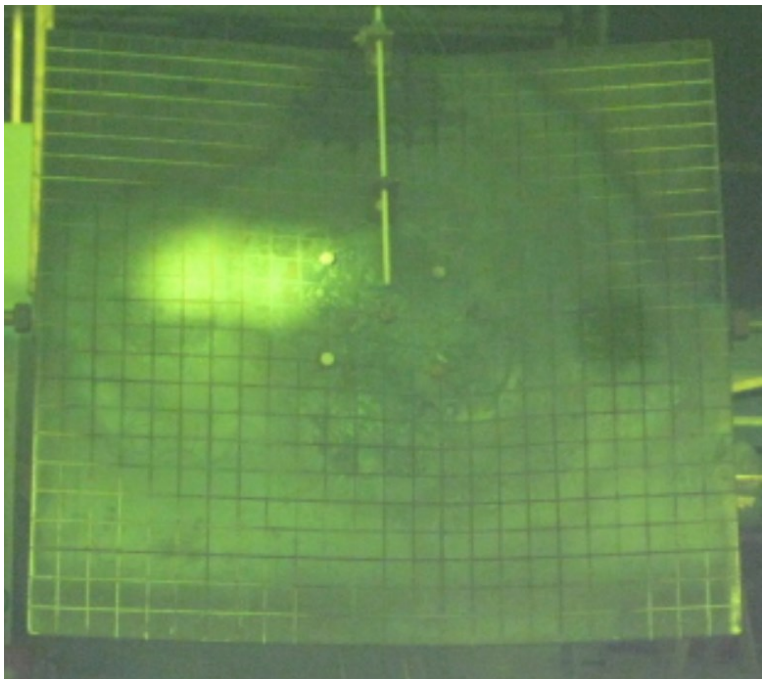

Figure 3-13. Focus image with all secondary reflectors covered except for outside 6" of secondary reflector #4.

Work was also conducted to test the theory of 'full support' of a reflector, at a small scale. 19.5"x13" and 13"x13" pieces of high density Styrofoam were cut to contain parabolic concave faces of 36" and 12" focal lengths respectively. These cuts were performed using a hot wire tool guided by to scale guides placed along the edge of the Styrofoam blocks. Pieces of Anomet reflectors were then epoxied to the Styrofoam pieces using a spray on adhesive. The immediate results were very impressive; due to the complete support of the reflectors, minimal surface irregularities and end conditions were observed, producing as close to perfect parabolic reflective surfaces as LIFE have ever produced. However, it was found in the coming weeks that the reflective surface didn't maintain its bond with the Styrofoam and the reflective surfaces fell off of their support backing. It was also concluded that while this could be an acceptable method for bench size reflectors, the logistics of fully supporting a large scale reflector (both size, and cost)

result in this not being a solution that should be presently pursued as the reflector holding method of choice.

3.1.3. Effect of Aspect Ratio

As discussed, several aspect ratios were used when developing these prototypes. It is desirable to maintain a 4'x8' reflector, but by providing a central support strip the effective aspect ratio can be changed to 2'x8'. The Solar+ 4600 uses such 2'x8' aspect ratio, and by comparing the resulting focal image from 2'x8' reflectors (Figure 3-14) with that of 4'x8' reflectors (Figure 3-15) the resulting focal quality can be seen to be greatly improved when using 2'x8' reflectors. For scaling reference, the plate in Figure 3-14 is 12" wide, while the plate in Figure 3-15 is 18" wide, and is scribed with a 1"x1" grid. The 2'x8' aspect ratio reflectors produce a focus that is completely contained within a 5" horizontal region. Meanwhile, the 4'x8' aspect ratio reflector has a focus that is horizontally contained within a 14" region.

It should be noted that this is not a quality single variable comparison between these two systems, as these two focal images are also the result of differences in material, focal length and holding methods. However it does offer partial indication that a narrower aspect ratio, consisting of a decreased span between the two curve defining edges, will yield a better reflector profile, and therefore tighter focal point.

It would be desirable to build various mirrors to different specifications, and accurately measure the deflection of the mirror at different locations, however limitations in available building tolerances and precision to not allow for this methodology of research.

Figure 3-14. Focus image resulting from 2'x8' aspect ratio.

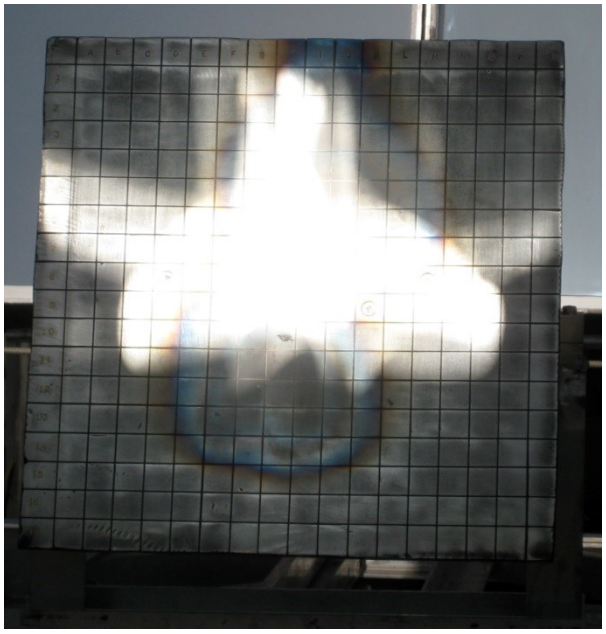

Figure 3-15. Focus image resulting from 4'x8' aspect ratio.

3.2.FEM

The process used to generate computer simulations of plates under different conditions is described in the following sections. The proposed plate simulations would then be laminated with a very thin reflective film.

3.2.1. Define Baseline Model

To accurately study the surface irregularities related to different design characteristics, a baseline model was formulated, upon which individual variables would be changed.

The curve that was selected for this baseline model is the same that is used for the primary reflector on LIFE's Solar+ 4600. The primary mirror of the Solar+ 4600 is an 8'x8' area, composed of two 4'x8' sheets. The sheets are curved to a parabolic shape with a 15' focal length. The section of the curve that is used is then offset from the zero region of the curve for geometric purposes and can be defined by formula 3.1:

$$y = \frac{x^2}{720} \quad \text{for } 75 \leq x \leq 165.85 \tag{3.1}$$

where; x and y are defined in inches.

As the reflectors to be modeled in this study will be mostly 8' in length, the arc length for the parabolic curve shall be set to 8'. Using the arc length equation 2.4, the parabolic formula and a lower limit of 75, the x value of the upper limit of the curve definition was determined in an iterative manner to give a curve arc length of 8':

$$\int_{75}^{U} \sqrt{1 + \frac{x^2}{129600}}\, dx = 96 \tag{3.2}$$

It was found that for a value of U=165.85, the solution to the integration is 96.0037, which is close enough to proceed. The determined value of U allows for two-dimensional graphing of the desired parabolic curve, while maintaining an arc length that matches that of an 8' reflector. A graph of this curve, with a focal length of 15', an arc length of 96.0037", a lower limit of x=75" and an iteratively solved upper limit of x=165.95 is shown in Figure 3-16.

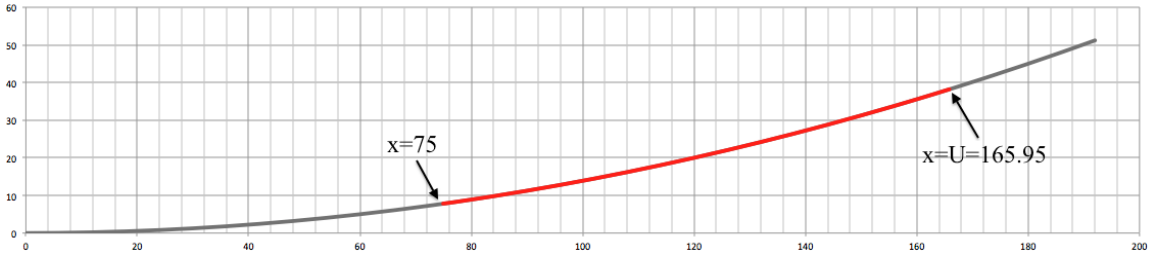

Figure 3-16 - Parabolic curve generation.

Data points were selected every 12" giving the following set of points:

Table 3-1. Baseline parabolic curve points in inches.

x	75.00	87.00	99.00	111.00	123.00	135.00	147.00	159.00	165.85
y	7.813	10.513	13.613	17.113	21.013	25.313	30.013	35.113	38.204

These values were then zeroed, by subtracting 75 from each x value and 7.813 from each y value:

Table 3-2. Zeroed baseline parabolic curve points in inches.

x	0.000	12.000	24.000	36.000	48.000	60.000	72.000	84.000	90.850
y	0.000	2.700	5.800	9.300	13.200	17.500	22.200	27.300	30.391

Finally, the values in inches were converted to mm by multiplying each value by 25.4, giving the curve points that would be used for the baseline model.

Table 3-3. Zeroed baseline parabolic curve points in mm.

x	0.00	304.80	609.60	914.40	1219.20	1524.00	1828.80	2133.60	2307.59
y	0.00	68.58	147.32	236.22	335.28	444.5	563.88	693.42	771.921

To simulate a 4'x8' sheet using Hypermesh v11.0, a curved line as defined above was plotted at z=0, and another line was plotted at z=1219.20. These two lines were then used to define a ruled surface.

Using the PSHELL Hyperworks card, a thickness of this surface is defined in mm. Using the MAT1 Hyperworks card, the material properties of a given material are entered in MPa and g/mm^3. In the PSHELL card, MID3 was intentionally left blank as to neglect transverse shear effects, and model the plates as a Kirchhoff plate. Using the GRAV Hyperworks card, a gravitational force was entered in mm/ms^2 and directed in the negative y direction.

A first order quadrilateral automatic mesh was then established over the curved surface, and the model was solved using the linear static OptiStruct solver.

The nodes along the 8' lengths of the surface were then constrained about all six degrees of freedom.

The solution file was then opened using Hyperview, and analyzed for displacement over its entire face. A displacement away from the initial (desired) location of reflector plate

represents a source of surface irregularity, the severity of which can be measured by the magnitude of the displacement. When looking at the results of these FEA models, an ideal case would show no displacement across the entire region of study.

3.2.2. Model Validation

To validate that the model output yielded results that could be trusted, a model validation was performed, comparing the results of a simple Hypermesh model with hand calculated displacement values for a similar plate.

By treating a flat 4'x8 'x1.628mm aluminum plate as a beam fully constrained along its 4' length, a maximum deflection along the center of the beam was calculated using the formula:

$$maximum\ deflection = \frac{WL^3}{384EI} \tag{3.3}$$

where the deflection is given in M, W is the load applied on the plate (in this case simply the gravitational weight of the plate) in N, L is the length of the plate in meters, E is the Young's modulus of aluminum in Pa, and I is the moment of inertia in m^4 which is given by the equation:

$$I = \frac{bh^3}{12} \tag{3.4}$$

where b and h are the base and height of the cross section of the plate respectively, given in meters.

Therefore it follows that the maximum deflection of such a beam under load of its own weight should be:

$$\max deflection = \frac{128.19 * 2.4384^3}{384 * 6.9 * 10^{10} * 4.38 * 10^{-10}} = 0.160\ m$$

A very simple Hyperworks computer model was then devised to simulate the same scenario and determine if the basics of the computer model are valid. The model used the same dimensions as noted above, 2428x1219x1.628 mm aluminum plate experiencing a vertical gravitational load using the Hyperworks GRAV card and which is equivalent to the 128.19 N load used in the hand calculation. By splitting the plate into only 3 cells, and executing the solver as described in section 3.2.1, a maximum deflection of 0.090 m was achieved. Such a coarse mesh size was chosen to make the model as simple as possible, however this very coarse mesh size can result in less accurate results, therefore the same model was run again using a 300 mm square mesh size (approximately 32 cells) and a 50 mm square mesh size (approximately 1170 cells). The results of these two models showed maximum deflections of 0.181 m and 0.158 m respectively. To see these maximum displacements converging towards the expected result of 0.160 m is very encouraging; particularly with the 50 mm square mesh size yielding a maximum deflection within 2% of the expected value.

A second validation model was analyzed comparing a 4'x8'x1.628 mm aluminum shell fully constrained on all 4 sides experiencing a gravitational force exerted normal to its large face. A Hypermesh model, set up as above, with a quadrilateral mesh size of 15 mm displayed a maximum deflection of 8.85 mm, located at its central most point.

The same plate scenario was then calculated by hand, using the classical plate theory equation:

$$\max deflection = c_1 \frac{pMin(L_x,L_y)^4}{Eh^3} \tag{3.5}$$

where c_1 = 0.0277 for an aspect ratio of 4'x8'.

The calculated maximum deflection for this case was then found to be 8.89 mm, which represents a difference between modeled and calculated results of less than 0.8%. It is therefore concluded that the basics of this Hypermesh model have been validated.

3.2.3. Convergence Analysis

To begin any meaningful modeling, a proper mesh size must be selected. As previously discussed, a finer mesh size will likely produce more accurate results, but at the expense of increasing computational demand.

An h-method convergence analysis was conducted on a 0.79375mm thick sheet of carbon steel set up as per the previous section. Several models were set up with progressively finer mesh sizes. In each case, the maximum displacement and the maximum vonMises stress were recorded. The results of this analysis are found in Table 3-4.

Table 3-4. Results of h-method convergence analysis.

Mesh Size (mm)	# of Elements	Max Displacement (mm)	Max Stress (MPa)	% Change in Max Stress
200	72	7.63	9.99	N/A
100	288	6.27	14.94	49.55
50	1176	6.13	23.91	60.04
25	4802	6.11	31.01	29.69

Mesh Size (mm)	# of Elements	Max Displacement (mm)	Max Stress (MPa)	% Change in Max Stress
15	13203	6.105	34.74	12.03
10	29768	6.105	37.04	6.62
8	46640	6.104	38.11	2.89
7	61176	6.104	38.69	1.52
6	83741	6.104	39.32	1.63
5	121190	6.103	40.02	1.78

The maximum displacement plotted against the number of mesh elements can be seen below in Figure 3-17.

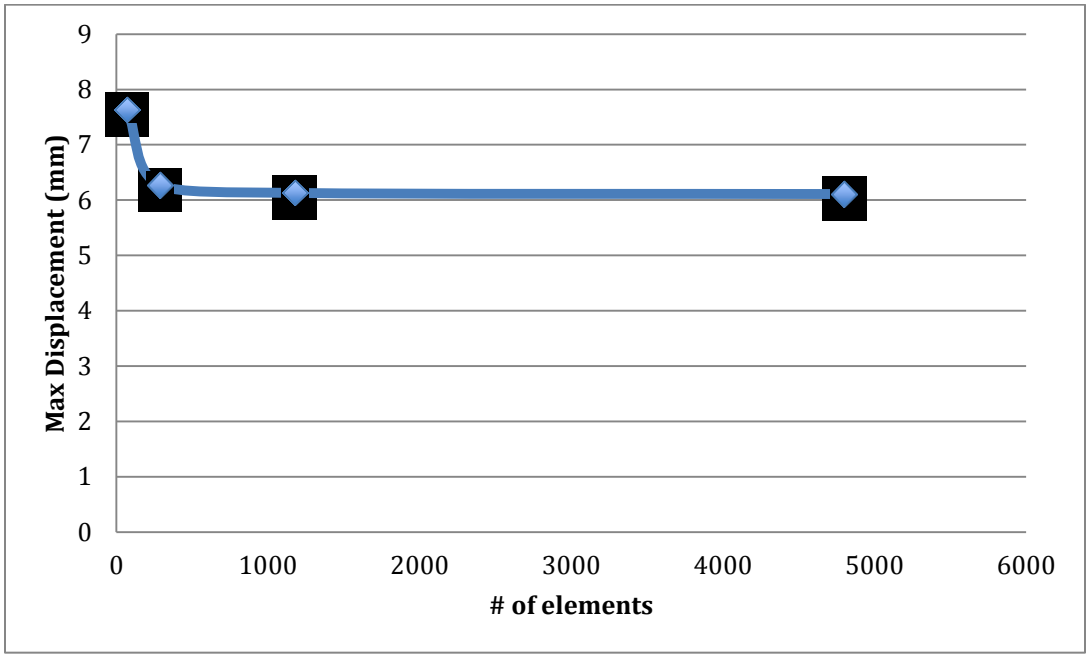

Figure 3-17. Maximum local displacement vs. # of mesh elements.

Likewise, the maximum vonMises stress is plotted against the number of mesh elements in Figure 3-18.

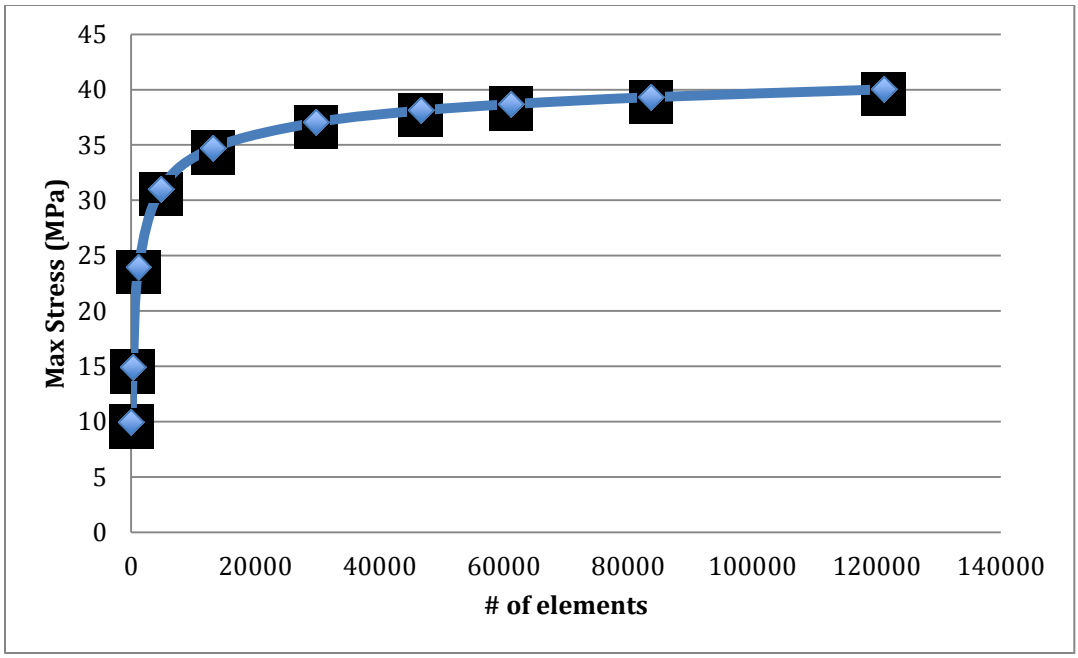

Figure 3-18. Maximum local vonMises stress vs. # of mesh elements.

Due to the analysis of these models being primarily based on the deflection results, it could be stated that a mesh size of 50mm (1176 elements) is sufficient to generate accurate results of the model. It is reasonable to select a mesh size that has converged by displacement rather than stress given the following:

1) Displacement is the primary value of interest.
2) Stresses values of approximately 40 MPa are well below a yield stress of 250 MPa for the material tested. A verification of max modeled stress compared to yield stress of the material being modeled should be performed after each model.

However, to give more confidence in the resulting model outputs, and to allow for better interpretation of this data should it be required, a mesh size of 8mm (46640 elements) was selected.

3.2.4. Effect of Material and Thickness

The effect of selected material and thickness of plate were studied simultaneously by comparing plain carbon steel and 6061 aluminum plates over a range of thicknesses. The reflectivity of each of these materials is irrelevant, as the final reflectivity will come from a reflective laminate film, and not the metal substrate plates. Each of the plates modeled in this section were 4'x8' and curved along the same points as defined in section 3.2.1. All variables, with the exception of material properties and thickness, were held constant between each model used in this section.

Steel plate thicknesses were selected using round imperial unit fractions and were based on having reasonable masses. While a very thick plate could well provide a resulting surface profile with less overall displacement, the requirements of building dual axis rotating structures with prohibitively heavy reflectors puts these plates out of the realm of possibility. The selected steel plate thicknesses are shown below in Table 3-5.

Table 3-5. Model numbers of aluminum thickness models.

Model #	Thickness (")	Approximate Gauge	Thickness (mm)	Weight (kg)
1	1/32	21.5	0.79375	18.87790
2	3/128	24	0.59531	14.15842
3	1/64	28	0.39688	9.43895
4	3/256	30	0.29766	7.07921
5	1/128	35	0.19844	4.71947

Aluminum plate thicknesses were then selected based on two criteria:

1) To match the weights of the steel plates, which provides an equal comparison from a mechanical design standpoint with respect to the rest of the concentrator's structure.
2) To match the thicknesses of the steel plates, which provides an equal comparison per unit volume of material.

The details of the aluminum plates modeled are shown in Table 3-6.

Table 3-6. Model numbers of aluminum thickness models.

Model #	Thickness (")	Approximate Gauge	Thickness (mm)	Weight (kg)
6		11	2.35185	18.87790
7		13.5	1.76389	14.15842
8		17	1.17593	9.43895
9		19.5	0.88194	7.07921
10	1/32	20	0.79750	6.40139
11	3/128	23	0.59531	4.77845
12		23	0.58796	4.71947
13	1/64	26	0.39688	3.18569
14	3/256	29	0.29766	2.38926
15	1/128	32	0.19844	1.59284

To remain in agreement with the rest of the inputs for this Hyperworks model, the thickness of plate was entered using mm.

For all of these models a gravitational force of 9.81 m/s^2 was applied in the negative y direction, and the two 8' lengths of the models were constrained in all degrees of freedom. Furthermore, the exact same mesh, as selected via the convergence analysis,

was used for each model. The material and force properties entered into Hyperworks for this analysis are found in Table 3-7.

Table 3-7. Material and force properties used for FEA modeling.

	ASTM A366 Steel	Aluminum 6061	Units
Gravity:	9.81E-03	9.81E-03	mm/ms^2
Young's modulus	2.10E+05	6.90E+04	MPa
Density	7.80E-03	2.70E-03	g/mm^3
Poison's ratio	3.00E-01	3.30E-01	

3.2.5. Effect of Holding Method

The effect of holding method on the resulting reflective field was studied independently of other variables. For all of the following models the plate was chosen to match the reflectors currently used as the primary mirror of the Solar+ 4600, a 14-gauge aluminum sheet that measures 1.628 mm in thickness. Sheet dimensions and curvature were selected to match the baseline model described in section 3.2.1. Standard aluminum mechanical properties were used as described in section 3.2.3.

Two main types of changes to the plate holding method were studied:

1) Holding the reflector along only its long edges compared with holding that same reflector along all four edges.
2) The method under which the reflector would be held along its edges.

To simulate two edges versus four edges, the constraints of the model were changed accordingly to provide limited degrees of freedom along only its long edges, or along all four edges.

Two methods by which each edge would be constrained were selected:

1) Full edge constraints. 6 degree of freedom limitation of every node along a given edge, simulating a full epoxy bond between the curves and the reflector. From a practical standpoint, this holding method reaches limitations when needing to replace a reflector, and increases the installation complexity of a large-scale device.
2) Select nodal constraints. Individual nodes along a given edge are limited about 6 degrees of freedom, simulating individual screws constraining the sheet at individual locations. The model being used was found to have a scale of 6" = 19 nodes. Therefore, nodes were chosen in two scenarios:
    a. Every 19 nodes, simulating a screw located every 6" along the edge of the reflector.
    b. Every 38 nodes, simulating a screw located every 12" along the edge of the reflector, the method currently used on the Solar+ 4600.

Table 3-8 outlines the holding method used for each of models 16 through 21.

Table 3-8. Model numbers of different holding methods

Model #	Holding Method
16	14 gauge aluminum, long edges fully constrained
17	14 gauge aluminum, all 4 edges fully constrained
18	14 gauge aluminum, screws every 6 inches along long sides

Model #	Holding Method
19	14 gauge aluminum, screws every 6 inches along all sides
20	14 gauge aluminum, screws every 12 inches along long sides
21	14 gauge aluminum, screws every 12 inches along all sides

3.2.6. Effect of Aspect Ratio

To study the effect of aspect ratio on the gravity induced displacement of a curved plate; plates of a constant material and thickness having various height and width dimensions were modeled.

Again, 14-gauge aluminum was selected as a baseline to stay consistent with the existing mirror used on the Solar+ 4600. In all models for this section, all four edges of the modeled plate were completely constrained about 6 degrees of freedom. Standard aluminum mechanical properties were used as described in previous sections.

A quadrilateral mesh size of 15 mm was selected to aid in computing time, given that the h-type convergence study had indicated that at a mesh size of 15 mm, maximum displacement of a similar curved plate had converged well within an acceptable tolerance.

For practical purposes, it was decided that the largest acceptable plate size should be 4'x8'. This selection was made to allow for all studied plates to be

- transported easily by a standard pickup truck,
- a minimal increase in overall unit packaged shipping dimensions,
- procured easily at a basic metals depot,
- easily manipulated during installation.

Three heights, and three widths were then selected by cutting the dimensions of the largest plate by a factor of two and a factor of four, yielding heights of 8', 4', 2' and widths of 4', 2', 1'. A model matrix, Table 3-9, was constructed outlying the 9 combinations of these dimensions to be modeled, and corresponding model numbers for each combination.

Table 3-9. Model matrix for effect of aspect ratio study.

		Length		
		2'	**4'**	**8'**
Width	**1'**	Model 30	Model 27	Model 24
	2'	Model 29	Model 26	Model 23
	4'	Model 28	Model 25	Model 22

It should be noted that, aside from mesh size, Model 22 has the exact same characteristics as Model 17 from the effect of holding method analysis, and should therefore yield a very similar result.

The 8' region of curve to be modeled was selected to match the curves used in the previous studies;

$$y = \frac{x^2}{720} \quad \text{for } 75 \leq x \leq 165.85 \tag{3.6}$$

where the arc length would give 96" height and the width would be defined by an identical line located at a given depth in the z direction. The outputs of this equation were then zeroed and converted to millimeters to match the unit scheme selected for use with Hyperworks.

The results of the previous studies, effect of material and thickness, and effect of holding method indicated that the area of maximum displacement was always found in the outermost region of the 8' curve, that is to say the area of the parabola that contained the most slope. To this end, both the 4' and 2' length dimensions were selected to consist of the steepest 4' and 2' sections of the 8' curve.

Therefore, for the 4' length:

$$\int_{U}^{165.85} \sqrt{1 + \frac{x^2}{129600}}\, dx = 48 \tag{3.7}$$

It was found that for a value of U=121.28, the solution to the integration is 48.0062, which is close enough to use, giving equation 3.8

$$y = \frac{x^2}{720} \quad \text{for } 121.28 \leq x \leq 165.85 \tag{3.8}$$

which is then solved, zeroed and converted to mm giving the x and y components to be modeled while the width would be defined by an identical line located at a given depth in the z direction.

And for the 2' length:

$$\int_{U}^{165.85} \sqrt{1 + \frac{x^2}{129600}}\, dx = 24 \tag{3.9}$$

It was found that for a value of U=143.80, the solution to the integration is 24.0054, which is close enough to use, giving equation 3.10:

$$y = \frac{x^2}{720} \quad \text{for } 24.0054 \leq x \leq 165.85 \tag{3.10}$$

which is then solved, zeroed and converted to mm giving the x and y components to be modeled while the width would be defined by an identical line located at a given depth in the z direction.

Chapter 4: RESULTS AND DISCUSSION

In the present research the displacement of curved plates under a gravitational load was studied, in order to identify the effect of material selection, plate thickness, holding method, and aspect ratio, on the resulting plate. The theoretical research was studied using FEA, and then compared with the results of practical experiments conducted on similarly curved reflective surfaces. The results will be presented and discussed in the following sections.

4.1. FEM

The results of computer simulations of plates under different conditions are described and discussed in the following sections.

4.1.1. Effect of Material and Thickness

The two materials chosen for testing, plain carbon steel and 6061 aluminum, were compared with one another on two sets of metrics; based on using the same volume of material, and based on using the same weight of material. These particular types of steel and aluminum were selected based on their availability and low cost. As these materials are only responsible for the shape of the reflector, and not the reflective face, the reflectivity and ability to withstand weathering were not of immediate concern. Tabulated results for this testing are found in Table 4-1. Graphical representations of each model output are found in Appendix A, however closer attention will be paid to a single model output as it is representative of all models discussed in this section.

Figure 4.1 displays the FEM results for model 7, the 1.76389 mm thick aluminum plate, fully constrained along its two 8' lengths, showing the displacement profile of the reflector after gravitational loading. As indicated by the label in the bottom left of the image, this image displays a top down view of the reflector with the more curved region of the reflector appearing on the left hand side of the image. The 'hamburger bun' effect that had been observed during physical experimentation is observed, occurring at the two unconstrained 4' lengths. Two localized maximum deflections are found at the middle points of the unconstrained sides, surrounded by smooth semicircular transition regions between the maximum points and 0 deflection locations which compromise most of the plate.

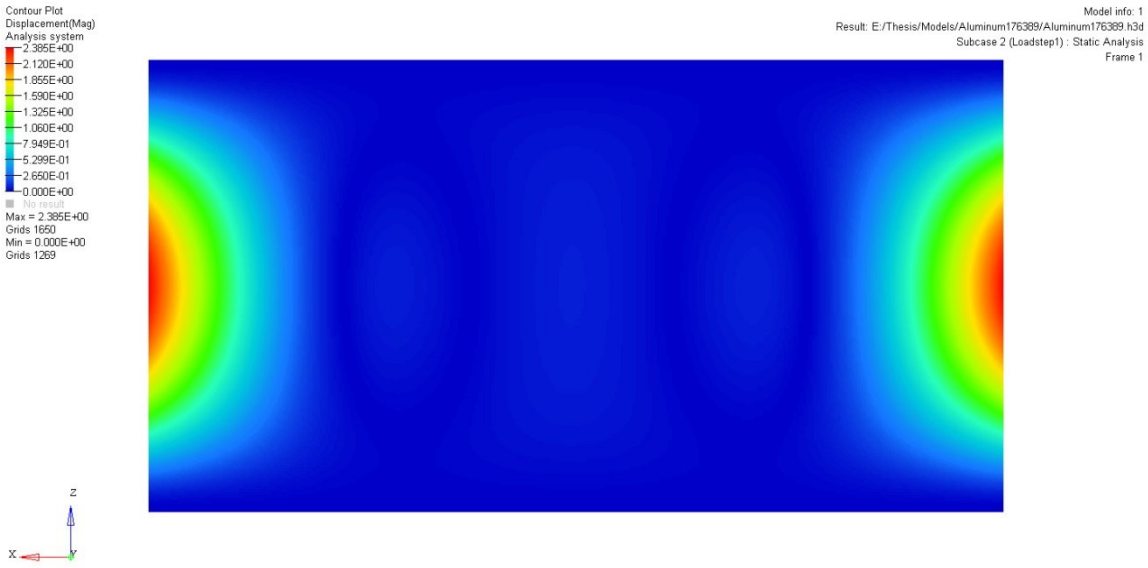

Figure 4-1. Model 7: 1.76389 mm thick aluminum plate, fully constrained along two 8' lengths.

It is observed that for each model discussed in this section the FEM outputs look quite similar with the only differences being the value of the maximum deflection points, and the sizes of the transition regions. Furthermore, it is observed that a thicker plate tends to

have both a larger maximum deflection and larger transition area, however the larger transition area is caused by the fact that in each case the color scale runs from blue = 0 to red = maximum, meaning that for a model with a larger maximum deflection, regions of small are more apt to appear as blue.

Table 4-1. Model results for effect of material and thickness study.

Model #	Material	Thickness (mm)	Max Displacement Mag (mm)	Max vonMises Stress (MPa)
1	ASTM A366 Steel	0.79750	6.13	23.91
2	ASTM A366 Steel	0.59531	8.56	44.5
3	ASTM A366 Steel	0.39688	13.58	54.65
4	ASTM A366 Steel	0.29766	18.67	62.69
5	ASTM A366 Steel	0.19844	28.97	75.29
6	Aluminum 6061	2.35185	1.62	6.65
7	Aluminum 6061	1.76389	2.39	8.04
8	Aluminum 6061	1.17593	4.00	10.37
9	Aluminum 6061	0.88194	5.68	12.26
10	Aluminum 6061	0.79750	6.41	12.98
11	Aluminum 6061	0.59531	9.16	15.3
12	Aluminum 6061	0.58796	9.16	15.3
13	Aluminum 6061	0.39688	14.31	18.69
14	Aluminum 6061	0.29766	19.65	21.45
15	Aluminum 6061	0.19844	30.46	25.77

On a per weight basis, the steel models 1, 2, 3, 4, and 5 correspond to aluminum models 6, 7, 8, 9, and 12. The maximum displacement of these models is shown plotted against plate weight in Figure 4-2.

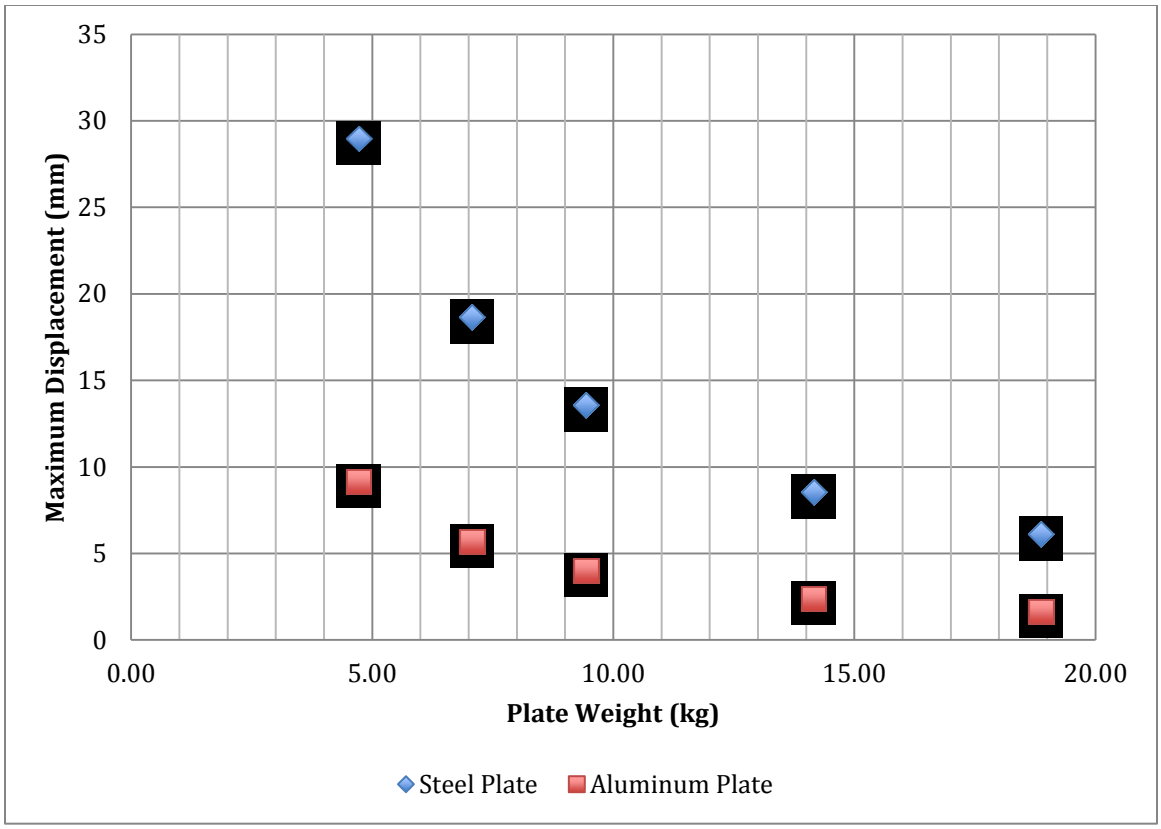

Figure 4-2. Maximum displacement of steel and aluminum plates of equal weight.

It is plainly seen that as the thickness and/or weight of a plate increases, the amount of maximum displacement in the plate is reduced, resulting in a face profile closer to that of the designed parabola, yielding a tighter solar focus.

For each given plate weight, the only difference between the two models were the material properties (Young's modulus, density and Poisson's ratio), and the thickness of the plate. To attain the same plate weight, the aluminum plate must be thicker due to the lower material density. The ratio by which the aluminum plate must be thicker is proportional to the ratio of densities of the two materials; in this case the aluminum must

be 2.89 times thicker. The section modulus of a rectangular cross section with a neutral axis running horizontally through its vertical midpoint is given as:

$$S = \frac{wh^2}{6} \tag{4.1}$$

where w is the width of the rectangle (unchanged for these models) and *h* is the height of the rectangle, or thickness in these cases. Since the *h* value is squared, an increase in thickness of 2.89 times would produce an increased section modulus of 8.35. When then also accounting for steel being 3.04 stiffer than aluminum, it would be expected for an aluminum plate to perform approximately 2.74 times better than a steel plate of the same weight based on the following equation:

$$\frac{S_{aluminum}/S_{steel}}{E_{steel}/E_{aluminum}} = \frac{8.35/1}{210000/69000} = \frac{8.35}{3.04} = 2.74 \tag{4.2}$$

When comparing individual data couples of these models it is seen that aluminum does perform better than steel on a per weight basis, at roughly the same rate as predicted. It should be noted that the 2.74 estimate is likely much less accurate than the FEA model results as it does not take into account the Poisson's ratio of the two materials, the, exact location of material bending in each plate or any membrane stresses in the plate.

Table 4-2. Relative difference in maximum displacement between steel and aluminum plates of same mass.

Weight (kg)	Steel Displacement (mm)	Aluminum Displacement (mm)	% Increase
18.87790	6.13	1.62	378
14.15842	8.56	2.39	358
9.43895	13.58	4.00	340
7.07921	18.67	5.68	329
4.71947	28.97	9.16	316

On a per thickness basis, the Steel models 1, 2, 3, 4, and 5 correspond to Aluminum models 10, 11, 13, 14, and 15. The Maximum displacement of these models is shown plotted against the plate thickness in Figure 4-3.

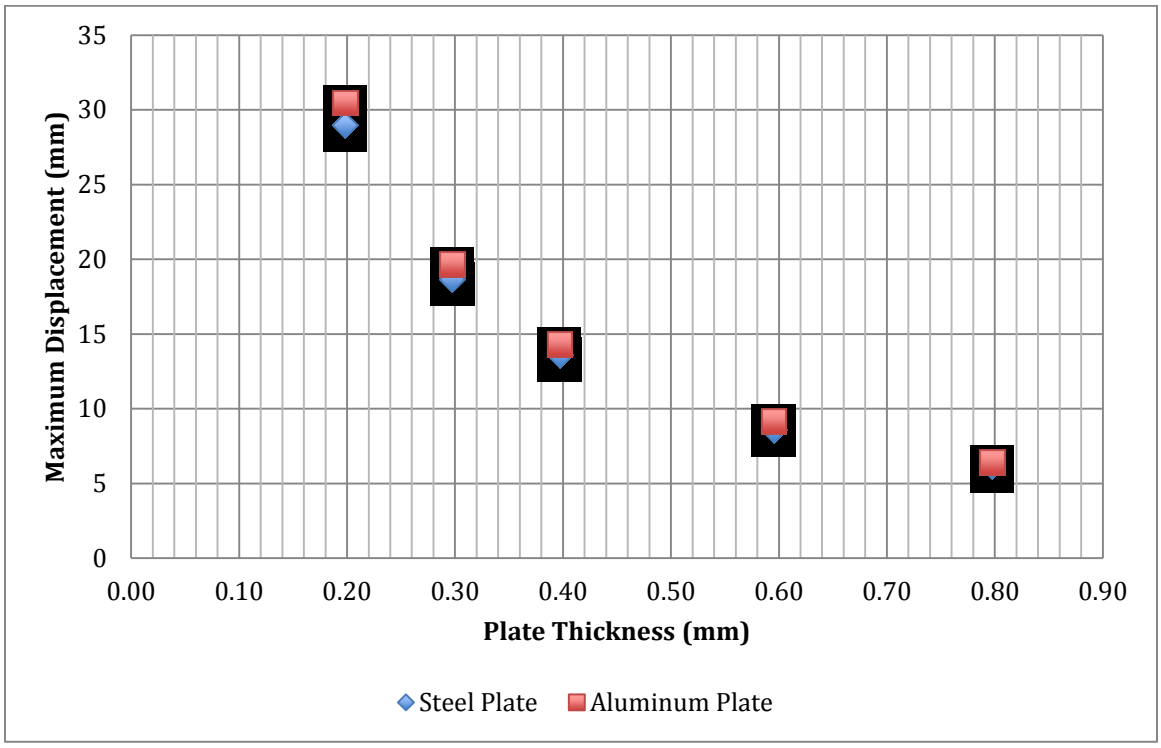

Figure 4-3. Maximum displacement of steel and aluminum plates of equal thickness.

In this case, with a constant plate thickness across each set, we have a defined difference for each set of both material properties and weight. The density value used for steel in these models was 2.89 times greater than that used for aluminum. Therefore steel plates of an equivalent thickness would weight 2.89 times more, and would have 2.89 times more gravitational force. Meanwhile, the value of Young's Modulus used for steel in these models was 3.04 times greater than that of aluminum, meaning that the steel plates should be 3.04 times stiffer than aluminum plates when nothing else is considered. When

combining these two values, one would expect a steel plate to deflect 5% less than an aluminum plate of equivalent thickness based on the following equation:

$$\frac{E_{Steel}/E_{aluminum}}{\rho_{steel}/\rho_{aluminum}} = \frac{210000/69000}{.0078/.0027} = \frac{3.04}{2.89} = 1.054 \quad (4.3)$$

When comparing individual data couples from these models, which are shown in Table 4-3, it is seen that the model results agree very closely with these expectations:

Table 4-3. Relative difference in maximum displacement between steel and aluminum plates of same thickness.

Thickness (mm)	Steel Displacement (mm)	Aluminum Displacement (mm)	% Increase
0.79750	6.13	6.41	4.57
0.59531	8.56	9.16	7.01
0.39688	13.58	14.31	5.38
0.29766	18.67	19.65	5.25
0.19844	28.97	30.46	5.14

Given that a steel plate weighs and costs much more than an aluminum plate of equivalent thickness, an increase in displacement of approximately 5% is not enough to justify the usage of steel plating for reflectors of this sort. For this reason, from this point onward, only aluminum plates shall be considered in the optimization of a two stage concentrators reflectors.

4.1.2. Effect of Holding Method

With aluminum determined to be a better material selection than Steel on both an economic and per unit weight basis, an aluminum plate of 1.628 mm thickness was

selected as a baseline for studying the effects of different holding methods on a curved reflective plate. The results of this modeling are found in Table 4-4. Graphical representations of each model output are found in Appendix A.

Table 4-4. Model results for effect of holding method study.

Model #	Number of Edges Constrained	Constraint Method	Max Displacement (mm)	Max vonMises Stress (MPa)
16	2	Full edge	2.648	8.47
17	4	Full edge	0.063	0.54
18	2	Nodes spaced by 6"	3.552	41.05
19	4	Nodes spaced by 6"	0.092	4.34
20	2	Nodes spaced by 12"	3.776	47.24
21	4	Nodes spaced by 12"	0.128	8.10

As can be seen, there are 3 sets of constraint methods, each modeled while constrained along two, and four edges. By dividing the maximum displacement of a two edge version of a constraint method (d_{max2}) by the maximum displacement of a four edge version of a constraint method (d_{max4}), an improvement factor ($IF_{2\text{-}4}$) is determined to quantify the improvement in maximum displacement by adding constraints along the third and fourth edges of the curved plate.

$$IF_{2-4} = \frac{d_{max2}}{d_{max4}} \tag{4.4}$$

Tabulated results of $IF_{2\text{-}4}$ are found in Table 4-5.

Table 4-5. Improvement Factor (IF_{2-4}) of constraining third and fourth edges for various holding methods

Constraint Method	Improvement Factor (IF_{2-4})
Full edges	41.71
Nodes spaced by 6"	38.63
Nodes spaced by 12"	29.52

It is expected that the improvement factor should be very large for all three of these cases. The maximum displacement for a two edge constrained curved plate as modeled is consistently found at the center of the unconstrained edge. Therefore, by adding full constraints to the third and fourth edges of the plate, what was once the area of maximum displacement has become a zero displacement location producing a much-improved overall profile.

Figure 4-4 shows the FEM output for model 17 an aluminum plate very similar to that shown in Figure 4-1, with the exception of a very small difference in material thickness, and all four sides of the reflector being constrained instead of only the two 8' lengths. It is observed that instead of the familiar 'hamburger bun' effect, the localized maximum points are now forced inward, and are again surrounded by transition regions to smaller displacement values. It should also be noted that while there is much blue area in this image, the entire color range of Figure 4-4's scale would be classified as blue in Figure 4-1.

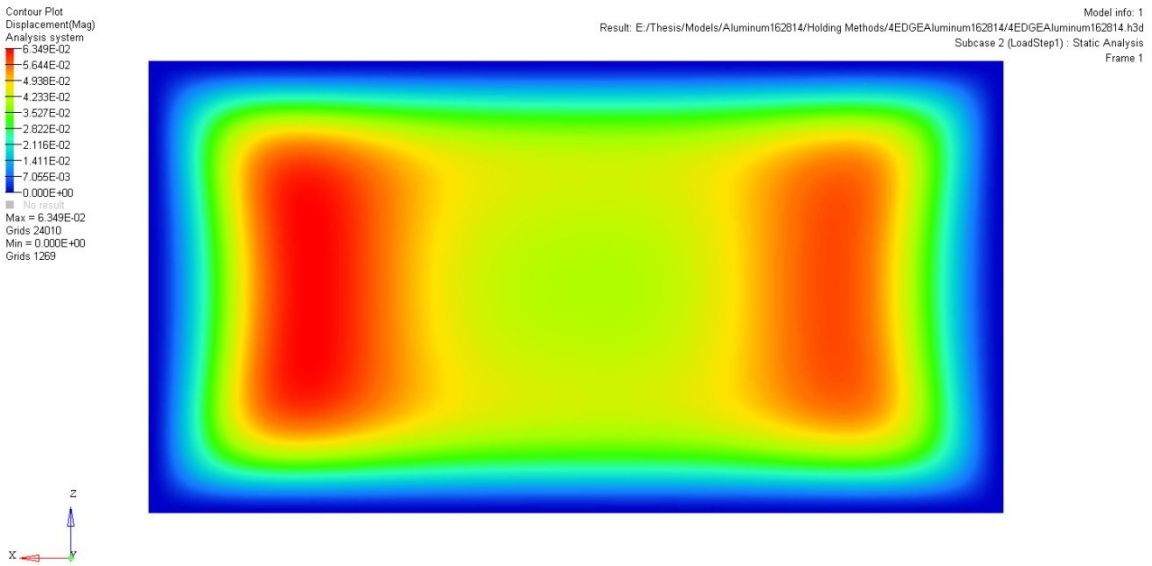

Figure 4-4. Model 17: 1.62814 mm thick aluminum plate, fully constrained along two 8' lengths and two 4' lengths.

When comparing different methods of constraining the plate to a given edge, as expected, it was shown that a plate with more constrained nodes resulted in a smaller maximum displacement.

With a mesh size of 8 mm selected, a 4'x8' plate consists of approximately 152 nodes along the 4' direction, and 305 nodes along the 8' direction. Therefore, when fully constraining all sides of a reflector plate, 910 nodes are constrained. When using screws spaced every 6", 44 nodes are constrained. When using screws spaced every 12", 20 nodes are constrained. It is seen in Table 4-6 that while systematically constraining more nodes will always yield a better maximum displacement, there are diminishing returns on each node constrained.

Table 4-6. Maximum displacement per constrained node for various four edge holding methods

Constraint Method	Nodes Constrained	Max Displacement (mm)	Max Displacement / Constrained Node (mm)
Full edges	910	0.0635	6.98E-05
Nodes spaced by 6"	44	0.0920	2.09E-03
Nodes spaced by 12"	20	0.1279	6.40E-03

Figure 4-5 shows model 21, an aluminum plate of same thickness as Figure 4-4, constrained along all four sides by nodal constraints spaced by 12". A wavelike pattern of 0 displacement transitioning to a small displacement is seen around each of the constrained nodes, and the overall effect results in localized maximum deflections of approximately twice those seen in the fully constrained variant. In Figure 4-6 model 19, the plate with four edges constrained by nodes spaced by 6" is shown, and it is observed that by doubling the number of constrained nodes on the outside edges, the resulting FEM output looks very similar to that of model 17, however with a larger maximum deflection, and smaller regions of 0 deflection around its outside border. Given that as you add more and more constrained nodes to the outside edge of a reflector it approaches the fully constrained edges, it is expected that as the constrained edge nodal spacing is decreased, the FEM outputs should look more and more like that of Figure 4-4.

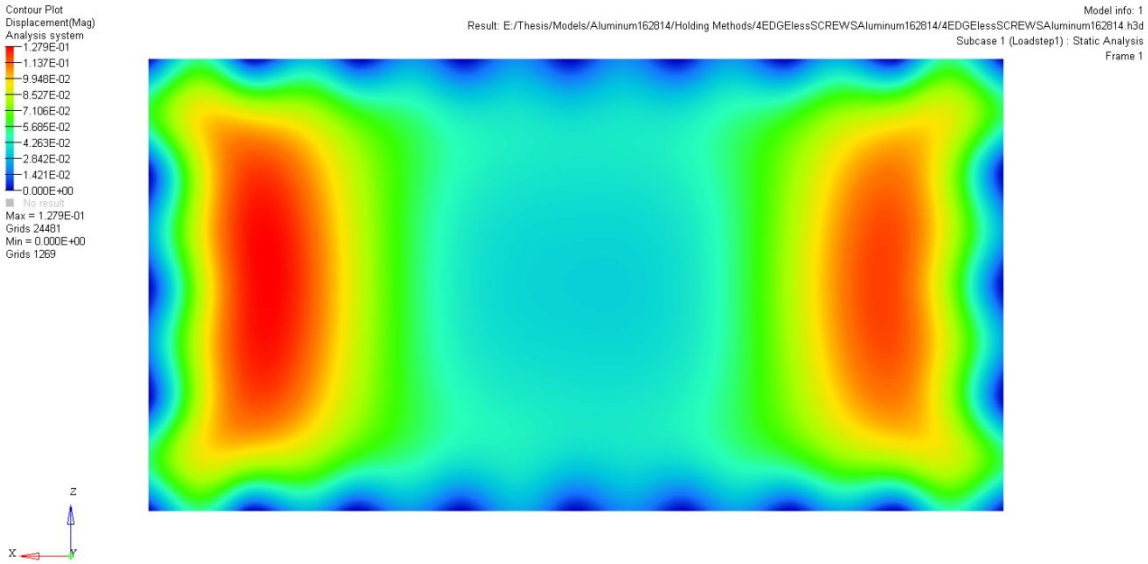

Figure 4-5. Model 21: 1.62814 mm thick aluminum plate, point constraints spaced every 12" along two 8' lengths and two 4' lengths.

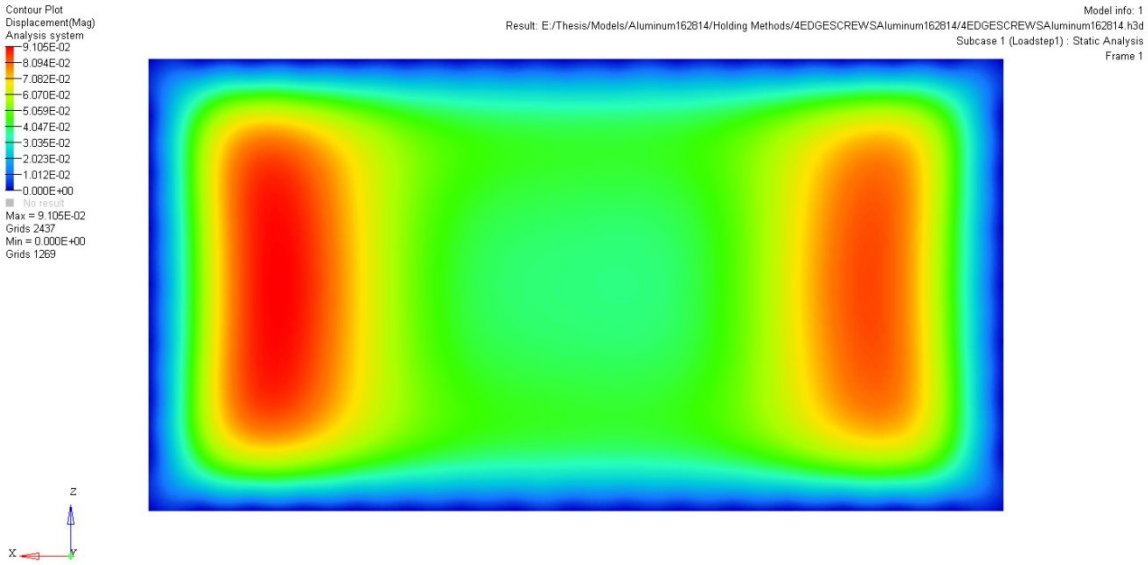

Figure 4-6. Model 19: 1.62814 mm thick aluminum plate, point constraints spaced every 6" along two 8' lengths and two 4' lengths.

Much like the other design criteria being considered, method for holding the mirrors becomes as much an economical design decision as it is a scientific design decision. It has been shown that a vast profile improvement is achieved by restraining all four edges of a reflecting plate, and in almost all cases this should be performed due to the minimal

cost of building a square plate frame compared to a strip mirror frame. This cost is close to inconsequential as the material constraining the 3rd and 4th edges mustn't be curved, like the longer edges, and therefore can be off the shelf metal stock, as opposed to CNC cut strips used for the 1st and 2nd edges.

Constraint method however, is a much more difficult decision. Full constraint along all four edges, most likely achieved by some sort of epoxy, offers the best focal profile of the methods selected, and requires relatively few labour hours, however in the event of a reflector being damaged and needing to be replaced, a repair process becomes much more complicated. The saving in labour hours due to simply applying an epoxy instead of accurately drilling and installing screws, is in part mitigated by the fact that if the installation of the reflector sheet to the curve strips is to be performed in the field, there is a significant reduction in quality control as opposed to an in shop procedure, and if the installation of the reflector sheet to the curve strips is performed in shop, there is a significant increase in shipping size and therefore shipping costs. If the decision is made to use screw based installation for reasons of ease of mirror replacement, maximizing in shop work load and minimizing shipping dimensions, a decision must be made on the spacing between the mounting screws. Assuming that the manufacturing will be conducted in a sophisticated environment that can automate the location of matching threaded holes on both the strips and plates, then it would seem that the improved surface profile would outweigh additional machining time and installation time per mirror. However, if the manufacturing is performed in a less sophisticated manufacturing environment where holes must be located and/or drilled by more manual means, then the

slightly improved surface profile is likely not worth the increase in manufacturing difficulty. Finally, the nature of the final application should be considered when considering the spacing requirement between mounting screws. An application that requires as high a temperature as possible (such as metal melting or chemical processing), will therefore require as tight a focus as possible, and it follows that it is more likely valid to choose an installation configuration with more mounting screws. Conversely, an application that requires a lower temperature over a wider area (such as steam production), could more likely justify sacrificing some quality in surface profile quality to minimize initial building costs.

4.1.3. Effect of Aspect Ratio

Three different widths and three different lengths of 1.62814 mm thick aluminum plates, being fully constrained about all four of their edges, were tested, yielding 9 different combinations as shown in Table 4-7.

Table 4-7. Model matrix for effect of aspect ratio study.

		Length		
		2'	**4'**	**8'**
Width	**1'**	Model 30	Model 27	Model 24
	2'	Model 29	Model 26	Model 23
	4'	Model 28	Model 25	Model 22

The maximum displacement of each of these models is shown in Table 4-8, while graphical outputs of each model are found in Appendix A.

Table 4-8. Maximum displacements (mm) for effect of aspect ratio study.

		Length		
		2'	**4'**	**8'**
Width	**1'**	0.02412	0.02399	0.02268
	2'	0.08439	0.08072	0.06993
	4'	0.09339	0.09950	0.06350

Initially, it was expected that as a single dimension grew, the resulting maximum displacement would increase, as a longer span between supported edges would indicate a larger bending moment from the gravitational force. While this is true for a length of 2', 4' and a width of 2', it is observed that there is very little difference in maximum displacement for all three plates with a width of 1', and there is very little difference between the 4'x'4, and 4'x2' plates, and the 8'x4' and 8'x2' plates.

By comparing Figures 4-7, 4-8 and 4-9, the transition between our benchmark 8'x4' plate to narrower 8'x2' and 8'x1' is observed. As shown, there is little change in the maximum displacement or general color profiles between the 8'x4' and 8'x2' FEM results, with both having localized maximum areas surrounded by transitional areas towards the constrained edges. In both cases the distance between the red/orange region to the 8' length, along the z-axis is measured to be approximately 8". However, due to the smaller z-axis dimension of the 8'x2' model, this results in a smaller, more circular, region of relatively large deflection. When looking at the 8'x1' model, Figure 4-9, it is observed that the maximum deflections are much smaller than in Figure 4-7 and 4-9, and also that the two localized areas of high deflection begin to approach one another, almost forming a continuous region of relatively large deflection.

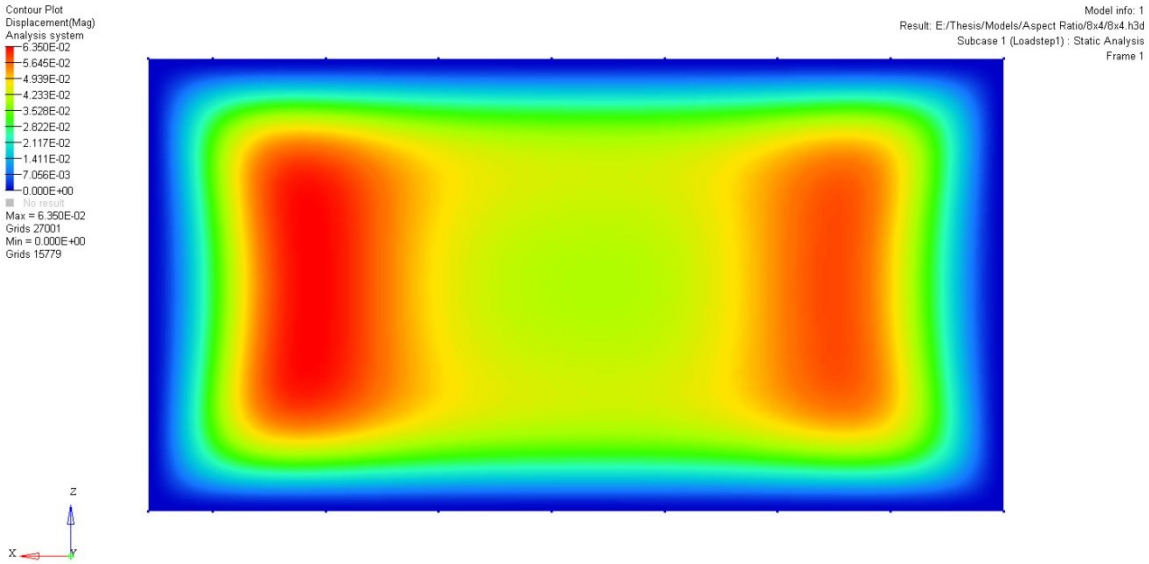

Figure 4-7. Model 22: 8'x4' 1.62814 mm thick aluminum plate, fully constrained about all edges.

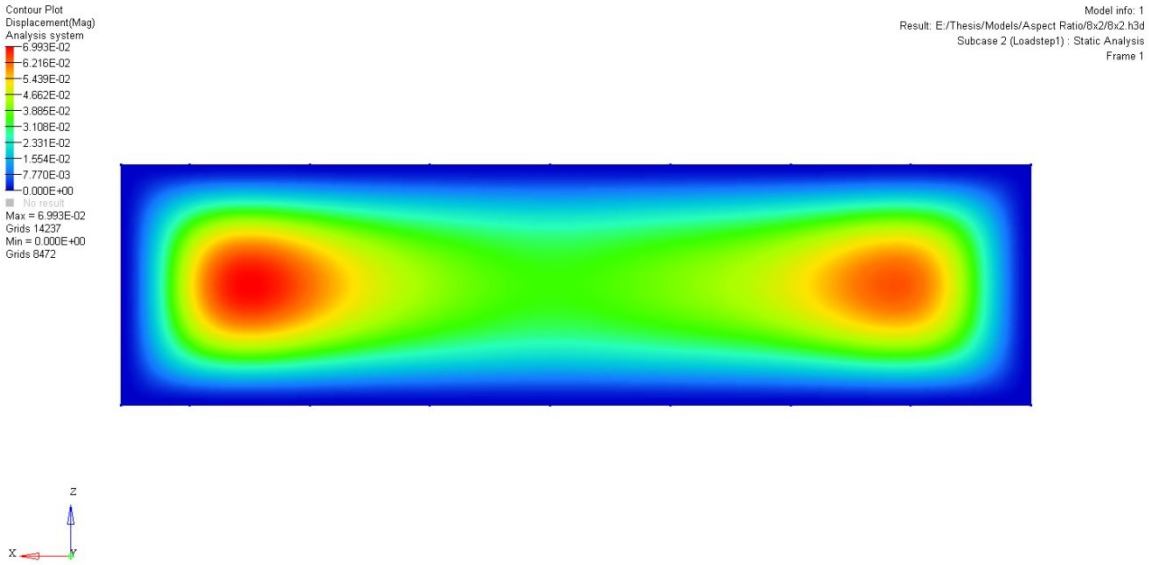

Figure 4-8. Model 23: 8'x2' 1.62814 mm thick aluminum plate, fully constrained about all edges.

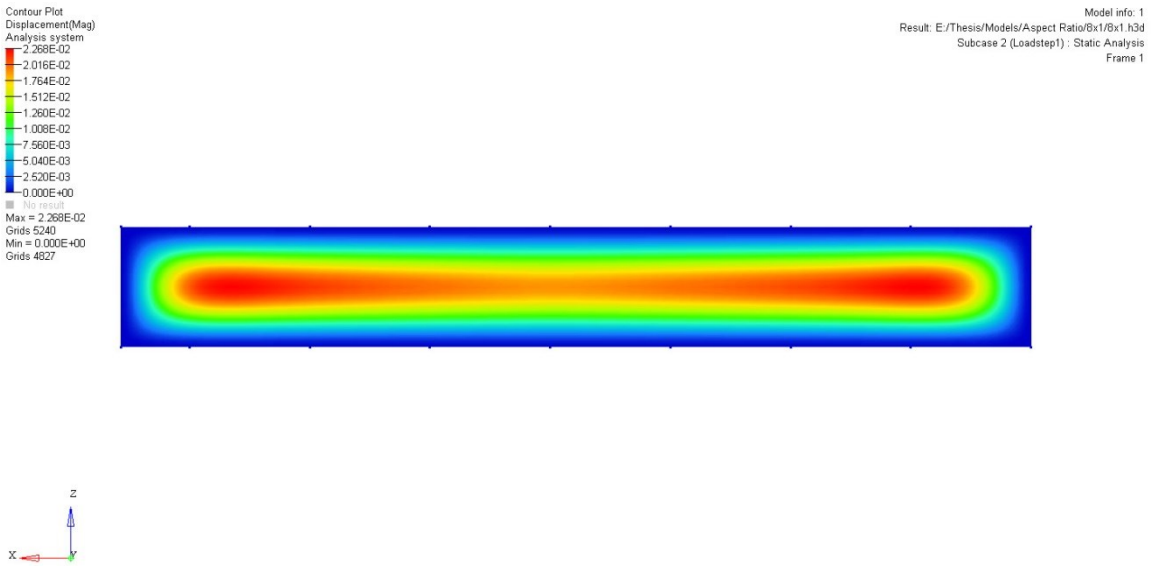

Figure 4-9. Model 24: 8'x1' 1.62814 mm thick aluminum plate, fully constrained about all edges.

By comparing Figures 4-7, 4-10 and 4-11, the FEM displacement outputs for 8'x4', 4'x4', and 2'x4' aluminum plates the effect of reducing the length of the plate is observed. It is found that by reducing the length of the reflector; the overall stiffness of the curved plate is decreased, resulting in a larger maximum deflection. This is observed as the maximum deflections of the two shorter plates are quite higher than that of the benchmark plate. While the 4'x4' plate output shown in Figure 4-10 looks very similar to the right half of the 8'x4' plate output in Figure 4-7, the 2'x4' plate output shown in Figure 4-11 appears to have a much more condensed region of high deflection, as the high deflection area is forced to be more concentrated to maintain a distance from the fully constrained edges. It is also observed by comparing Figure 4-8 with Figure 4-10 and Figure 4-9 with Figure 4-11, two pairs of mirrors that have the same total face area via different dimensions, that decreasing the width of the reflector plate is a preferable

method of decreasing area of reflector piece, as Figures 4-8 and 4-9 show smaller maximum deflections.

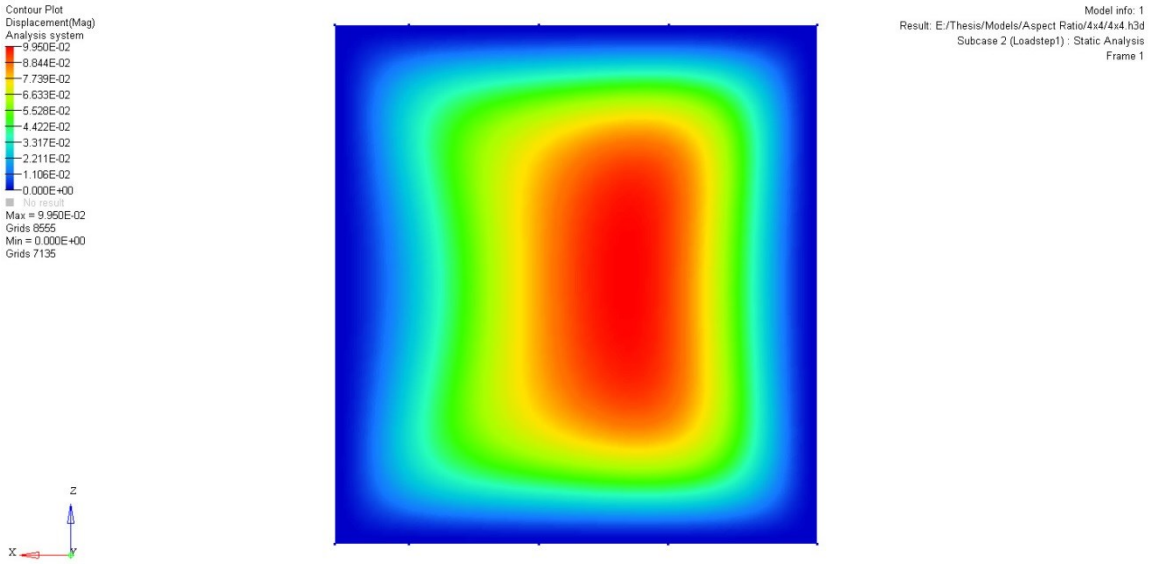

Figure 4-10. Model 25: 4'x4' 1.62814 mm thick aluminum plate, fully constrained about all edges.

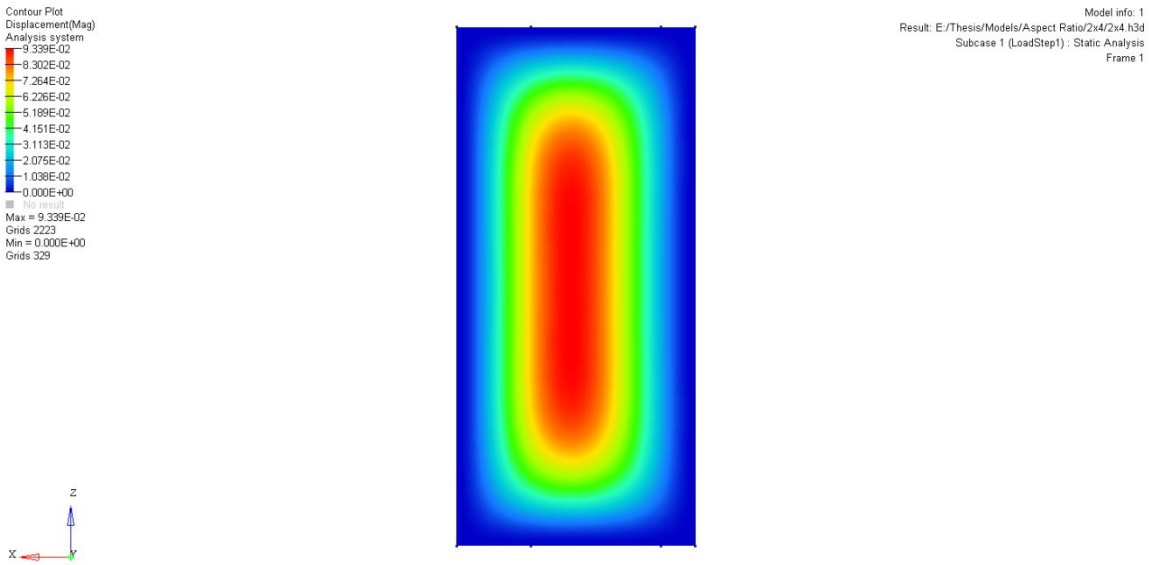

Figure 4-11. Model 28: 2'x4' 1.62814 mm thick aluminum plate, fully constrained about all edges.

To confirm that this model was working correctly, some additional trouble shooting models were studied. For the 4' length models, the top half of the 8' curve had been selected as it was expected to have a greater maximum displacement than the lower half of the 8' curve. Three 4' models were prepared and analyzed using the lower portion of the curve instead of the upper portion of the curve. The results of these models, which are shown in Table 4-9, demonstrate lower displacement values as had been anticipated, but still show the same trend that had been observed for the 4' length plates using the upper portion of the 8' plate.

Table 4-9. Maximum displacements (mm) for 4' length models using bottom half of 8' curve.

Width (')	**Maximum Displacement (mm)**
1	0.0272
2	0.06338
4	0.07573

Next, the entire range of models 22-30 was studied again, but using flat plates of the same dimensions. The results of this experiment are shown in Table 4-10. It is observed here that there is an increase in all dimensions compared to the parabolic plates, because of the inherent stiffness associated with the pre-curvature of a surface. In the case of the flat plate with a normal gravitational force, there will be no membrane forces through the plate, and only predictable bending should be experienced. While these values do follow the trending direction that would be expected, their lack of consistency between the values of different rows and columns, implies that the results of such a study are very complex, and it is well possible that the results displayed in Table 4-8 are accurate.

Table 4-10. Maximum displacements (mm) for flat plate analysis

		Length		
		2'	**4'**	**8'**
Width	**1'**	0.03379	0.03477	0.03477
	2'	0.2704	0.5408	0.5572
	4'	0.5408	4.328	8.663

Finally, to verify that the constraints chosen were not responsible for the unexpected results of Table 4-8, the exact same models were studied but with constraints only applied to the 8’ length edges of the plates, leaving the 4’ length edges free. These results are shown in Table 4-11. While the values in Table 4-11 are much greater than those in Table 4-8, which is to be expected given the difference in holding method, some of the same trends are observed. Again, there is minimal difference in the 1’ width plates, the 2’ width plates, and the 4’ width plates. However, an upward trend is experienced whenever a length is held constant, as would be expected. Given that we are now only applying constraints along the length and not the width, it is intuitive that the effect of width would be much more pronounced.

Table 4-11. Maximum displacements (mm) for effect of aspect ratio study, 2 constraints per sheet.

		Length		
		2'	**4'**	**8'**
Width	**1'**	0.03433	0.03516	0.03575
	2'	0.39727	0.4048	0.3926
	4'	3.104	3.039	2.648

It is therefore concluded that the results of Table 4-8 are correct, and are the product of a very complex balance between bending and membrane forces. It is observed that the state of stresses dictates a stiffening effect as the length of the plate increases.

The selection of aspect ratios is quite straightforward. The 8' length has been shown to have the smallest maximum deflect in all cases, and therefore should be used. It is likely that segments of more than 8' could be beneficial due to the increase in stiffness of longer plates, however for practical purposes 8' has been selected as the maximum length to be analyzed. When looking at the width, there is minimal difference between the 2' dimension and the 4' dimension, and therefore the selection comes down to an 8'x4' sheet, or an 8'x1' sheet. As stated in discussing the plate thickness and holding method, this selection becomes an application based economic analysis. A 1' wide mirror array will require 4 times as many connections as a 4' wide mirror array, and therefore will result in much higher manufacturing and installation costs. Therefore, unless the specified application requires the highest possible amount of precision and temperature, it is recommended that an 8'x4' aspect ratio reflector be selected.

4.2. EXPERIMENTAL

In this section, the results of the practical experiments will be summarized, and then will be compared with the results of the computer models outlined in section 4.1.

4.2.1. Effect of Material and Thickness

By testing different material reflectors (polished steel, glass mirrors, plexiglass mirrors, Anolux reflective aluminum sheets, Reflectec aluminum reflective film), it was found

that the greatest combination of durability and quality of focal image was achieved when laminating a reflective foil to a metal substrate plate. Polished steel and plexiglass mirrors were found to not offer sufficient reflectivity, glass mirrors were found to be too fragile and lacked the required flexibility for smaller focal lengths, and the Anolux reflective sheets were found to be too thin to hold a desired shape without the addition of a substrate plate and adhesives or epoxies which resulted in many surface irregularities. The reflective film, which is designed to be laminated to a backing plate, offered the reflectivity and smooth surface required for tight concentration with a good balance of durability, flexibility and rigidity to be properly suited for solar concentrator. The FEM research conducted on effect of material and thickness was not conducted in parallel with this practical experimentation, but rather was conducted using the conclusions of the experimental research to optimize the specific characteristics of the substrate plate that should be chosen. The initial experimental hypothesis that a 1.62814 mm thick aluminum sheet should be used as the reflector substrate was found to be reasonable. Theoretical experimentation confirms that aluminum is a better material for these plates than steel, and 1.62814 mm provides enough thickness to control the plate surface profile better than the vast majority of the reasonable thicknesses studied.

The only experimentation performed on the effect of thickness of a same material is not appropriate for comparison with the theoretical models as the reflectors studied have their reflective layer located at the back a clear substrate, instead of at the front of a substrate as modeled. To accurately compare the models of different thicknesses, reflective foils

should have been laminated to aluminum plates of different thicknesses, and the resulting images and/or surface profiles should have been compared.

4.2.2. Effect of Holding Method

Experimentally, it was found that by stiffening the ends of a glass reflector, a better focus image was achieved. Using a more rigid stiffener on glass mirrors installed on the same solar concentrator prototype as glass mirrors with less rigid stiffeners further strengthened this hypothesis. By switching from fragile glass mirrors to more durable metal-based reflector, the abilities to attach the reflectors to curved surfaces by means of screws instead of friction, and to constrain all four ends of the reflectors were gained. Experimentally, it was found that by constraining all four ends, instead of constraining two ends and stiffening the other ends yielded a much better solar focus. These findings were verified by means of computer models, the results of which are shown in section 4.1.2. Both experimental observations and theoretical modeling showed that constraining four ends is far superior to constraining two ends. Both experimental and theoretical testing was also conducted on the effect of using point constraints to hold the reflector to the appropriate curve. An experimental hypothesis had been drawn that the benefit of placing screws every 6” would not outweigh the additional labour costs over placing screws every 12”, while this was not tested experimentally due to cost constraints, model results showed that the 12” spacing yielded a maximum displacement of 0.1279 mm while the 6” spacing yielded a maximum displacement of 0.0920 mm. Given that the locating and drilling of these holes is the most time intensive portion of the construction of such a mirror set, it is reasonable to say that unless a maximum temperature application is being designed, the 12” mirror spacing is adequate.

4.2.3. Effect of Aspect Ratio

Experimentally it was found that of all tested reflector aspect ratios, the best focal characteristics were achieved from using an 8'x2' reflector. It is noted that this analysis was not a controlled single variable experiment, however it is still observed that this experimental result is in partial agreement with the theoretical computer models. Computer results indicated the smallest plate deflections for 1' wide plates, however no 1' plates were physically tested as from a commercial standpoint they fall outside the realm of reasonable. Of the remaining set of plates, the 8'x2' reflector performed 2nd best, having a maximum deflection approximately 10.13% larger than the 8'x4' reflector but a maximum deflection 13.38% smaller than the next best reflector of this set.

The small disagreement between experimental and computational results is attributed to the fact that this particular physical experiment was conducted without isolating the single variable to be analyzed, and was performed in a qualitative manner. It would be desirable to conduct this physical experiment in a controlled and qualitative manner to give an accurate comparison between the physical and computational results, however this is outside the currently available technical and manufacturing ability. It is concluded that the computational results are more accurate than the physical results in this case.

Chapter 5: FUTURE WORK & CONSIDERATIONS

There are a number of possible directions future work on this topic could take to progress the research outlined in this report and to further optimize the design selection of plates to be used for substrates on a two stage-stage solar reflector.

To provide a consistent basis for comparison between different materials, thicknesses, holding methods, and aspect ratios, the curve orientation of the plates studied, and loading forces applied to the plates were held constant throughout all theoretical tests. It would be useful for future work to consider both the secondary reflector, which is curved about a vertical axis rather than a horizontal axis, and is formed using a shorter focal length, in addition to the primary reflector. It would also be useful to study the mirrors at a range of angles to a datum set of coordinates, to represent the rotation of the two-stage concentrator throughout its daily motion. Furthermore, while the work in this report only used a gravitational loading, it would be of value for future work to consider wind loading on the reflector plates at a range of wind speeds, as prescribed by the manufacturer of the two-stage concentrator.

While the theoretical experimental section accurately describes the effect of gravitational loading on a parabolic curved plate, a study based on the displacement of the plate profile simply indicates the overall quality of the plate under different design conditions, and fails to show how the displacement of plate at different points will affect the resulting focus image. To this end, it is advised that later work uses the model outputs achieved in this work, in conjunction with similarly created horizontal mirror models, and

implements ray tracing methods to determine the exact path of a field of incident and reflected sun rays, which would result in a focal area at a prescribed target location. By defining a certain acceptable target area, it could then be determined what percentage of incident light rays end up within the acceptable area, providing an overall focus score for the given mirror design selections, and allowing for an estimate of the achievable temperatures and power ratings of given the projected solar focus dimensions.

At times, this report determines that different design selections could be legitimate, given different economic conditions. It is advised that future work perform a full economic analysis of a two-stage concentrator design using various mirror design selections. The economic analysis, which would need to be performed in conjunction with the two-stage concentrator patent holder LIFE, should consider the overall construction, commissioning and maintenance cost of the two-stage concentrator over its entire lifetime, given the requirements to safety apply each of the selected design constraints. Furthermore, the analysis should also indicate what applications would be possible, given the estimated temperature and power ratings, and factor in estimated profits generated by the two-stage solar concentrator over its lifespan.

Chapter 6: CONCLUSIONS

Backgrounds of concentrated solar power and finite element analysis have been provided, along with further technical details on the physics of parabolic light concentration and classical plate theory. The concept of optical efficiency has been outlined, including the 5 contributing factors: the cosine effect, mirror reflectivity, blocking and shadowing, atmospheric attenuation and surface irregularities. Surface irregularities have been identified as the least predictable factor of optical efficiency, making them the subject of the experimental section.

Steel and aluminum were considered as material selections for the reflector plates. These two materials have been compared on a thickness basis and a weight basis. It has been shown that on an equal weight basis, aluminum is preferable material selection yielding a maximum deflection of less than one third that of an equivalently weighted steel plate. On a per thickness basis, steel has been shown to deflect approximately 5% less than an equally thick aluminum plate, however due to the additional weight and cost of a same thickness steel plate, aluminum is recommended as the preferable material for solar reflectors.

Thickness of plate has been shown to be an economic decision more than a scientific decision. It is observed that a thicker plate will deflect less, however additional design strength of the whole CSP device would need to be implemented to carry the additional weight of the thicker reflector. It is recommended to use the thickest plates that can be reasonably supported and afforded.

Three sets of constraint methods, each modeled while constrained along two, and four edges were considered. It was shown that in all cases constraining four edges yielded much smaller plate displacements, resulting in improvement factors ranging from 29.52 to 41.71. Choosing between full edge constraints or a series of point constraints is determined to be an economic decision, which should consider the focal quality requirement of a given application. It was found that point constraints spaced every 12" resulted in a maximum displacement roughly twice as large of the maximum displacement when all edges were fully constrained, with point constraints spaced every 6" falling very close to the middle of this range

Nine different mirror sizes were considered, having widths of 1', 2', and 4' and lengths of 2', 4', and 8'. It was shown that reducing the width from 4' to 2' has a much smaller impact than reducing the width from 2' to 1'. It was also shown that reducing the length of the mirror increases the maximum deflection in the mirror as the overall stiffness of the curved plate is reduced. The selection of reflector sizes is therefore narrowed down to 8'x4' or 8'x1' based on analysis of required focal quality, and cost to build.

REFERENCES

1. Ummadisingu, A., Soni, M., (2001). Concentrating solar power – Technology, potential and policy in India. Renewable and Sustainable Energy Reviews, 15, 5169-5175.
2. Clifton, J., Boruff, B., (2010). Assessing the potential for concentrated solar power development in rural Australia. Energy Policy, 38, 5272-5280.
3. Groulx, D., Sponagle, B., (2009). Ray-Tracing Analysis of a Two-Stage Solar Concentrator. <http://www.tcsme.org/Papers/Vol34/Vol34No2Paper6.pdf>. Accessed August 8, 2013.
4. PEGASE Group, (2013). Production of Electricity from Gas and Solar Energy. <http://www.promes.cnrs.fr/pegase/index.php>. Accessed August 8, 2013.
5. Maag, G., Zanganeh, G., Steinfeld, A., (2009). Solar thermal cracking of methane in a particle-flow reactor for the co-production of hydrogen and carbon. International Journal of Hydrogen Energy 34, 7676-7685.
6. Flamant, G., Luxembourg, D., Robert, J.F., Laplaze, D., (2004). Optimizing fullerene synthesis in a 50 kW solar reactor. Solar Energy, 77, 73-80.
7. Ahcene, T., Monty, C., Kouam, J., Thorel, A., Petot-Ervas, G., Djemel, A., (2007). Preparation by solar physical vapor deposition (SPVD) and nanostructural study of pure and Bi doped ZnO nanopowders. Journal of the European Ceramic Society, 27, 3413-342.
8. Akin, E., (2009). Finite Element Analysis Methods. <http://www.clear.rice.edu/mech403/HelpFiles/FEM_intro.pdf>. Accessed August 8, 2013.

9. Turner, M.J., Clough, H.C., Martin, H.C., Topp L.P., (1956). Stiffness and deflection analysis of complex structures. Journal of Aerosoi Science, 23, 805-823.
10. Clough, H.C., (1960). The finite element method in plane stress analysis, Proc. ASCE 2nd Conference on Electronic Computation, 345-379.
11. Argyris, J.H., (1963). Recent advances in matrix methods of structural analysis by finite element. Elmsford, New York: Pergamon Press.
12. Babuska, I., Aziz, A.K., (1972). Survey lectures on the mathematical foundation of the finite element method. In The Mathematical Foundations of the Finite Element Method with Applications to Partial Differential Equations (pp. 5-359). New York: Academic Press.
13. Strang, G., Fix, G.J., (1973). An analysis of the finite element methods. Englewood Cliffs, N.J: Prentice-Hall Inc.
14. Oden, J.T., Reddy, J.N., (1976). Introduction to Mathematical Theory of Finite Elements. New York: John Wiley and Sons.
15. Zenkiwicz, O.C., Taylor, R.L., (1989). The Finite Element Method, Volume 1, Basic Formulation and Linear Problems. New York: McGraw-Hill
16. Holand, I., (1969). Stiffness matrices for plate bending elements. In I. Holand and K Bell (Eds.), Finite Element Methods in Stress Analysis (pp 159-178). Trondeim, Norway: Tapir Press 159-178.
17. Ashwell, G. H., Gallagher, R. H., (1976). Finite Elements for Thin Shells and Curved Members. New York: Wiley..

18. Parisch, H., (1979). A critical survey of the 9-node degenerated shell element with special emphasis on thin shell application and reduced integration. Computational Methods in Applied Mechanics And Engineering, 20, 323-350.
19. Batoz, J.L., Bathe, K.J., Ho, L.W., (1980). A study of three-node triangular plate bending elements. International Journal for Numerical Methods in Engineering, 15, 1771-1812.
20. Hrabok, M.M., Hrudey, T.M., (1984). A review and catalogue of plate bending finite elements. Computer Structures, 19, 479-498.
21. Ortiz, M., Morris, G.R., (1988). C^0 finite element discretization of Kirchhoff's equations of thin plate bending. International Journal for Numerical Methods in Engineering, 26, 1551-1566.
22. Kurowski, P., (1994). Avoiding Pitfalls in FEA. Machine Design, Nov. 7, 1994.
23. Dassault Systemes SolidWorks Corp. (2010). Understanding Nonlinear Analysis. <files.solidworks.com/whitepapers/2010/Nonlinear_Analysis_2010_ENG_FINAL.pdf>. Accessed November 19, 2013.
24. ESI Group, (2013). Element Types for CFD-ACE+ Stress Module. <http://www.esi-cfd.com/content/view/67/192/>. Accessed August 8, 2013.
25. Euler, L., (1766). De motu vibratorio tympanorum. Novi Commentari Acad Petropolit, 10, 243-260
26. Bernoulli, J., Jr., (1789). Essai théorique sure les vibrations de plaques élastiques rectangulaires et libres. Nova Acta Acad Petropolit, 5, 197-219.
27. Germain, S., (1826). Remarques sur la nature, les bornes e l'étendue de la question des surfaces élastiques et équation général de ces surfaces, Paris.

28. Lagrange, J.L., (1828). Ann Chim, Vol. 39, 149-207.

29. Poisson, S.D., (1829). Memoire sur l'équilibre et le mouvement des corps élastiques, Mem Acad Sci, 8, 357.

30. Navier, C.L.M.H., (1823). Bulletin des Sciences de la Societe Philomanthique de Paris.

31. Love, A.E.H., (1888). On the small free vibrations and deformations of elastic shells. Philosophical Transactions of the Royal Society of London, 179, 491-546.

32. Kirchhoff, G.R., (1850). Über das gleichgewicht und die bewegung einer elastischem scheibe. J. Feuer die Reine und Angewandte Mathematik, 40, 51-88.

33. Timoshenko, S., Woinowsky-Krieger, S., (1959). Theory of Plates and Shells. New York: McGraw-Hill

34. Mindlin, R.D., (1951). Influence of rotatory inertia and shear on flexural motions of isotropic elastic plates. ASME Journal of Applied Mechanics, 18, 31-38.

35. Föpple, A., (1907). Vorlesungen uber technische Mechanik. Leipzig, Germany: B.G. Tuebner.

36. Hencky, H., (1915). On the stress state in circular plates with vanishing bending stiffness. Zeitschrift fur Mathematik und Physik, 63, 311-317.

37. Stine, W., Geyer, M., (2001). Power from the Sun. <http://www.powerfromthesun.net/book.html>. Accessed August 8, 2013.

38. Danielli, A., Yatir, Y., Mor, O., (2011). Improving the optical efficiency of a concentrated solar power field using a concatenated micro-tower configuration. Solar Energy 85, 931-937.

39. Kreider, J., Kreith, F., (1981). Solar Energy Handbook. New York: McGraw-Hill

40. Barlev, D., Vidu, R., Stroeve, P., (2011). Innovation in concentrated solar power. Solar Energy Materials & Solar Cells 95, 2703-2725.
41. Collado, F., (2008). Quick evaluation of the annual heliostat field efficiency. Solar Energy 82, 379-284.
42. Collado, F., (2009). Preliminary design of surrounding heliostat fields. Renewable Energy 34, 1359-1363
43. Ventsel, E., Krauthammer, T., (2001). Thin Plates and Shells: Theory, Analysis and Applications. New York: Marcel Dekker, Inc.

Appendix A – Graphical Outputs of Computer Models

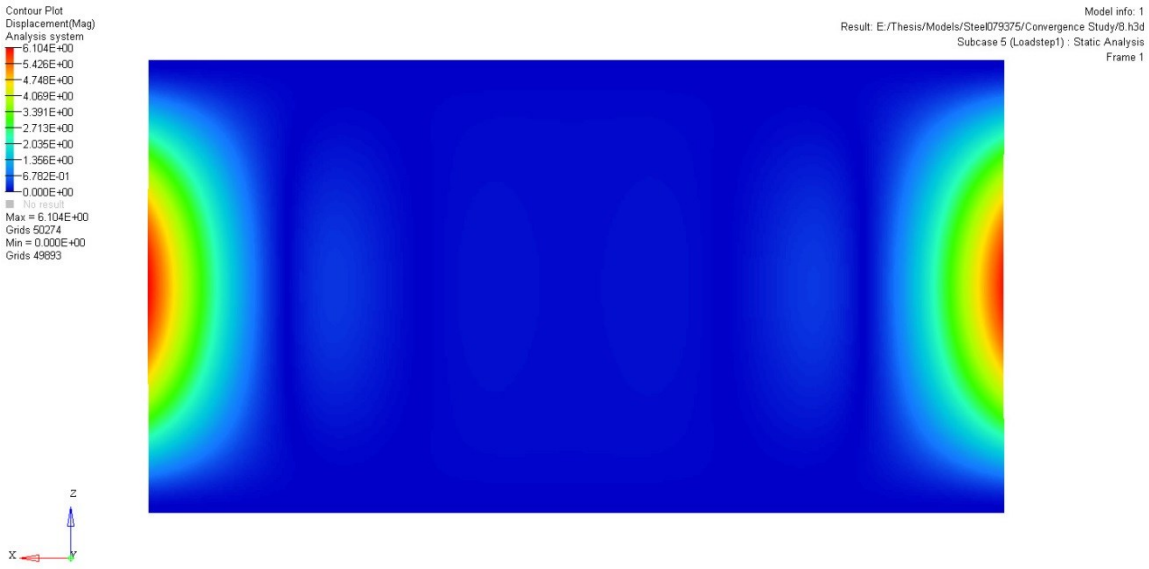

Figure A-1. Model 1: 0.79750 mm thick steel plate, fully constrained along two 8' lengths.

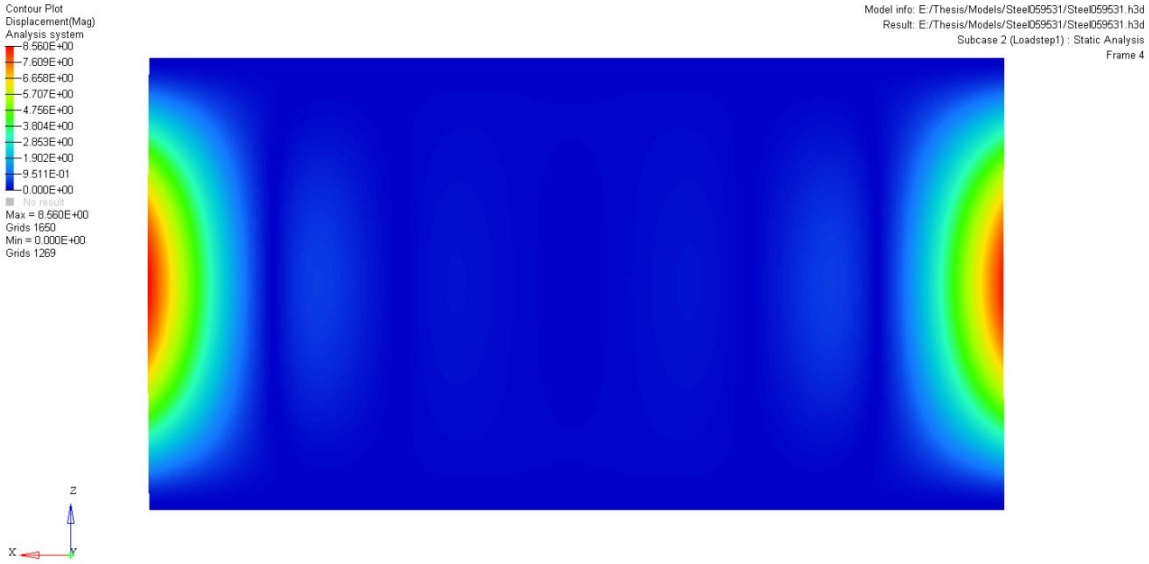

Figure A-2. Model 2: 0.59531 mm thick steel plate, fully constrained along two 8' lengths.

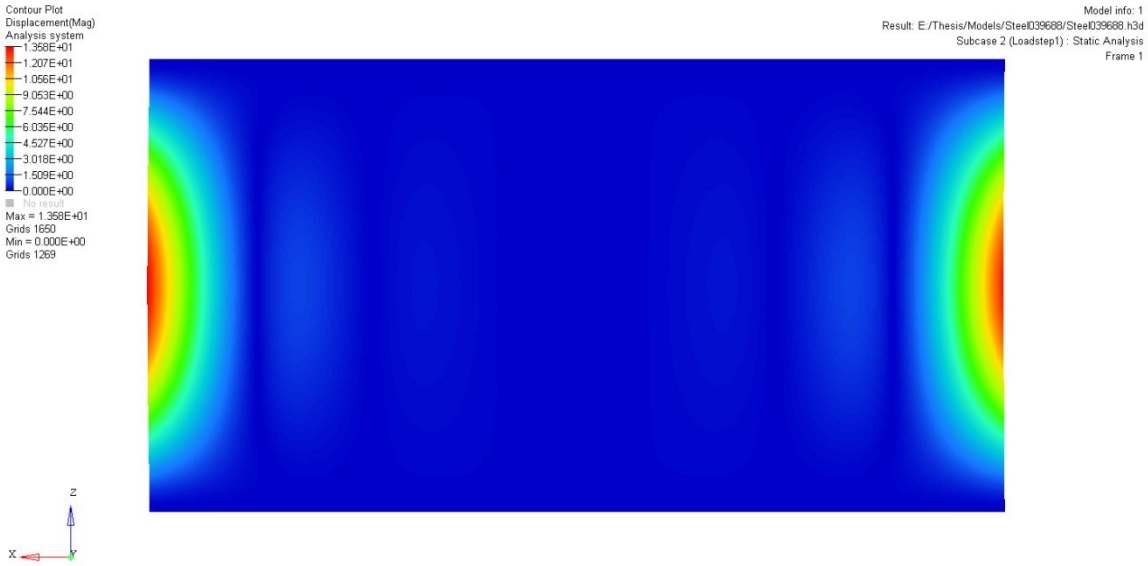

Figure A-3. Model 3: 0.39688 mm thick steel plate, fully constrained along two 8' lengths.

Figure A-4. Model 4: 0.29766 mm thick steel plate, fully constrained along two 8' lengths.

Figure A-5. Model 5: 0.19844 mm thick steel plate, fully constrained along two 8' lengths.

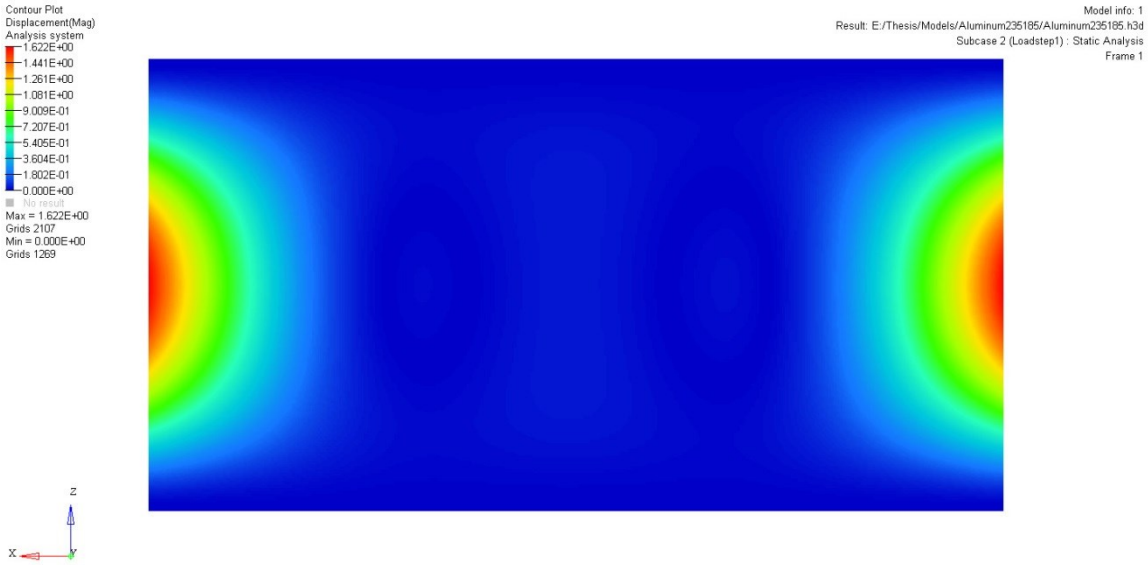

Figure A-6. Model 6: 2.35185 mm thick aluminum plate, fully constrained along two 8' lengths.

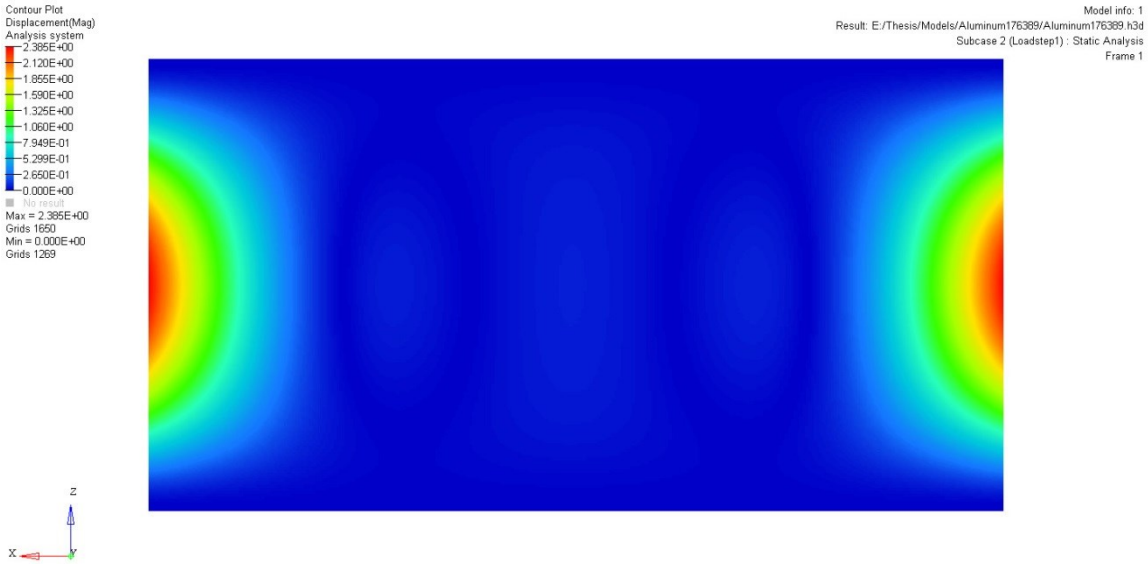

Figure A-7. Model 7: 1.76389 mm thick aluminum plate, fully constrained along two 8' lengths.

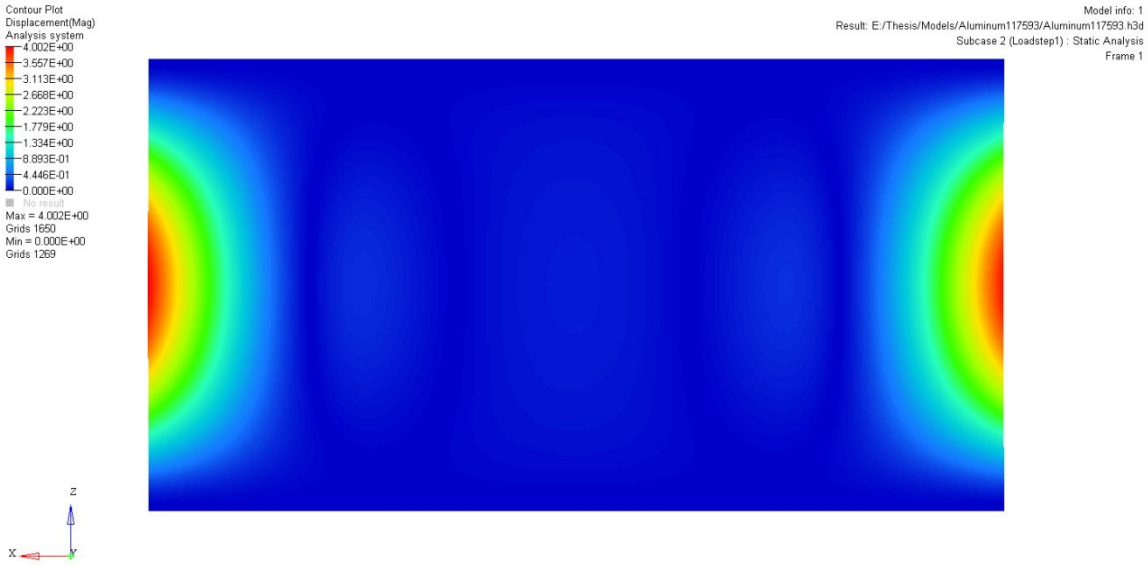

Figure A-8. Model 8: 1.17593 mm thick aluminum plate, fully constrained along two 8' lengths.

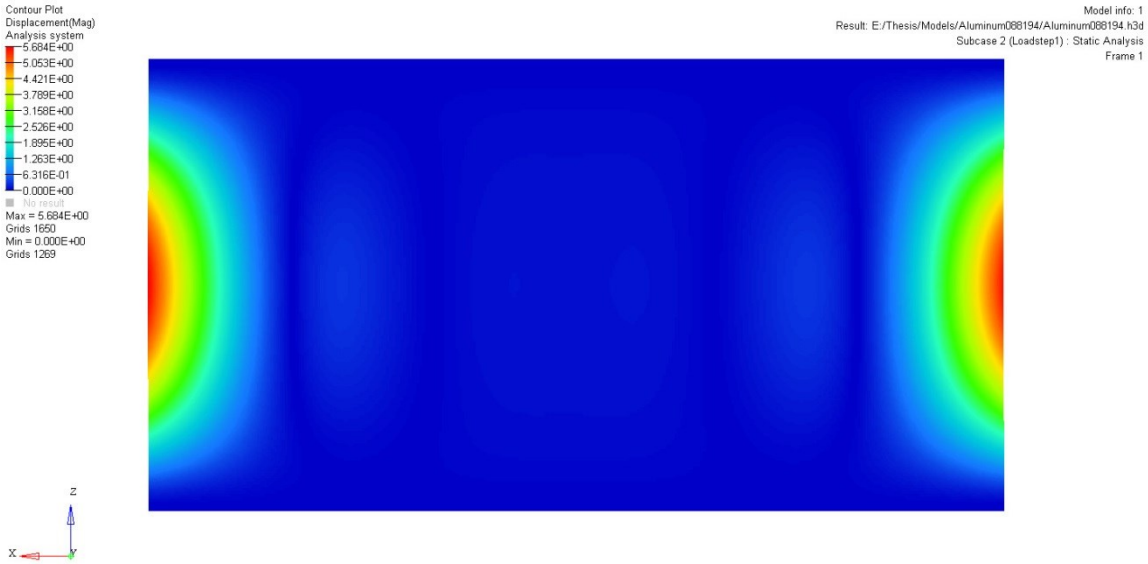

Figure A-9. Model 9: 0.88194 mm thick aluminum plate, fully constrained along two 8' lengths.

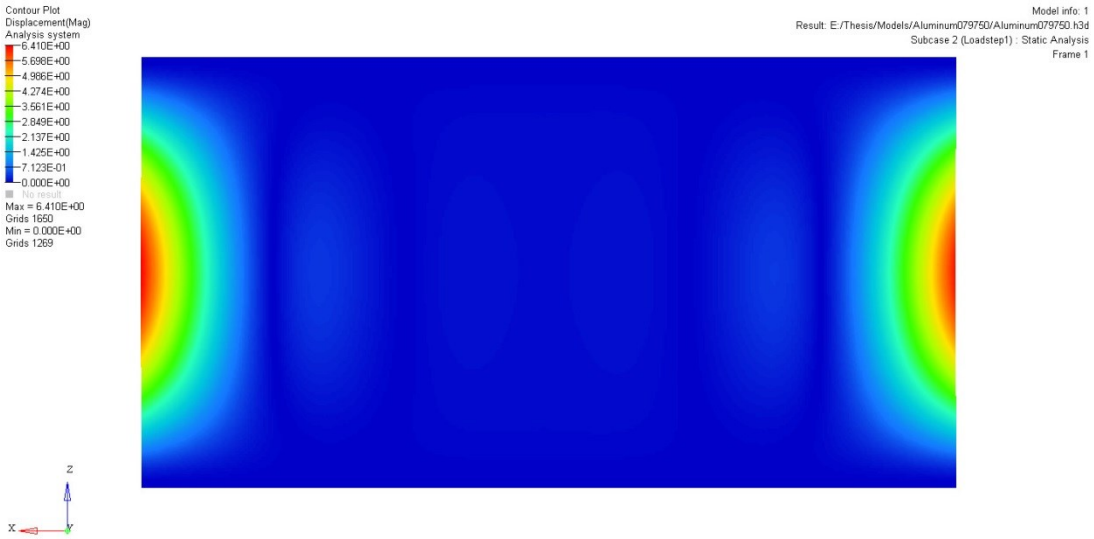

Figure A-10. Model 10: 0.79750 mm thick aluminum plate, fully constrained along two 8' lengths.

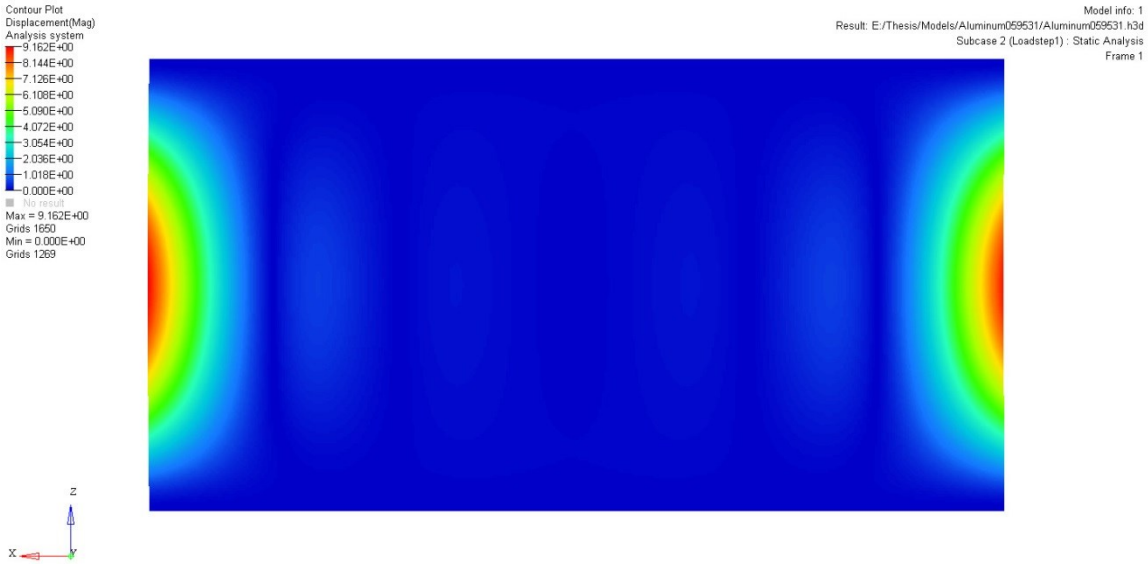

Figure A-11. Model 11: 0.59531 mm thick aluminum plate, fully constrained along two 8' lengths.

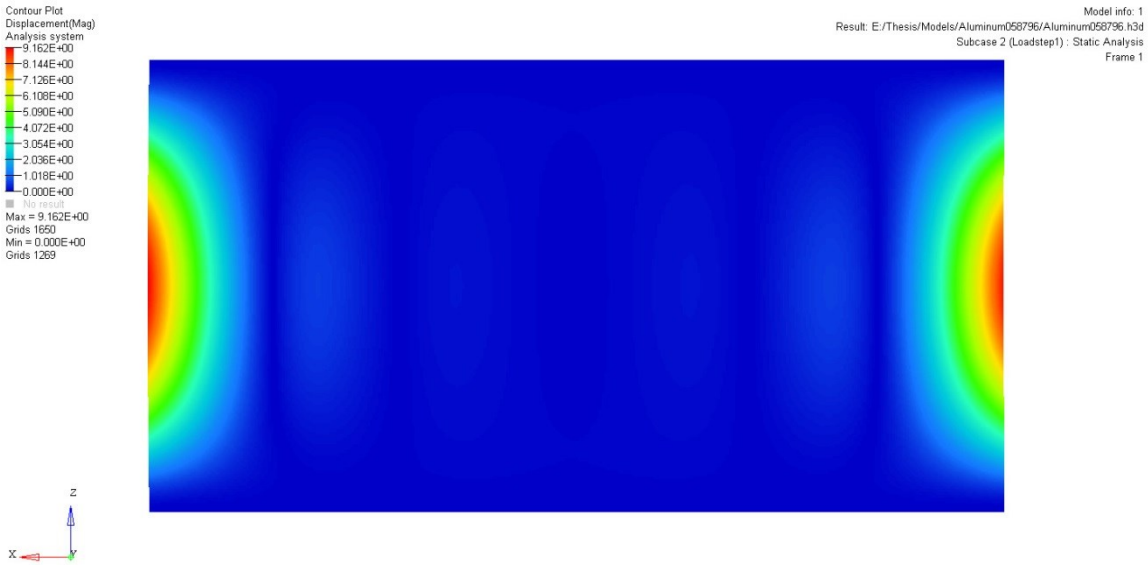

Figure A-12. Model 12: 0.58796 mm thick aluminum plate, fully constrained along two 8' lengths.

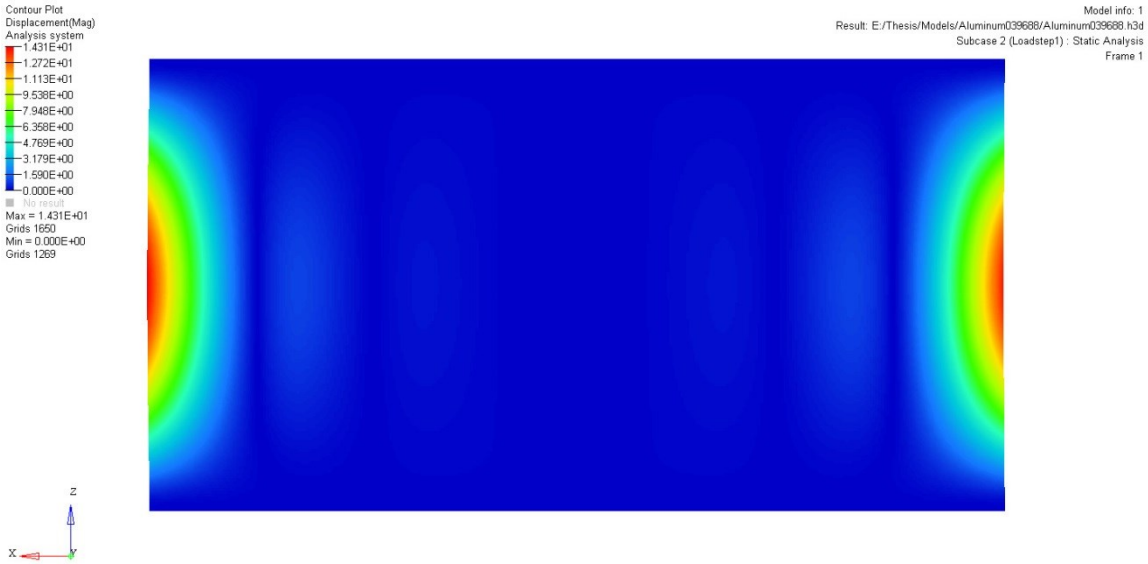

Figure A-13. Model 13: 0.39688 mm thick aluminum plate, fully constrained along two 8' lengths.

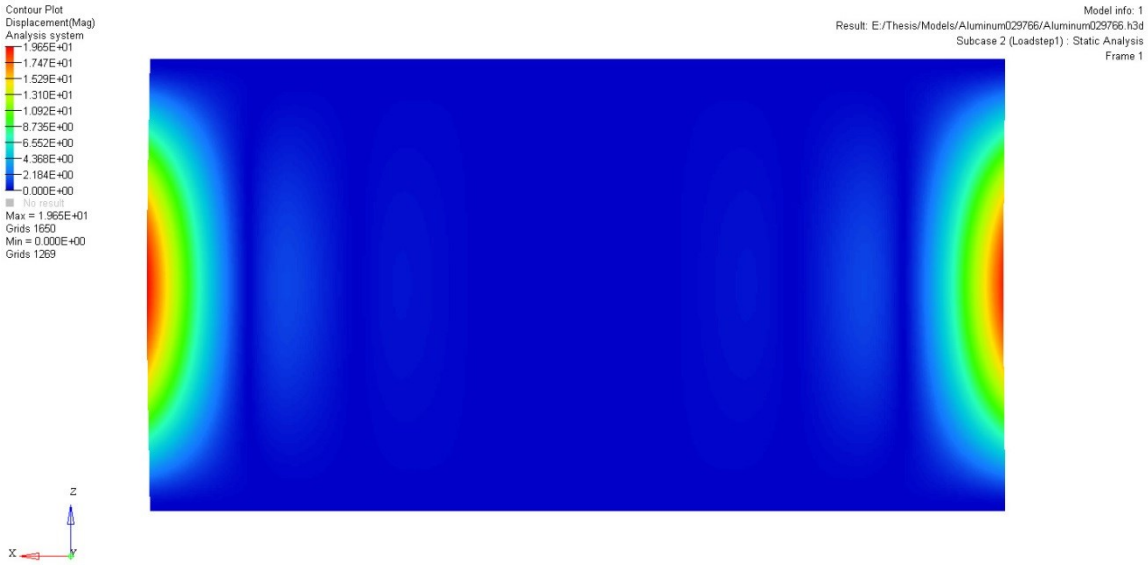

Figure A-14. Model 14: 0.29766 mm thick aluminum plate, fully constrained along two 8' lengths.

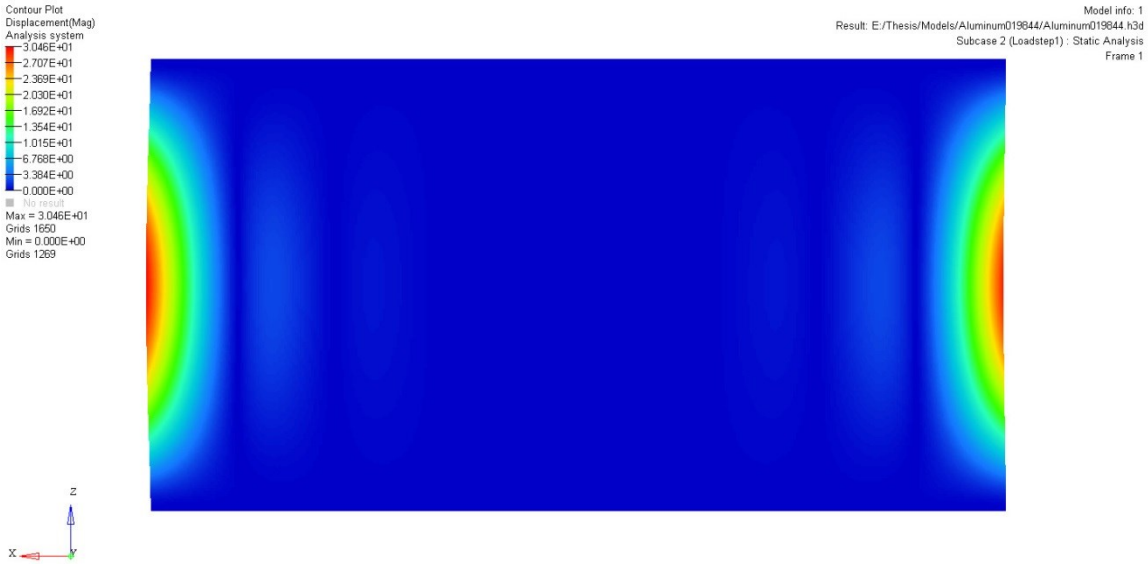

Figure A-15. Model 15: 0.19844 mm thick aluminum plate, fully constrained along two 8' lengths.

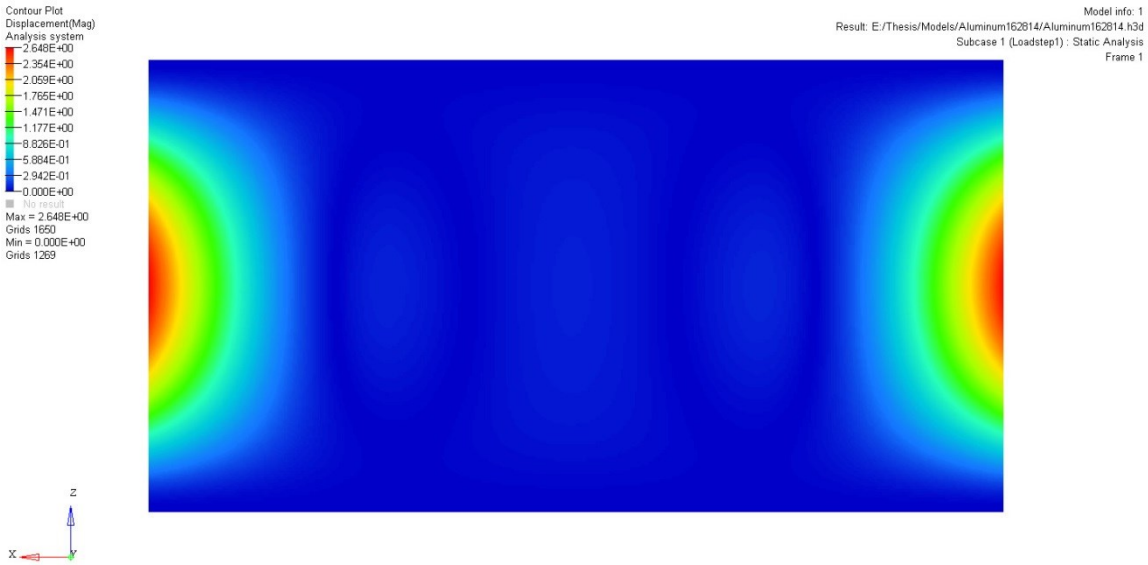

Figure A-16. Model 16: 1.62814 mm thick aluminum plate, fully constrained along two 8' lengths.

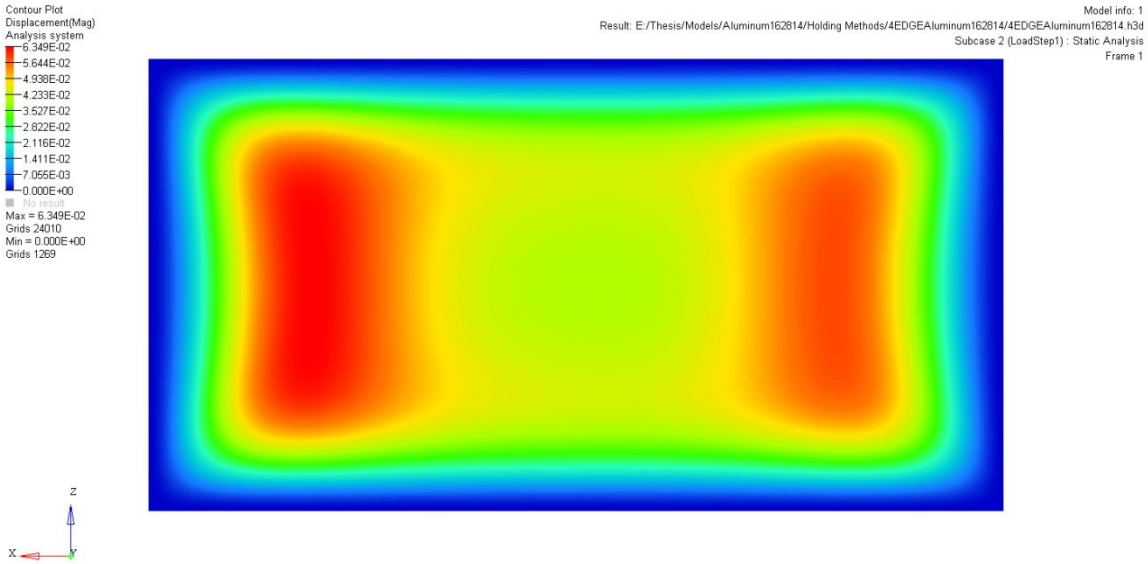

Figure A-17. Model 17: 1.62814 mm thick aluminum plate, fully constrained along two 8' lengths and two 4' lengths.

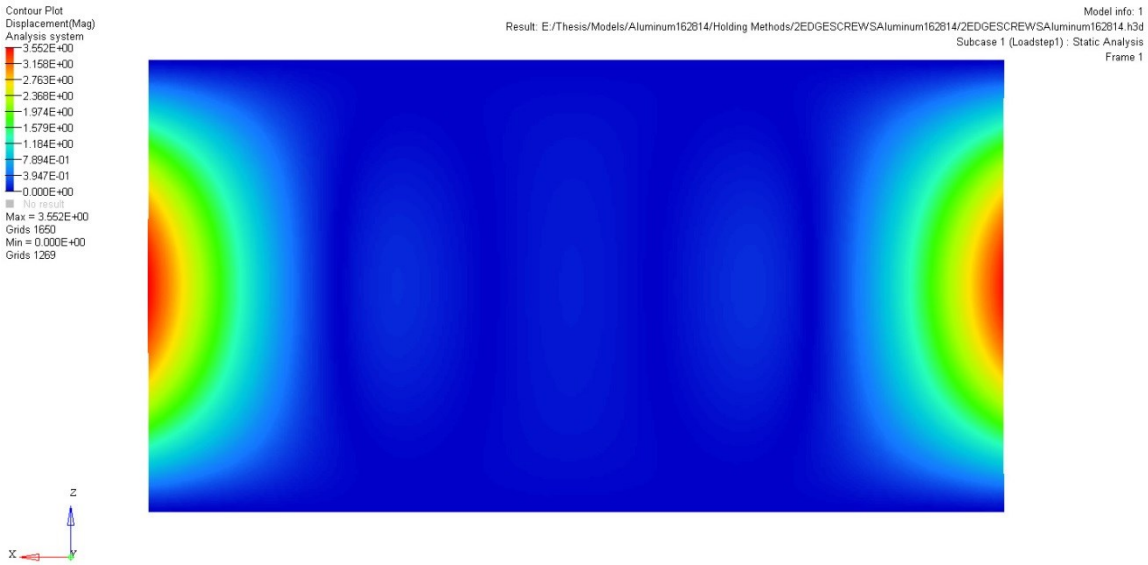

Figure A-18. Model 18: 1.62814 mm thick aluminum plate, point constraints spaced every 6" along two 8' lengths.

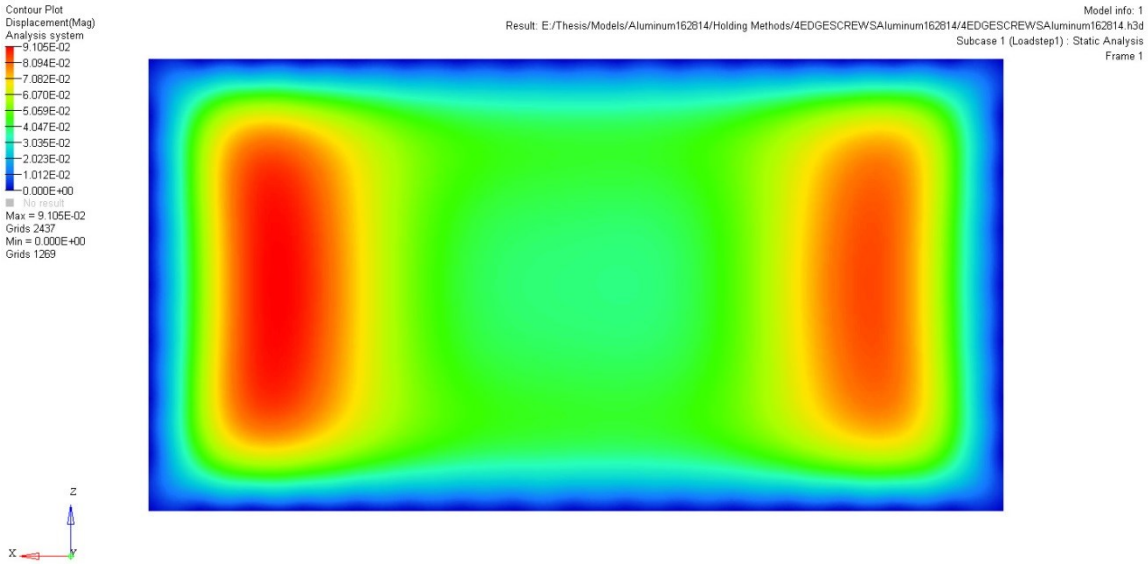

Figure A-19. Model 19: 1.62814 mm thick aluminum plate, point constraints spaced every 6" along two 8' lengths and two 4' lengths.

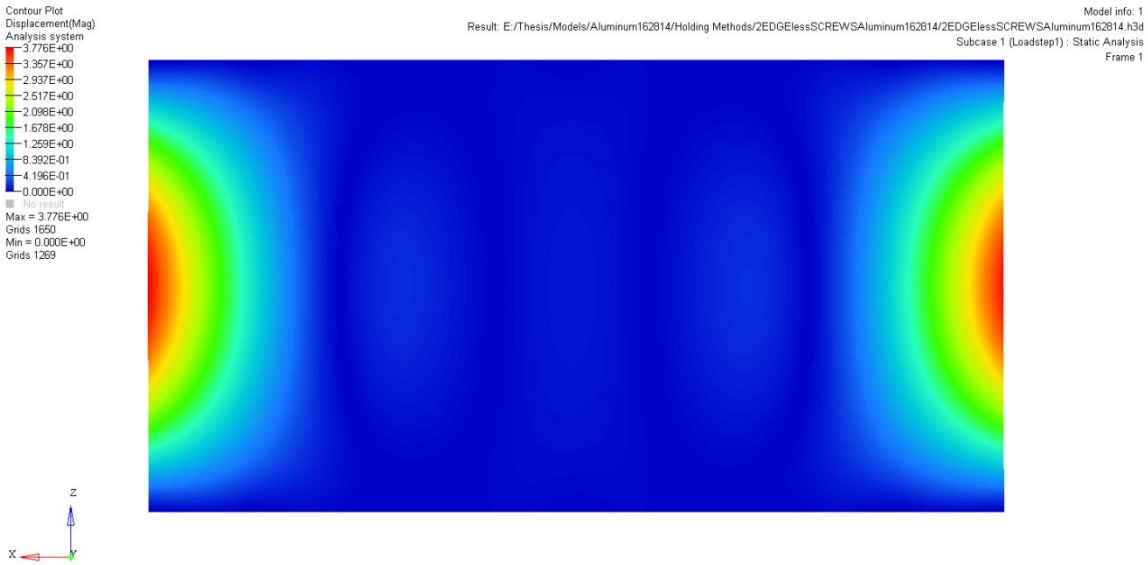

Figure A-20. Model 20: 1.62814 mm thick aluminum plate, point constraints spaced every 12" along two 8' lengths.

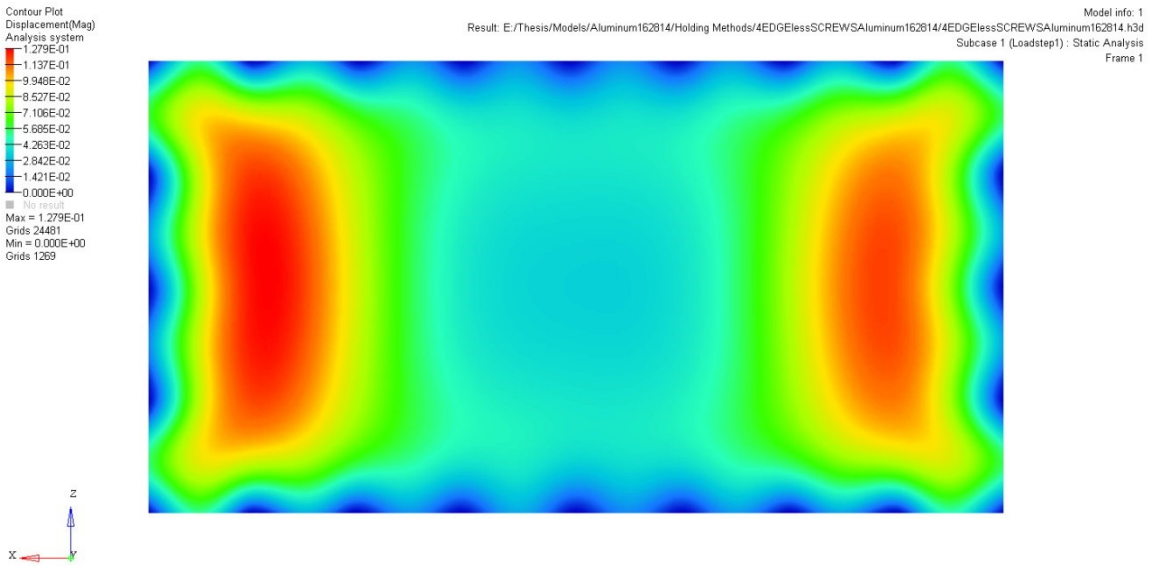

Figure A-21. Model 21: 1.62814 mm thick aluminum plate, point constraints spaced every 12" along two 8' lengths and two 4' lengths.

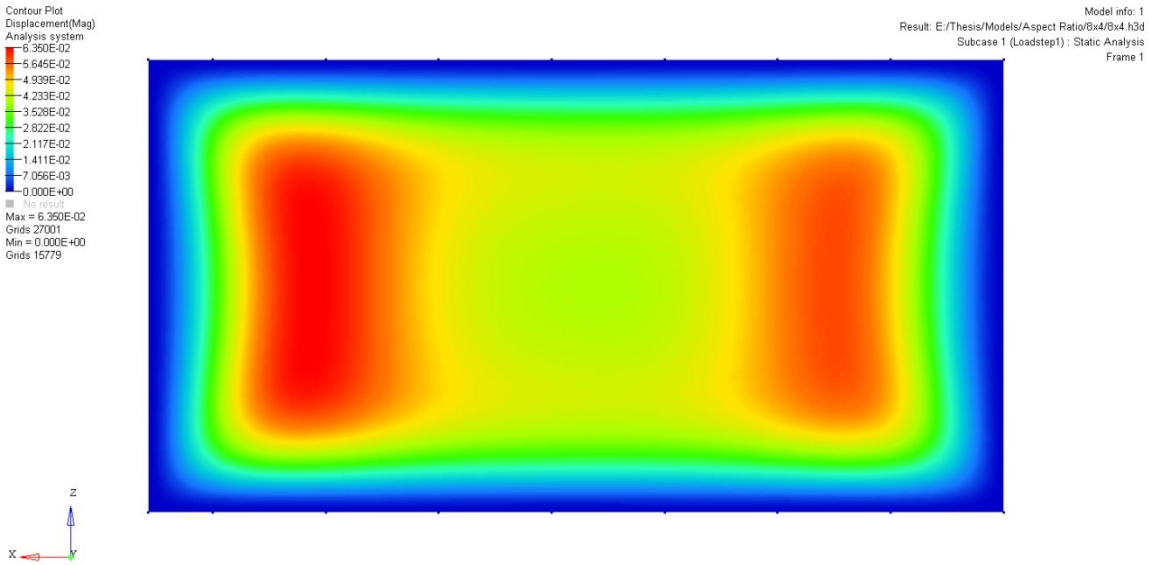

Figure A-22. Model 22: 8'x4' 1.62814 mm thick aluminum plate, fully constrained about all edges.

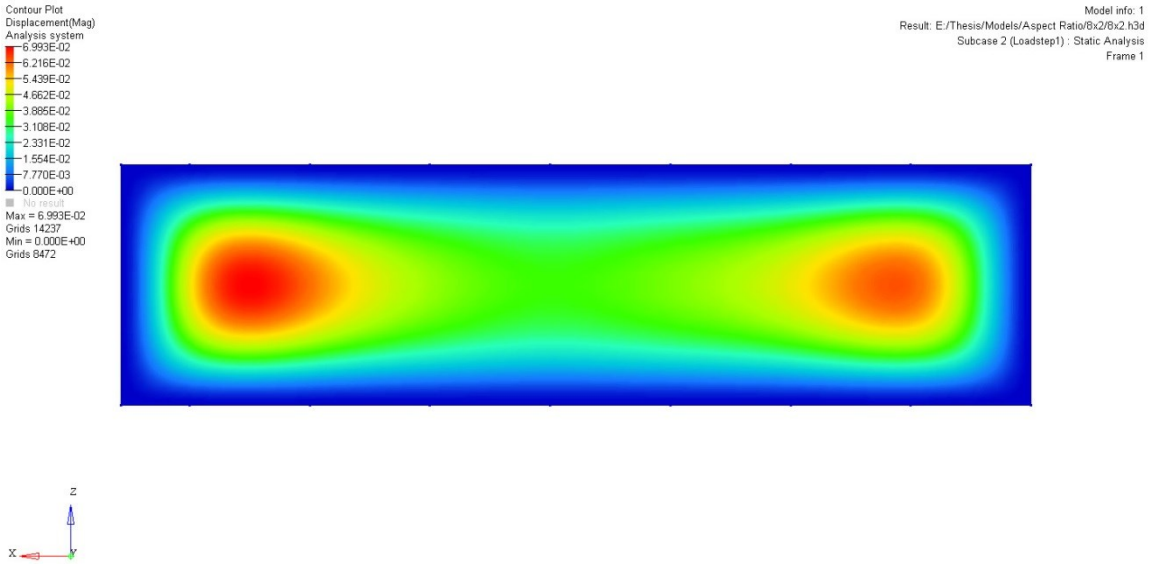

Figure A-23. Model 23: 8'x2' 1.62814 mm thick aluminum plate, fully constrained about all edges.

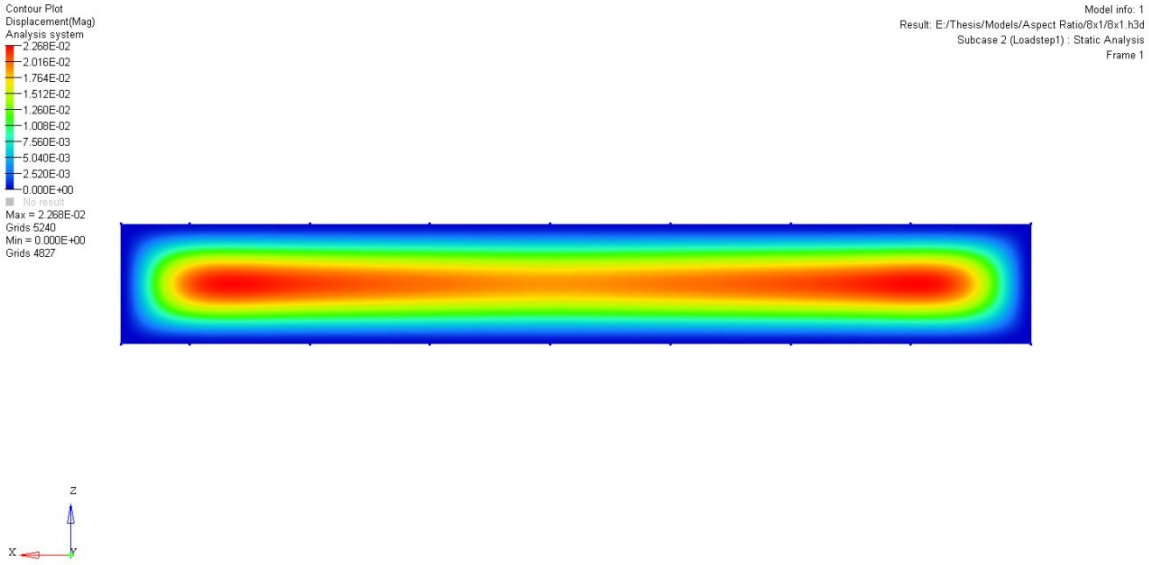

Figure A-24. Model 24: 8'x1' 1.62814 mm thick aluminum plate, fully constrained about all edges.

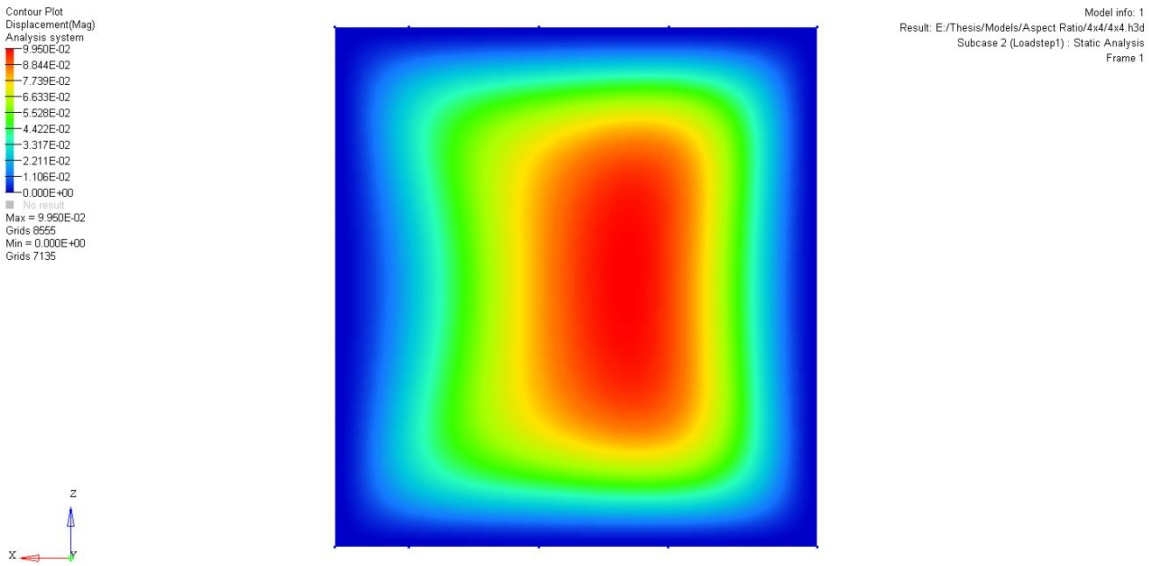

Figure A-25. Model 25: 4'x4' 1.62814 mm thick aluminum plate, fully constrained about all edges.

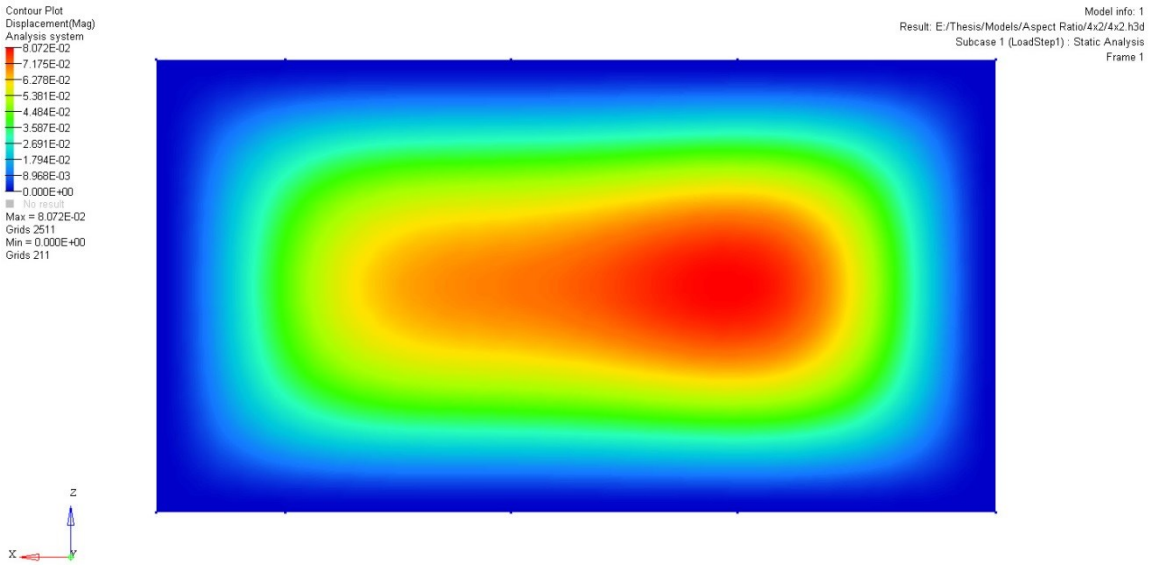

Figure A-26. Model 26: 4'x2' 1.62814 mm thick aluminum plate, fully constrained about all edges.

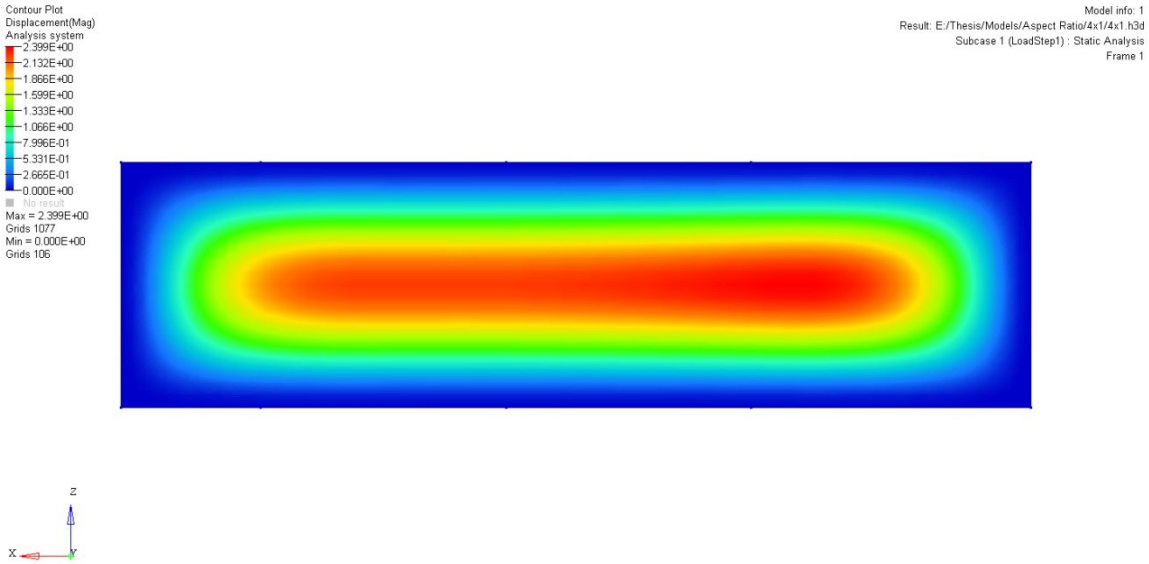

Figure A-27. Model 27: 4'x1' 1.62814 mm thick aluminum plate, fully constrained about all edges.

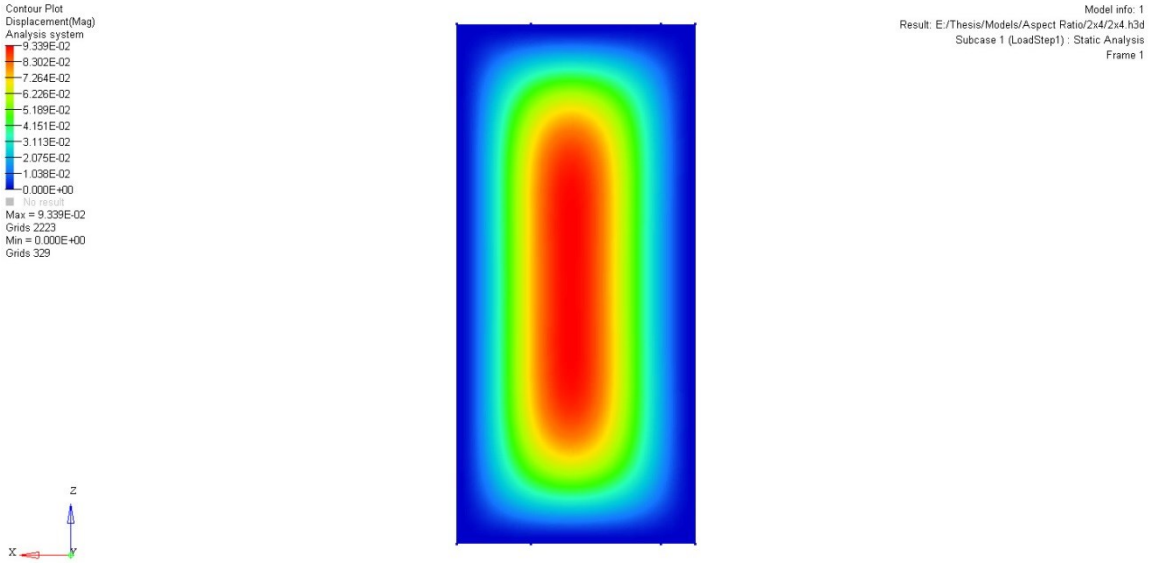

Figure A-28. Model 28: 2'x4' 1.62814 mm thick aluminum plate, fully constrained about all edges.

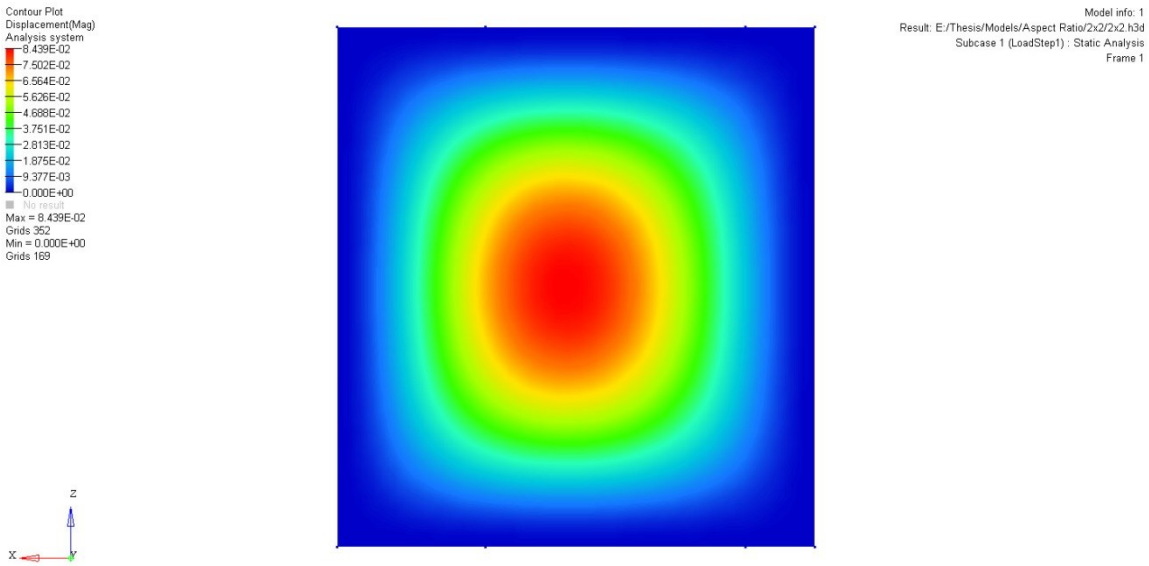

Figure A-29. Model 29: 2'x2' 1.62814 mm thick aluminum plate, fully constrained about all edges.

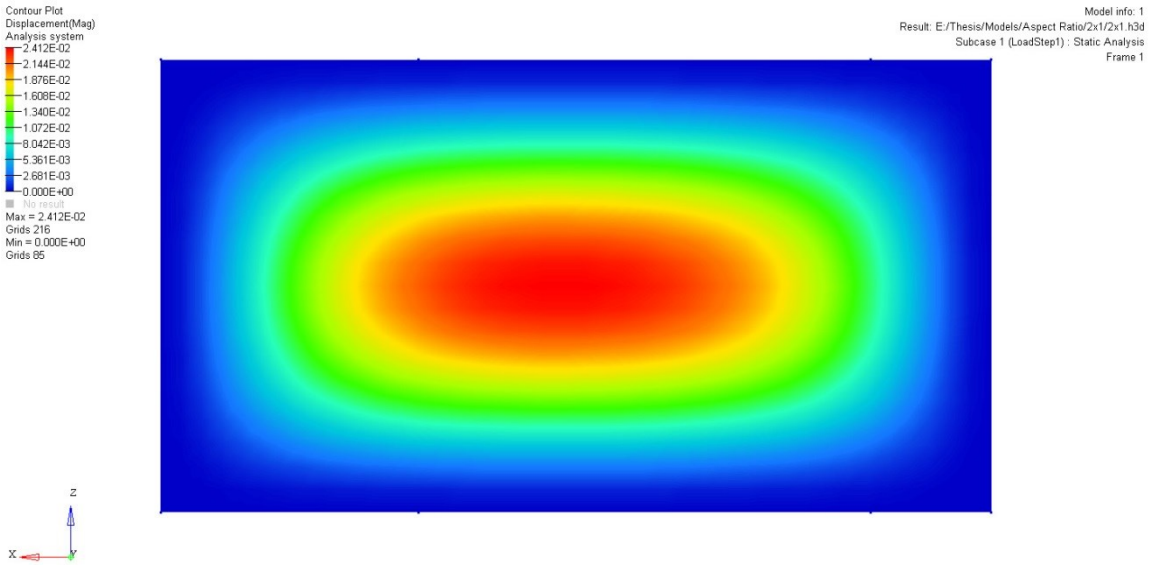

Figure A-30. Model 30: 2'x1' 1.62814 mm thick aluminum plate, fully constrained about all edges.

Appendix B – Sample FEA output report.

RADIOSS 11.0 Report

Problem submitted Wed Jul 03 15:47:00 2013
Input file E:/Thesis/Models/Aspect Ratio/8x4/8x4.fem

Problem summary

- Problem parameters: *E:/Thesis/Models/Aspect Ratio/8x4/8x4.fem*
- Finite element model: *E:/Thesis/Models/Aspect Ratio/8x4/8x4.fem*
- Output files prefix: *8x4*

- **Finite element model information**

  Number of nodes: 13466
  Number of elements: 13203
  Number of degrees of freedom: 77760
  Number of non-zero stiffness terms: 2112336

  - **Elements**

    Number of QUAD4 elements: 13203

  - **Loads and boundaries**

    Number of FORCE sets: 1
    Number of SPC sets: 1

  - **Materials and properties**

    Number of PSHELL cards: 1
    Number of MAT1 cards: 1

- **Subcases & loadcases information**
  - **Static subcases**

Subcase ID	SPC ID	Force ID	Weight
1	4	3	1.00

Results summary

- **Subcase 1 - Loadstep1**
  - Maximum displacement is 0.635E-01 at grid 27001.
  - Maximum 2-D element stress is 0.488 in element 28301.

Appendix C – Sample .fem FEA Input File

```
$$
$$ Optistruct Input Deck Generated by HyperMesh Version  : 11.0.0.47
$$ Generated using HyperMesh-Optistruct Template Version : 11.0.0.47
$$
$$   Template:  optistruct
$$
$$
$$ optistruct
$
$$------------------------------------------------------------------------------$
$$                     Case Control Cards                                       $
$$------------------------------------------------------------------------------$
$
$HMNAME LOADSTEP               1"LoadStep1"       1
$
SUBCASE       1
  SPC =        2
  LOAD =        1
$$---------------------------------------------------------------
$$ HYPERMESH TAGS
$$---------------------------------------------------------------
$$BEGIN TAGS
$$END TAGS
$
BEGIN BULK
$$
$$  Stacking Information for Ply-Based Composite Definition
$$
$$
$$  DESVARG Data
$$
$$
$$  GRID Data
$$
GRID           1        0.0     0.0     0.0
GRID           2        81.28   32.828090.0
GRID           3        386.08  162.36810.0
GRID           4        560.07  240.869 0.0
GRID           5        560.07  240.869 304.8
GRID           6        386.08  162.3681304.8
GRID           7        81.28   32.82809304.8
GRID           8        0.0     0.0     304.8
GRID          85        0.0     0.0     0.0
GRID          86        13.792775.5598670.0
GRID          87        27.5784111.1374 0.0
GRID          88        41.3569416.732440.0
GRID          89        55.1284122.344850.0
GRID          90        68.8928527.974480.0
GRID          91        82.6503 33.621180.0
GRID          92        96.4007939.2848 0.0
GRID          93        110.144444.9652 0.0
GRID          94        123.881 50.662220.0
GRID          95        137.610956.375710.0
GRID          96        151.333962.105540.0
GRID          97        165.050267.851550.0
GRID          98        178.759773.613590.0
GRID          99        192.462679.391520.0
GRID         100        206.158885.185190.0
GRID         101        219.848490.994450.0
GRID         102        233.531496.819170.0
GRID         103        247.2079102.65920.0
GRID         104        260.8779108.51440.0
GRID         105        274.5415114.38450.0
GRID         106        288.1987120.26960.0
GRID         107        301.8495126.16930.0
```

```
GRID        108        315.4941132.08370.0
GRID        109        329.1323138.01240.0
GRID        110        342.7644143.95550.0
GRID        111        356.3903149.91260.0
GRID        112        370.01  155.88380.0
GRID        113        383.6237161.86880.0
GRID        114        397.2313167.86760.0
GRID        115        410.833 173.87990.0
GRID        116        424.4287179.90560.0
GRID        117        438.0185185.94450.0
GRID        118        451.6025191.99660.0
GRID        119        465.1807198.06170.0
GRID        120        478.7531204.13970.0
GRID        121        492.3199210.23030.0
GRID        122        505.881 216.33350.0
GRID        123        519.4365222.44910.0
GRID        124        532.9865228.577 0.0
GRID        125        546.531 234.717 0.0
GRID        126        560.07  240.869 0.0
GRID        127        560.07  240.869 15.24
GRID        128        560.07  240.869 30.48
GRID        129        560.07  240.869 45.72
GRID        130        560.07  240.869 60.96
GRID        131        560.07  240.869 76.2
GRID        132        560.07  240.869 91.44
GRID        133        560.07  240.869 106.68
GRID        134        560.07  240.869 121.92
GRID        135        560.07  240.869 137.16
GRID        136        560.07  240.869 152.4
GRID        137        560.07  240.869 167.64
GRID        138        560.07  240.869 182.88
GRID        139        560.07  240.869 198.12
GRID        140        560.07  240.869 213.36
GRID        141        560.07  240.869 228.6
GRID        142        560.07  240.869 243.84
GRID        143        560.07  240.869 259.08
GRID        144        560.07  240.869 274.32
GRID        145        560.07  240.869 289.56
GRID        146        560.07  240.869 304.8
GRID        147        546.531 234.717 304.8
GRID        148        532.9865228.577 304.8
GRID        149        519.4365222.4491304.8
GRID        150        505.881 216.3335304.8
GRID        151        492.3199210.2303304.8
GRID        152        478.7532204.1397304.8
GRID        153        465.1807198.0617304.8
GRID        154        451.6025191.9966304.8
GRID        155        438.0185185.9445304.8
GRID        156        424.4287179.9056304.8
GRID        157        410.833 173.8799304.8
GRID        158        397.2313167.8676304.8
GRID        159        383.6237161.8688304.8
GRID        160        370.01  155.8838304.8
GRID        161        356.3903149.9126304.8
GRID        162        342.7644143.9555304.8
GRID        163        329.1323138.0124304.8
GRID        164        315.4941132.0837304.8
GRID        165        301.8495126.1693304.8
GRID        166        288.1987120.2696304.8
GRID        167        274.5415114.3845304.8
GRID        168        260.8779108.5143304.8
GRID        169        247.2079102.6592304.8
GRID        170        233.531496.81917304.8
GRID        171        219.848490.99445304.8
GRID        172        206.158885.18519304.8
GRID        173        192.462679.39152304.8
GRID        174        178.759773.61359304.8
GRID        175        165.050267.85154304.8
GRID        176        151.333962.10554304.8
```

```
GRID        177       137.610956.37571304.8
GRID        178       123.881 50.66222304.8
GRID        179       110.144444.9652 304.8
GRID        180       96.4007939.2848 304.8
GRID        181       82.6503133.62119304.8
GRID        182       68.8928527.97448304.8
GRID        183       55.1284222.34486304.8
GRID        184       41.3569316.73244304.8
GRID        185       27.5783911.13739304.8
GRID        186       13.792785.559869304.8
GRID        187       0.0     0.0     304.8
GRID        188       0.0     0.0     289.56
GRID        189       0.0     0.0     274.32
GRID        190       0.0     0.0     259.08
GRID        191       0.0     0.0     243.84
GRID        192       0.0     0.0     228.6
GRID        193       0.0     0.0     213.36
GRID        194       0.0     0.0     198.12
GRID        195       0.0     0.0     182.88
GRID        196       0.0     0.0     167.64
GRID        197       0.0     0.0     152.4
GRID        198       0.0     0.0     137.16
GRID        199       0.0     0.0     121.92
GRID        200       0.0     0.0     106.68
GRID        201       0.0     0.0     91.44
GRID        202       0.0     0.0     76.2
GRID        203       0.0     0.0     60.96
GRID        204       0.0     0.0     45.72
GRID        205       0.0     0.0     30.48
GRID        206       0.0     0.0     15.24
GRID        207       288.1944120.2677289.5705
GRID        208       288.1938120.2674274.3695
GRID        209       288.1939120.2675259.08
GRID        210       288.1939120.2675243.84
GRID        211       288.1939120.2675228.6
GRID        212       288.1939120.2675213.36
GRID        213       288.1939120.2675198.12
GRID        214       288.1939120.2675182.88
GRID        215       288.1939120.2675167.64
GRID        216       288.1939120.2675152.4
GRID        217       288.1939120.2675137.16
GRID        218       288.1939120.2675121.92
GRID        219       288.1939120.2675106.68
GRID        220       288.1939120.267591.44
GRID        221       288.1939120.267576.2
GRID        222       288.1939120.267560.96
GRID        223       288.1939120.267545.72
GRID        224       288.1938120.267530.43045
GRID        225       288.1944120.267715.22951
GRID        226       301.8458126.1677152.4
GRID        227       315.4914132.0825152.4
GRID        228       329.1455138.0182152.4
GRID        229       342.7803143.9624152.4
GRID        230       356.4087149.9207152.4
GRID        231       370.0306155.8928152.4
GRID        232       383.646 161.8787152.4
GRID        233       397.2551167.8781152.4
GRID        234       410.8578173.8908152.4
GRID        235       424.4541179.9168152.4
GRID        236       438.044 185.9559152.4
GRID        237       451.6275192.0078152.4
GRID        238       465.2048198.0725152.4
GRID        239       478.7757204.1498152.4
GRID        240       492.3403210.2395152.4
GRID        241       505.8851216.3354152.4
GRID        242       519.44  222.4507152.4
GRID        243       532.989 228.5781152.4
GRID        244       546.5323234.7176152.4
GRID        245       424.4541179.9168167.64
```

```
GRID        246       424.4541179.9168182.88
GRID        247       424.4541179.9168198.12
GRID        248       424.4541179.9168213.36
GRID        249       424.4541179.9168228.6
GRID        250       424.4541179.9168243.84
GRID        251       424.4541179.9168259.08
GRID        252       424.453 179.9164274.3457
GRID        253       424.4488179.9145289.5654
GRID        254       410.8578173.8908228.6
GRID        255       397.2551167.8781228.6
GRID        256       383.646 161.8787228.6
GRID        257       370.0306155.8928228.6
GRID        258       356.4087149.9207228.6
GRID        259       342.7803143.9624228.6
GRID        260       329.1455138.0182228.6
GRID        261       315.4914132.0825228.6
GRID        262       301.8458126.1677228.6
GRID        263       356.4087149.9207213.36
GRID        264       356.4087149.9207198.12
GRID        265       356.4087149.9207182.88
GRID        266       356.4087149.9207167.64
GRID        267       370.0306155.8928198.12
GRID        268       383.646 161.8787198.12
GRID        269       397.2551167.8781198.12
GRID        270       410.8578173.8908198.12
GRID        271       383.646 161.8787213.36
GRID        272       370.0306155.8928213.36
GRID        273       397.2551167.8781213.36
GRID        274       410.8578173.8908213.36
GRID        275       383.646 161.8787167.64
GRID        276       383.646 161.8787182.88
GRID        277       370.0306155.8928167.64
GRID        278       370.0306155.8928182.88
GRID        279       410.8578173.8908167.64
GRID        280       397.2551167.8781167.64
GRID        281       410.8578173.8908182.88
GRID        282       397.2551167.8781182.88
GRID        283       301.8458126.1677198.12
GRID        284       315.4914132.0825198.12
GRID        285       329.1455138.0182198.12
GRID        286       342.7803143.9624198.12
GRID        287       315.4914132.0825213.36
GRID        288       301.8458126.1677213.36
GRID        289       329.1455138.0182213.36
GRID        290       342.7803143.9624213.36
GRID        291       315.4914132.0825167.64
GRID        292       315.4914132.0825182.88
GRID        293       301.8458126.1677167.64
GRID        294       301.8458126.1677182.88
GRID        295       342.7803143.9624167.64
GRID        296       329.1455138.0182167.64
GRID        297       342.7803143.9624182.88
GRID        298       329.1455138.0182182.88
GRID        299       356.4049149.9191289.5687
GRID        300       356.4079149.9204274.3616
GRID        301       356.4086149.9207259.08
GRID        302       356.4087149.9207243.84
GRID        303       370.0298155.8925274.3589
GRID        304       383.6452161.8783274.3559
GRID        305       397.2542167.8777274.3526
GRID        306       410.8568173.8904274.3492
GRID        307       383.6415161.8767289.5675
GRID        308       370.0264155.891 289.5681
GRID        309       397.2502167.8759289.5669
GRID        310       410.8527173.8886289.5662
GRID        311       383.646 161.8787243.84
GRID        312       383.646 161.8787259.08
GRID        313       370.0306155.8928243.84
GRID        314       370.0306155.8928259.08
```

```
GRID        315       410.8578173.8908243.84
GRID        316       397.2551167.8781243.84
GRID        317       410.8578173.8908259.08
GRID        318       397.2551167.8781259.08
GRID        319       301.8456126.1676274.3688
GRID        320       315.4978132.0853274.3676
GRID        321       329.1392138.0154274.366
GRID        322       342.7797143.9622274.364
GRID        323       315.4969132.0849289.5694
GRID        324       301.846 126.1678289.5703
GRID        325       329.138 138.0149289.569
GRID        326       342.7771143.961 289.5692
GRID        327       315.4914132.0825243.84
GRID        328       315.4914132.0825259.08
GRID        329       301.8458126.1677243.84
GRID        330       301.8458126.1677259.08
GRID        331       342.7803143.9624243.84
GRID        332       329.1455138.0182243.84
GRID        333       342.7803143.9624259.08
GRID        334       329.1455138.0182259.08
GRID        335       546.5323234.7176228.6
GRID        336       532.989 228.5781228.6
GRID        337       519.44  222.4507228.6
GRID        338       505.8851216.3354228.6
GRID        339       492.3403210.2395228.6
GRID        340       478.7757204.1498228.6
GRID        341       465.2048198.0725228.6
GRID        342       451.6275192.0078228.6
GRID        343       438.044 185.9559228.6
GRID        344       492.3403210.2395213.36
GRID        345       492.3403210.2395198.12
GRID        346       492.3403210.2395182.88
GRID        347       492.3403210.2395167.64
GRID        348       505.8851216.3354198.12
GRID        349       519.44  222.4507198.12
GRID        350       532.989 228.5781198.12
GRID        351       546.5323234.7176198.12
GRID        352       519.44  222.4507213.36
GRID        353       505.8851216.3354213.36
GRID        354       532.989 228.5781213.36
GRID        355       546.5323234.7176213.36
GRID        356       519.44  222.4507167.64
GRID        357       519.44  222.4507182.88
GRID        358       505.8851216.3354167.64
GRID        359       505.8851216.3354182.88
GRID        360       546.5323234.7176167.64
GRID        361       532.989 228.5781167.64
GRID        362       546.5323234.7176182.88
GRID        363       532.989 228.5781182.88
GRID        364       438.044 185.9559198.12
GRID        365       451.6275192.0078198.12
GRID        366       465.2048198.0725198.12
GRID        367       478.7757204.1498198.12
GRID        368       451.6275192.0078213.36
GRID        369       438.044 185.9559213.36
GRID        370       465.2048198.0725213.36
GRID        371       478.7757204.1498213.36
GRID        372       451.6275192.0078167.64
GRID        373       451.6275192.0078182.88
GRID        374       438.044 185.9559167.64
GRID        375       438.044 185.9559182.88
GRID        376       478.7757204.1498167.64
GRID        377       465.2048198.0725167.64
GRID        378       478.7757204.1498182.88
GRID        379       465.2048198.0725182.88
GRID        380       492.3309210.2352289.5626
GRID        381       492.3403210.2395274.32
GRID        382       492.3403210.2395259.08
GRID        383       492.3403210.2395243.84
```

```
GRID        384       505.8851216.3354274.32
GRID        385       519.44  222.4507274.32
GRID        386       532.989 228.5781274.32
GRID        387       546.5323234.7176274.32
GRID        388       519.4389222.4502289.5674
GRID        389       505.8839216.3348289.5725
GRID        390       532.9883228.5778289.5634
GRID        391       546.5319234.7174289.5609
GRID        392       519.44  222.4507243.84
GRID        393       519.44  222.4507259.08
GRID        394       505.8851216.3354243.84
GRID        395       505.8851216.3354259.08
GRID        396       546.5323234.7176243.84
GRID        397       532.989 228.5781243.84
GRID        398       546.5323234.7176259.08
GRID        399       532.989 228.5781259.08
GRID        400       438.0429185.9554274.3421
GRID        401       451.6265192.0073274.3385
GRID        402       465.2048198.0725274.32
GRID        403       478.7757204.1498274.32
GRID        404       451.6223192.0055289.564
GRID        405       438.0387185.9535289.5647
GRID        406       465.1997198.0703289.5633
GRID        407       478.771 204.1476289.5626
GRID        408       451.6275192.0078243.84
GRID        409       451.6275192.0078259.08
GRID        410       438.044 185.9559243.84
GRID        411       438.044 185.9559259.08
GRID        412       478.7757204.1498243.84
GRID        413       465.2048198.0725243.84
GRID        414       478.7757204.1498259.08
GRID        415       465.2048198.0725259.08
GRID        416       424.4488179.914515.23456
GRID        417       424.4531179.916430.45434
GRID        418       424.4541179.916845.72
GRID        419       424.4541179.916860.96
GRID        420       424.4541179.916876.2
GRID        421       424.4541179.916891.44
GRID        422       424.4541179.9168106.68
GRID        423       424.4541179.9168121.92
GRID        424       424.4541179.9168137.16
GRID        425       410.8578173.890876.2
GRID        426       397.2551167.878176.2
GRID        427       383.646 161.878776.2
GRID        428       370.0306155.892876.2
GRID        429       356.4087149.920776.2
GRID        430       342.7803143.962476.2
GRID        431       329.1455138.018276.2
GRID        432       315.4914132.082576.2
GRID        433       301.8458126.167776.2
GRID        434       356.4087149.920760.96
GRID        435       356.4087149.920745.72
GRID        436       356.4079149.920430.43843
GRID        437       356.4049149.919115.23132
GRID        438       370.0306155.892845.72
GRID        439       383.646 161.878745.72
GRID        440       397.2551167.878145.72
GRID        441       410.8578173.890845.72
GRID        442       383.646 161.878760.96
GRID        443       370.0306155.892860.96
GRID        444       397.2551167.878160.96
GRID        445       410.8578173.890860.96
GRID        446       383.6415161.876715.23249
GRID        447       383.6452161.878330.44414
GRID        448       370.0264155.891 15.23188
GRID        449       370.0298155.892530.44114
GRID        450       410.8527173.888615.23384
GRID        451       397.2502167.875915.23315
GRID        452       410.8568173.890430.45079
```

```
GRID        453        397.2542167.877730.44737
GRID        454        301.8458126.167745.72
GRID        455        315.4914132.082545.72
GRID        456        329.1455138.018245.72
GRID        457        342.7803143.962445.72
GRID        458        315.4914132.082560.96
GRID        459        301.8458126.167760.96
GRID        460        329.1455138.018260.96
GRID        461        342.7803143.962460.96
GRID        462        315.4969132.084915.23055
GRID        463        315.4978132.085330.4324
GRID        464        301.846 126.167815.22967
GRID        465        301.8456126.167630.4312
GRID        466        342.7771143.961 15.23084
GRID        467        329.138 138.014915.23097
GRID        468        342.7797143.962230.43604
GRID        469        329.1392138.015430.43402
GRID        470        356.4087149.9207137.16
GRID        471        356.4087149.9207121.92
GRID        472        356.4087149.9207106.68
GRID        473        356.4087149.920791.44
GRID        474        370.0306155.8928121.92
GRID        475        383.646 161.8787121.92
GRID        476        397.2551167.8781121.92
GRID        477        410.8578173.8908121.92
GRID        478        383.646 161.8787137.16
GRID        479        370.0306155.8928137.16
GRID        480        397.2551167.8781137.16
GRID        481        410.8578173.8908137.16
GRID        482        383.646 161.878791.44
GRID        483        383.646 161.8787106.68
GRID        484        370.0306155.892891.44
GRID        485        370.0306155.8928106.68
GRID        486        410.8578173.890891.44
GRID        487        397.2551167.878191.44
GRID        488        410.8578173.8908106.68
GRID        489        397.2551167.8781106.68
GRID        490        301.8458126.1677121.92
GRID        491        315.4914132.0825121.92
GRID        492        329.1455138.0182121.92
GRID        493        342.7803143.9624121.92
GRID        494        315.4914132.0825137.16
GRID        495        301.8458126.1677137.16
GRID        496        329.1455138.0182137.16
GRID        497        342.7803143.9624137.16
GRID        498        315.4914132.082591.44
GRID        499        315.4914132.0825106.68
GRID        500        301.8458126.167791.44
GRID        501        301.8458126.1677106.68
GRID        502        342.7803143.962491.44
GRID        503        329.1455138.018291.44
GRID        504        342.7803143.9624106.68
GRID        505        329.1455138.0182106.68
GRID        506        546.5323234.717676.2
GRID        507        532.989 228.578176.2
GRID        508        519.44  222.450776.2
GRID        509        505.8851216.335476.2
GRID        510        492.3403210.239576.2
GRID        511        478.7757204.149876.2
GRID        512        465.2048198.072576.2
GRID        513        451.6275192.007876.2
GRID        514        438.044 185.955976.2
GRID        515        492.3403210.239560.96
GRID        516        492.3403210.239545.72
GRID        517        492.3403210.239530.48
GRID        518        492.3309210.235215.23743
GRID        519        505.8851216.335445.72
GRID        520        519.44  222.450745.72
GRID        521        532.989 228.578145.72
```

```
GRID        522       546.5323234.717645.72
GRID        523       519.44  222.450760.96
GRID        524       505.8851216.335460.96
GRID        525       532.989 228.578160.96
GRID        526       546.5323234.717660.96
GRID        527       519.4389222.450215.2326
GRID        528       519.44  222.450730.48
GRID        529       505.8839216.334815.22744
GRID        530       505.8851216.335430.48
GRID        531       546.5319234.717415.23911
GRID        532       532.9883228.577815.23656
GRID        533       546.5323234.717630.48
GRID        534       532.989 228.578130.48
GRID        535       438.044 185.955945.72
GRID        536       451.6275192.007845.72
GRID        537       465.2048198.072545.72
GRID        538       478.7757204.149845.72
GRID        539       451.6275192.007860.96
GRID        540       438.044 185.955960.96
GRID        541       465.2048198.072560.96
GRID        542       478.7757204.149860.96
GRID        543       451.6223192.005515.23602
GRID        544       451.6265192.007330.46154
GRID        545       438.0387185.953515.23529
GRID        546       438.0429185.955430.45794
GRID        547       478.7709204.147615.23739
GRID        548       465.1997198.070215.23672
GRID        549       478.7757204.149830.48
GRID        550       465.2048198.072530.48
GRID        551       492.3403210.2395137.16
GRID        552       492.3403210.2395121.92
GRID        553       492.3403210.2395106.68
GRID        554       492.3403210.239591.44
GRID        555       505.8851216.3354121.92
GRID        556       519.44  222.4507121.92
GRID        557       532.989 228.5781121.92
GRID        558       546.5323234.7176121.92
GRID        559       519.44  222.4507137.16
GRID        560       505.8851216.3354137.16
GRID        561       532.989 228.5781137.16
GRID        562       546.5323234.7176137.16
GRID        563       519.44  222.450791.44
GRID        564       519.44  222.4507106.68
GRID        565       505.8851216.335491.44
GRID        566       505.8851216.3354106.68
GRID        567       546.5323234.717691.44
GRID        568       532.989 228.578191.44
GRID        569       546.5323234.7176106.68
GRID        570       532.989 228.5781106.68
GRID        571       438.044 185.9559121.92
GRID        572       451.6275192.0078121.92
GRID        573       465.2048198.0725121.92
GRID        574       478.7757204.1498121.92
GRID        575       451.6275192.0078137.16
GRID        576       438.044 185.9559137.16
GRID        577       465.2048198.0725137.16
GRID        578       478.7757204.1498137.16
GRID        579       451.6275192.007891.44
GRID        580       451.6275192.0078106.68
GRID        581       438.044 185.955991.44
GRID        582       438.044 185.9559106.68
GRID        583       478.7757204.149891.44
GRID        584       465.2048198.072591.44
GRID        585       478.7757204.1498106.68
GRID        586       465.2048198.0725106.68
GRID        587       151.319562.0995 289.5664
GRID        588       151.316262.09812274.3528
GRID        589       151.321862.10049259.08
GRID        590       151.321862.10049243.84
```

```
GRID        591       151.321862.10049228.6
GRID        592       151.321862.10049213.36
GRID        593       151.321862.10049198.12
GRID        594       151.321862.10049182.88
GRID        595       151.321862.10049167.64
GRID        596       151.321862.10049152.4
GRID        597       151.321862.10049137.16
GRID        598       151.321862.10049121.92
GRID        599       151.321862.10049106.68
GRID        600       151.321862.1004991.44
GRID        601       151.321862.1004976.2
GRID        602       151.321862.1004960.96
GRID        603       151.321862.1004945.72
GRID        604       151.316262.0981130.44719
GRID        605       151.319562.0995 15.23362
GRID        606       165.038367.84657152.4
GRID        607       178.748273.60875152.4
GRID        608       192.451679.38688152.4
GRID        609       206.148485.18081152.4
GRID        610       219.838890.99037152.4
GRID        611       233.522696.81543152.4
GRID        612       247.2   102.6558152.4
GRID        613       260.871 108.5114152.4
GRID        614       274.5356114.382 152.4
GRID        615       165.038367.84657228.6
GRID        616       178.748273.60875228.6
GRID        617       192.451679.38688228.6
GRID        618       206.148485.18081228.6
GRID        619       219.838890.99037228.6
GRID        620       233.522696.81543228.6
GRID        621       247.2   102.6558228.6
GRID        622       260.871 108.5114228.6
GRID        623       274.5356114.382 228.6
GRID        624       219.838890.99037243.84
GRID        625       219.838890.99037259.08
GRID        626       219.839290.99056274.3664
GRID        627       219.840890.99126289.5698
GRID        628       206.148485.1808 259.08
GRID        629       192.451679.38688259.08
GRID        630       178.748273.60875259.08
GRID        631       165.038367.84657259.08
GRID        632       192.451679.38688243.84
GRID        633       206.148485.18081243.84
GRID        634       178.748273.60875243.84
GRID        635       165.038367.84657243.84
GRID        636       192.454279.38798289.5689
GRID        637       192.452279.38715274.3621
GRID        638       206.150885.1818 289.5694
GRID        639       206.149 85.18104274.3644
GRID        640       165.041367.84782289.5677
GRID        641       178.751 73.60993289.5683
GRID        642       165.039167.84691274.3562
GRID        643       178.749 73.60906274.3593
GRID        644       274.5356114.382 259.08
GRID        645       260.871 108.5114259.08
GRID        646       247.2   102.6558259.08
GRID        647       233.522696.81543259.08
GRID        648       260.871 108.5114243.84
GRID        649       274.5356114.382 243.84
GRID        650       247.2   102.6558243.84
GRID        651       233.522696.81543243.84
GRID        652       260.8722108.5119289.5705
GRID        653       260.8711108.5114274.3697
GRID        654       274.5365114.3824289.5706
GRID        655       274.5356114.382 274.3698
GRID        656       233.524496.81619289.5702
GRID        657       247.2015102.6565289.5704
GRID        658       233.523 96.81557274.368
GRID        659       247.2003102.6559274.3691
```

```
GRID        660        219.838890.99037167.64
GRID        661        219.838890.99037182.88
GRID        662        219.838890.99037198.12
GRID        663        219.838890.99037213.36
GRID        664        206.148485.18081182.88
GRID        665        192.451679.38688182.88
GRID        666        178.748273.60875182.88
GRID        667        165.038367.84657182.88
GRID        668        192.451679.38688167.64
GRID        669        206.148485.18081167.64
GRID        670        178.748273.60875167.64
GRID        671        165.038367.84657167.64
GRID        672        192.451679.38688213.36
GRID        673        192.451679.38688198.12
GRID        674        206.148485.18081213.36
GRID        675        206.148485.18081198.12
GRID        676        165.038367.84657213.36
GRID        677        178.748273.60875213.36
GRID        678        165.038367.84657198.12
GRID        679        178.748273.60875198.12
GRID        680        274.5356114.382 182.88
GRID        681        260.871 108.5114182.88
GRID        682        247.2   102.6558182.88
GRID        683        233.522696.81543182.88
GRID        684        260.871 108.5114167.64
GRID        685        274.5356114.382 167.64
GRID        686        247.2   102.6558167.64
GRID        687        233.522696.81543167.64
GRID        688        260.871 108.5114213.36
GRID        689        260.871 108.5114198.12
GRID        690        274.5356114.382 213.36
GRID        691        274.5356114.382 198.12
GRID        692        233.522696.81543213.36
GRID        693        247.2   102.6558213.36
GRID        694        233.522696.81543198.12
GRID        695        247.2   102.6558198.12
GRID        696        165.038367.8465776.2
GRID        697        178.748273.6087576.2
GRID        698        192.451679.3868876.2
GRID        699        206.148485.1808 76.2
GRID        700        219.838890.9903776.2
GRID        701        233.522696.8154376.2
GRID        702        247.2   102.655876.2
GRID        703        260.871 108.511476.2
GRID        704        274.5356114.382 76.2
GRID        705        219.838890.9903791.44
GRID        706        219.838890.99037106.68
GRID        707        219.838890.99037121.92
GRID        708        219.838890.99037137.16
GRID        709        206.148485.18081106.68
GRID        710        192.451679.38688106.68
GRID        711        178.748273.60875106.68
GRID        712        165.038367.84657106.68
GRID        713        192.451679.3868891.44
GRID        714        206.148485.1808191.44
GRID        715        178.748273.6087591.44
GRID        716        165.038367.8465791.44
GRID        717        192.451679.38688137.16
GRID        718        192.451679.38688121.92
GRID        719        206.148485.18081137.16
GRID        720        206.148485.18081121.92
GRID        721        165.038367.84657137.16
GRID        722        178.748273.60875137.16
GRID        723        165.038367.84657121.92
GRID        724        178.748273.60875121.92
GRID        725        274.5356114.382 106.68
GRID        726        260.871 108.5114106.68
GRID        727        247.2   102.6558106.68
GRID        728        233.522696.81543106.68
```

```
GRID        729       260.871 108.511491.44
GRID        730       274.5356114.382 91.44
GRID        731       247.2   102.655891.44
GRID        732       233.522696.8154391.44
GRID        733       260.871 108.5114137.16
GRID        734       260.871 108.5114121.92
GRID        735       274.5356114.382 137.16
GRID        736       274.5356114.382 121.92
GRID        737       233.522696.81543137.16
GRID        738       247.2   102.6558137.16
GRID        739       233.522696.81543121.92
GRID        740       247.2   102.6558121.92
GRID        741       219.840890.9912615.23015
GRID        742       219.839290.9905630.43357
GRID        743       219.838890.9903745.72
GRID        744       219.838890.9903760.96
GRID        745       206.149 85.1810330.43555
GRID        746       192.452279.3871530.43793
GRID        747       178.749 73.6090630.4407
GRID        748       165.039167.8469130.4438
GRID        749       192.454279.3879815.23107
GRID        750       206.150885.1818 15.23057
GRID        751       178.751 73.6099315.23165
GRID        752       165.041367.8478215.2323
GRID        753       192.451679.3868860.96
GRID        754       192.451679.3868845.72
GRID        755       206.148485.1808 60.96
GRID        756       206.148485.1808 45.72
GRID        757       165.038367.8465760.96
GRID        758       178.748273.6087560.96
GRID        759       165.038367.8465745.72
GRID        760       178.748273.6087545.72
GRID        761       274.5356114.382 30.43014
GRID        762       260.8712108.511430.43031
GRID        763       247.2003102.655930.43094
GRID        764       233.523 96.8155730.43203
GRID        765       260.8722108.511915.22947
GRID        766       274.5365114.382415.22944
GRID        767       247.2015102.656515.2296
GRID        768       233.524496.8162 15.22983
GRID        769       260.871 108.511460.96
GRID        770       260.871 108.511445.72
GRID        771       274.5356114.382 60.96
GRID        772       274.5356114.382 45.72
GRID        773       233.522696.8154360.96
GRID        774       247.2   102.655860.96
GRID        775       233.522696.8154345.72
GRID        776       247.2   102.655845.72
GRID        777       13.790455.558929152.4
GRID        778       27.5739 11.13557152.4
GRID        779       41.3505616.72985152.4
GRID        780       55.1204522.3416 152.4
GRID        781       68.8686627.96457152.4
GRID        782       82.6241733.61044152.4
GRID        783       96.3735139.27355152.4
GRID        784       110.116744.95373152.4
GRID        785       123.853650.65081152.4
GRID        786       137.584356.36462152.4
GRID        787       68.8686627.96457167.64
GRID        788       68.8686627.96457182.88
GRID        789       68.8686627.96457198.12
GRID        790       68.8686627.96457213.36
GRID        791       68.8686627.96457228.6
GRID        792       68.8686627.96457243.84
GRID        793       68.8686627.96457259.08
GRID        794       68.8686627.96457274.32
GRID        795       68.8788727.96876289.5629
GRID        796       55.1204522.3416 228.6
GRID        797       41.3505616.72985228.6
```

```
GRID        798        27.5739 11.13557228.6
GRID        799        13.790455.558929228.6
GRID        800        55.1204522.3416 182.88
GRID        801        41.3505616.72985182.88
GRID        802        27.5739 11.13557182.88
GRID        803        13.790455.558929182.88
GRID        804        41.3505616.72985167.64
GRID        805        55.1204522.3416 167.64
GRID        806        27.5739 11.13557167.64
GRID        807        13.790455.558929167.64
GRID        808        41.3505616.72985213.36
GRID        809        41.3505616.72985198.12
GRID        810        55.1204522.3416 213.36
GRID        811        55.1204522.3416 198.12
GRID        812        13.790455.558929213.36
GRID        813        27.5739 11.13557213.36
GRID        814        13.790455.558929198.12
GRID        815        27.5739 11.13557198.12
GRID        816        55.1204522.3416 259.08
GRID        817        41.3505616.72985259.08
GRID        818        27.5739 11.13557259.08
GRID        819        13.790455.558929259.08
GRID        820        41.3505616.72985243.84
GRID        821        55.1204522.3416 243.84
GRID        822        27.5739 11.13557243.84
GRID        823        13.790455.558929243.84
GRID        824        41.3518316.73036289.5692
GRID        825        41.3505616.72985274.32
GRID        826        55.1219922.34223289.5754
GRID        827        55.1204522.3416 274.32
GRID        828        13.790955.559132289.5611
GRID        829        27.5748211.13595289.5643
GRID        830        13.790455.558928274.32
GRID        831        27.5739 11.13557274.32
GRID        832        137.584356.36462228.6
GRID        833        123.853650.65081228.6
GRID        834        110.116744.95373228.6
GRID        835        96.3735139.27355228.6
GRID        836        82.6241733.61044228.6
GRID        837        110.116744.95373213.36
GRID        838        110.116744.95373198.12
GRID        839        110.116744.95373182.88
GRID        840        110.116744.95373167.64
GRID        841        123.853650.65081198.12
GRID        842        137.584356.36462198.12
GRID        843        123.853650.65081213.36
GRID        844        137.584356.36462213.36
GRID        845        123.853650.65081182.88
GRID        846        137.584356.36462182.88
GRID        847        123.853650.65081167.64
GRID        848        137.584356.36462167.64
GRID        849        82.6241733.61044198.12
GRID        850        96.3735139.27355198.12
GRID        851        82.6241733.61044213.36
GRID        852        96.3735139.27355213.36
GRID        853        82.6241733.61044182.88
GRID        854        96.3735139.27355182.88
GRID        855        82.6241733.61044167.64
GRID        856        96.3735139.27355167.64
GRID        857        110.122444.95612289.5646
GRID        858        110.117844.95422274.3415
GRID        859        110.116744.95373259.08
GRID        860        110.116744.95373243.84
GRID        861        123.854750.65129274.3454
GRID        862        137.591356.36755274.3492
GRID        863        123.859350.65317289.5654
GRID        864        137.594756.36898289.5656
GRID        865        123.853650.65081259.08
GRID        866        137.584356.36462259.08
```

```
GRID        867       123.853650.65081243.84
GRID        868       137.584356.36462243.84
GRID        869       82.6241733.61044274.32
GRID        870       96.3747139.27404274.3376
GRID        871       82.6296833.61271289.5631
GRID        872       96.3792239.27591289.5638
GRID        873       82.6241733.61044259.08
GRID        874       96.3735139.27355259.08
GRID        875       82.6241733.61044243.84
GRID        876       96.3735139.27355243.84
GRID        877       68.8788727.9687615.23706
GRID        878       68.8686627.9645730.48
GRID        879       68.8686627.9645745.72
GRID        880       68.8686627.9645760.96
GRID        881       68.8686627.9645776.2
GRID        882       68.8686627.9645791.44
GRID        883       68.8686627.96457106.68
GRID        884       68.8686627.96457121.92
GRID        885       68.8686627.96457137.16
GRID        886       55.1204522.3416 76.2
GRID        887       41.3505616.7298576.2
GRID        888       27.5739 11.1355776.2
GRID        889       13.790455.55892976.2
GRID        890       55.1204522.3416 30.48
GRID        891       41.3505616.7298530.48
GRID        892       27.5739 11.1355730.48
GRID        893       13.790455.55892930.48
GRID        894       41.3518316.7303615.2308
GRID        895       55.1219922.3422315.22459
GRID        896       27.5748311.1359515.23567
GRID        897       13.790965.55913415.23886
GRID        898       41.3505616.7298560.96
GRID        899       41.3505616.7298545.72
GRID        900       55.1204522.3416 60.96
GRID        901       55.1204522.3416 45.72
GRID        902       13.790455.55892960.96
GRID        903       27.5739 11.1355760.96
GRID        904       13.790455.55892945.72
GRID        905       27.5739 11.1355745.72
GRID        906       55.1204522.3416 106.68
GRID        907       41.3505616.72985106.68
GRID        908       27.5739 11.13557106.68
GRID        909       13.790455.558929106.68
GRID        910       41.3505616.7298591.44
GRID        911       55.1204522.3416 91.44
GRID        912       27.5739 11.1355791.44
GRID        913       13.790455.55892991.44
GRID        914       41.3505616.72985137.16
GRID        915       41.3505616.72985121.92
GRID        916       55.1204522.3416 137.16
GRID        917       55.1204522.3416 121.92
GRID        918       13.790455.558929137.16
GRID        919       27.5739 11.13557137.16
GRID        920       13.790455.558929121.92
GRID        921       27.5739 11.13557121.92
GRID        922       137.584356.3646276.2
GRID        923       123.853650.6508176.2
GRID        924       110.116744.9537376.2
GRID        925       96.3735139.2735576.2
GRID        926       82.6241633.6104476.2
GRID        927       110.116744.9537360.96
GRID        928       110.116744.9537345.72
GRID        929       110.117844.9542230.45848
GRID        930       110.122444.9561215.23541
GRID        931       123.853650.6508145.72
GRID        932       137.584356.3646245.72
GRID        933       123.853650.6508160.96
GRID        934       137.584356.3646260.96
GRID        935       123.854750.6512830.4546
```

```
GRID         936        137.591356.3675530.45081
GRID         937        123.859350.6531715.23463
GRID         938        137.594756.3689815.23442
GRID         939        82.6241633.6104445.72
GRID         940        96.3735139.2735545.72
GRID         941        82.6241633.6104460.96
GRID         942        96.3735139.2735560.96
GRID         943        82.6241633.6104430.48
GRID         944        96.3747139.2740430.46235
GRID         945        82.6296833.6127115.23693
GRID         946        96.3792239.2759 15.23618
GRID         947        110.116744.95373137.16
GRID         948        110.116744.95373121.92
GRID         949        110.116744.95373106.68
GRID         950        110.116744.9537391.44
GRID         951        123.853650.65081121.92
GRID         952        137.584356.36462121.92
GRID         953        123.853650.65081137.16
GRID         954        137.584356.36462137.16
GRID         955        123.853650.65081106.68
GRID         956        137.584356.36462106.68
GRID         957        123.853650.6508191.44
GRID         958        137.584356.3646291.44
GRID         959        82.6241633.61044121.92
GRID         960        96.3735139.27355121.92
GRID         961        82.6241633.61044137.16
GRID         962        96.3735139.27355137.16
GRID         963        82.6241633.61044106.68
GRID         964        96.3735139.27355106.68
GRID         965        82.6241633.6104491.44
GRID         966        96.3735139.2735591.44
$$
$$  SPOINT Data
$$
$
$  CQUAD4 Elements
$
CQUAD4        61       1     271     272     267     268
CQUAD4        62       1     272     263     264     267
CQUAD4        63       1     256     257     272     271
CQUAD4        64       1     257     258     263     272
CQUAD4        65       1     268     269     273     271
CQUAD4        66       1     271     273     255     256
CQUAD4        67       1     248     274     270     247
CQUAD4        68       1     274     273     269     270
CQUAD4        69       1     249     254     274     248
CQUAD4        70       1     254     255     273     274
CQUAD4        71       1     275     277     231     232
CQUAD4        72       1     277     266     230     231
CQUAD4        73       1     276     278     277     275
CQUAD4        74       1     278     265     266     277
CQUAD4        75       1     268     267     278     276
CQUAD4        76       1     267     264     265     278
CQUAD4        77       1     245     279     234     235
CQUAD4        78       1     279     280     233     234
CQUAD4        79       1     280     275     232     233
CQUAD4        80       1     247     270     281     246
CQUAD4        81       1     246     281     279     245
CQUAD4        82       1     276     282     269     268
CQUAD4        83       1     282     281     270     269
CQUAD4        84       1     275     280     282     276
CQUAD4        85       1     280     279     281     282
CQUAD4        86       1     287     288     283     284
CQUAD4        87       1     288     212     213     283
CQUAD4        88       1     261     262     288     287
CQUAD4        89       1     262     211     212     288
CQUAD4        90       1     284     285     289     287
CQUAD4        91       1     287     289     260     261
CQUAD4        92       1     263     290     286     264
```

```
CQUAD4         93       1      290      289      285      286
CQUAD4         94       1      258      259      290      263
CQUAD4         95       1      259      260      289      290
CQUAD4         96       1      291      293      226      227
CQUAD4         97       1      293      215      216      226
CQUAD4         98       1      292      294      293      291
CQUAD4         99       1      294      214      215      293
CQUAD4        100       1      284      283      294      292
CQUAD4        101       1      283      213      214      294
CQUAD4        102       1      266      295      229      230
CQUAD4        103       1      295      296      228      229
CQUAD4        104       1      296      291      227      228
CQUAD4        105       1      264      286      297      265
CQUAD4        106       1      265      297      295      266
CQUAD4        107       1      292      298      285      284
CQUAD4        108       1      298      297      286      285
CQUAD4        109       1      291      296      298      292
CQUAD4        110       1      296      295      297      298
CQUAD4        111       1      307      308      303      304
CQUAD4        112       1      308      299      300      303
CQUAD4        113       1      159      160      308      307
CQUAD4        114       1      160      161      299      308
CQUAD4        115       1      304      305      309      307
CQUAD4        116       1      307      309      158      159
CQUAD4        117       1      253      310      306      252
CQUAD4        118       1      310      309      305      306
CQUAD4        119       1      156      157      310      253
CQUAD4        120       1      157      158      309      310
CQUAD4        121       1      311      313      257      256
CQUAD4        122       1      313      302      258      257
CQUAD4        123       1      312      314      313      311
CQUAD4        124       1      314      301      302      313
CQUAD4        125       1      304      303      314      312
CQUAD4        126       1      303      300      301      314
CQUAD4        127       1      250      315      254      249
CQUAD4        128       1      315      316      255      254
CQUAD4        129       1      316      311      256      255
CQUAD4        130       1      252      306      317      251
CQUAD4        131       1      251      317      315      250
CQUAD4        132       1      312      318      305      304
CQUAD4        133       1      318      317      306      305
CQUAD4        134       1      311      316      318      312
CQUAD4        135       1      316      315      317      318
CQUAD4        136       1      323      324      319      320
CQUAD4        137       1      324      207      208      319
CQUAD4        138       1      164      165      324      323
CQUAD4        139       1      165      166      207      324
CQUAD4        140       1      320      321      325      323
CQUAD4        141       1      323      325      163      164
CQUAD4        142       1      299      326      322      300
CQUAD4        143       1      326      325      321      322
CQUAD4        144       1      161      162      326      299
CQUAD4        145       1      162      163      325      326
CQUAD4        146       1      327      329      262      261
CQUAD4        147       1      329      210      211      262
CQUAD4        148       1      328      330      329      327
CQUAD4        149       1      330      209      210      329
CQUAD4        150       1      320      319      330      328
CQUAD4        151       1      319      208      209      330
CQUAD4        152       1      302      331      259      258
CQUAD4        153       1      331      332      260      259
CQUAD4        154       1      332      327      261      260
CQUAD4        155       1      300      322      333      301
CQUAD4        156       1      301      333      331      302
CQUAD4        157       1      328      334      321      320
CQUAD4        158       1      334      333      322      321
CQUAD4        159       1      327      332      334      328
CQUAD4        160       1      332      331      333      334
CQUAD4        161       1      352      353      348      349
```

```
CQUAD4        162       1       353       344       345       348
CQUAD4        163       1       337       338       353       352
CQUAD4        164       1       338       339       344       353
CQUAD4        165       1       349       350       354       352
CQUAD4        166       1       352       354       336       337
CQUAD4        167       1       140       355       351       139
CQUAD4        168       1       355       354       350       351
CQUAD4        169       1       141       335       355       140
CQUAD4        170       1       335       336       354       355
CQUAD4        171       1       356       358       241       242
CQUAD4        172       1       358       347       240       241
CQUAD4        173       1       357       359       358       356
CQUAD4        174       1       359       346       347       358
CQUAD4        175       1       349       348       359       357
CQUAD4        176       1       348       345       346       359
CQUAD4        177       1       137       360       244       136
CQUAD4        178       1       360       361       243       244
CQUAD4        179       1       361       356       242       243
CQUAD4        180       1       139       351       362       138
CQUAD4        181       1       138       362       360       137
CQUAD4        182       1       357       363       350       349
CQUAD4        183       1       363       362       351       350
CQUAD4        184       1       356       361       363       357
CQUAD4        185       1       361       360       362       363
CQUAD4        186       1       368       369       364       365
CQUAD4        187       1       369       248       247       364
CQUAD4        188       1       342       343       369       368
CQUAD4        189       1       343       249       248       369
CQUAD4        190       1       365       366       370       368
CQUAD4        191       1       368       370       341       342
CQUAD4        192       1       344       371       367       345
CQUAD4        193       1       371       370       366       367
CQUAD4        194       1       339       340       371       344
CQUAD4        195       1       340       341       370       371
CQUAD4        196       1       372       374       236       237
CQUAD4        197       1       374       245       235       236
CQUAD4        198       1       373       375       374       372
CQUAD4        199       1       375       246       245       374
CQUAD4        200       1       365       364       375       373
CQUAD4        201       1       364       247       246       375
CQUAD4        202       1       347       376       239       240
CQUAD4        203       1       376       377       238       239
CQUAD4        204       1       377       372       237       238
CQUAD4        205       1       345       367       378       346
CQUAD4        206       1       346       378       376       347
CQUAD4        207       1       373       379       366       365
CQUAD4        208       1       379       378       367       366
CQUAD4        209       1       372       377       379       373
CQUAD4        210       1       377       376       378       379
CQUAD4        211       1       388       389       384       385
CQUAD4        212       1       389       380       381       384
CQUAD4        213       1       149       150       389       388
CQUAD4        214       1       150       151       380       389
CQUAD4        215       1       385       386       390       388
CQUAD4        216       1       388       390       148       149
CQUAD4        217       1       145       391       387       144
CQUAD4        218       1       391       390       386       387
CQUAD4        219       1       146       147       391       145
CQUAD4        220       1       147       148       390       391
CQUAD4        221       1       392       394       338       337
CQUAD4        222       1       394       383       339       338
CQUAD4        223       1       393       395       394       392
CQUAD4        224       1       395       382       383       394
CQUAD4        225       1       385       384       395       393
CQUAD4        226       1       384       381       382       395
CQUAD4        227       1       142       396       335       141
CQUAD4        228       1       396       397       336       335
CQUAD4        229       1       397       392       337       336
CQUAD4        230       1       144       387       398       143
```

```
CQUAD4        231       1       143       398       396       142
CQUAD4        232       1       393       399       386       385
CQUAD4        233       1       399       398       387       386
CQUAD4        234       1       392       397       399       393
CQUAD4        235       1       397       396       398       399
CQUAD4        236       1       404       405       400       401
CQUAD4        237       1       405       253       252       400
CQUAD4        238       1       154       155       405       404
CQUAD4        239       1       155       156       253       405
CQUAD4        240       1       401       402       406       404
CQUAD4        241       1       404       406       153       154
CQUAD4        242       1       380       407       403       381
CQUAD4        243       1       407       406       402       403
CQUAD4        244       1       151       152       407       380
CQUAD4        245       1       152       153       406       407
CQUAD4        246       1       408       410       343       342
CQUAD4        247       1       410       250       249       343
CQUAD4        248       1       409       411       410       408
CQUAD4        249       1       411       251       250       410
CQUAD4        250       1       401       400       411       409
CQUAD4        251       1       400       252       251       411
CQUAD4        252       1       383       412       340       339
CQUAD4        253       1       412       413       341       340
CQUAD4        254       1       413       408       342       341
CQUAD4        255       1       381       403       414       382
CQUAD4        256       1       382       414       412       383
CQUAD4        257       1       409       415       402       401
CQUAD4        258       1       415       414       403       402
CQUAD4        259       1       408       413       415       409
CQUAD4        260       1       413       412       414       415
CQUAD4        261       1       442       443       438       439
CQUAD4        262       1       443       434       435       438
CQUAD4        263       1       427       428       443       442
CQUAD4        264       1       428       429       434       443
CQUAD4        265       1       439       440       444       442
CQUAD4        266       1       442       444       426       427
CQUAD4        267       1       419       445       441       418
CQUAD4        268       1       445       444       440       441
CQUAD4        269       1       420       425       445       419
CQUAD4        270       1       425       426       444       445
CQUAD4        271       1       446       448       112       113
CQUAD4        272       1       448       437       111       112
CQUAD4        273       1       447       449       448       446
CQUAD4        274       1       449       436       437       448
CQUAD4        275       1       439       438       449       447
CQUAD4        276       1       438       435       436       449
CQUAD4        277       1       416       450       115       116
CQUAD4        278       1       450       451       114       115
CQUAD4        279       1       451       446       113       114
CQUAD4        280       1       418       441       452       417
CQUAD4        281       1       417       452       450       416
CQUAD4        282       1       447       453       440       439
CQUAD4        283       1       453       452       441       440
CQUAD4        284       1       446       451       453       447
CQUAD4        285       1       451       450       452       453
CQUAD4        286       1       458       459       454       455
CQUAD4        287       1       459       222       223       454
CQUAD4        288       1       432       433       459       458
CQUAD4        289       1       433       221       222       459
CQUAD4        290       1       455       456       460       458
CQUAD4        291       1       458       460       431       432
CQUAD4        292       1       434       461       457       435
CQUAD4        293       1       461       460       456       457
CQUAD4        294       1       429       430       461       434
CQUAD4        295       1       430       431       460       461
CQUAD4        296       1       462       464       107       108
CQUAD4        297       1       464       225       106       107
CQUAD4        298       1       463       465       464       462
CQUAD4        299       1       465       224       225       464
```

```
CQUAD4        300       1       455       454       465       463
CQUAD4        301       1       454       223       224       465
CQUAD4        302       1       437       466       110       111
CQUAD4        303       1       466       467       109       110
CQUAD4        304       1       467       462       108       109
CQUAD4        305       1       435       457       468       436
CQUAD4        306       1       436       468       466       437
CQUAD4        307       1       463       469       456       455
CQUAD4        308       1       469       468       457       456
CQUAD4        309       1       462       467       469       463
CQUAD4        310       1       467       466       468       469
CQUAD4        311       1       478       479       474       475
CQUAD4        312       1       479       470       471       474
CQUAD4        313       1       232       231       479       478
CQUAD4        314       1       231       230       470       479
CQUAD4        315       1       475       476       480       478
CQUAD4        316       1       478       480       233       232
CQUAD4        317       1       424       481       477       423
CQUAD4        318       1       481       480       476       477
CQUAD4        319       1       235       234       481       424
CQUAD4        320       1       234       233       480       481
CQUAD4        321       1       482       484       428       427
CQUAD4        322       1       484       473       429       428
CQUAD4        323       1       483       485       484       482
CQUAD4        324       1       485       472       473       484
CQUAD4        325       1       475       474       485       483
CQUAD4        326       1       474       471       472       485
CQUAD4        327       1       421       486       425       420
CQUAD4        328       1       486       487       426       425
CQUAD4        329       1       487       482       427       426
CQUAD4        330       1       423       477       488       422
CQUAD4        331       1       422       488       486       421
CQUAD4        332       1       483       489       476       475
CQUAD4        333       1       489       488       477       476
CQUAD4        334       1       482       487       489       483
CQUAD4        335       1       487       486       488       489
CQUAD4        336       1       494       495       490       491
CQUAD4        337       1       495       217       218       490
CQUAD4        338       1       227       226       495       494
CQUAD4        339       1       226       216       217       495
CQUAD4        340       1       491       492       496       494
CQUAD4        341       1       494       496       228       227
CQUAD4        342       1       470       497       493       471
CQUAD4        343       1       497       496       492       493
CQUAD4        344       1       230       229       497       470
CQUAD4        345       1       229       228       496       497
CQUAD4        346       1       498       500       433       432
CQUAD4        347       1       500       220       221       433
CQUAD4        348       1       499       501       500       498
CQUAD4        349       1       501       219       220       500
CQUAD4        350       1       491       490       501       499
CQUAD4        351       1       490       218       219       501
CQUAD4        352       1       473       502       430       429
CQUAD4        353       1       502       503       431       430
CQUAD4        354       1       503       498       432       431
CQUAD4        355       1       471       493       504       472
CQUAD4        356       1       472       504       502       473
CQUAD4        357       1       499       505       492       491
CQUAD4        358       1       505       504       493       492
CQUAD4        359       1       498       503       505       499
CQUAD4        360       1       503       502       504       505
CQUAD4        361       1       523       524       519       520
CQUAD4        362       1       524       515       516       519
CQUAD4        363       1       508       509       524       523
CQUAD4        364       1       509       510       515       524
CQUAD4        365       1       520       521       525       523
CQUAD4        366       1       523       525       507       508
CQUAD4        367       1       130       526       522       129
CQUAD4        368       1       526       525       521       522
```

```
CQUAD4      369       1      131      506      526      130
CQUAD4      370       1      506      507      525      526
CQUAD4      371       1      527      529      122      123
CQUAD4      372       1      529      518      121      122
CQUAD4      373       1      528      530      529      527
CQUAD4      374       1      530      517      518      529
CQUAD4      375       1      520      519      530      528
CQUAD4      376       1      519      516      517      530
CQUAD4      377       1      127      531      125      126
CQUAD4      378       1      531      532      124      125
CQUAD4      379       1      532      527      123      124
CQUAD4      380       1      129      522      533      128
CQUAD4      381       1      128      533      531      127
CQUAD4      382       1      528      534      521      520
CQUAD4      383       1      534      533      522      521
CQUAD4      384       1      527      532      534      528
CQUAD4      385       1      532      531      533      534
CQUAD4      386       1      539      540      535      536
CQUAD4      387       1      540      419      418      535
CQUAD4      388       1      513      514      540      539
CQUAD4      389       1      514      420      419      540
CQUAD4      390       1      536      537      541      539
CQUAD4      391       1      539      541      512      513
CQUAD4      392       1      515      542      538      516
CQUAD4      393       1      542      541      537      538
CQUAD4      394       1      510      511      542      515
CQUAD4      395       1      511      512      541      542
CQUAD4      396       1      543      545      117      118
CQUAD4      397       1      545      416      116      117
CQUAD4      398       1      544      546      545      543
CQUAD4      399       1      546      417      416      545
CQUAD4      400       1      536      535      546      544
CQUAD4      401       1      535      418      417      546
CQUAD4      402       1      518      547      120      121
CQUAD4      403       1      547      548      119      120
CQUAD4      404       1      548      543      118      119
CQUAD4      405       1      516      538      549      517
CQUAD4      406       1      517      549      547      518
CQUAD4      407       1      544      550      537      536
CQUAD4      408       1      550      549      538      537
CQUAD4      409       1      543      548      550      544
CQUAD4      410       1      548      547      549      550
CQUAD4      411       1      559      560      555      556
CQUAD4      412       1      560      551      552      555
CQUAD4      413       1      242      241      560      559
CQUAD4      414       1      241      240      551      560
CQUAD4      415       1      556      557      561      559
CQUAD4      416       1      559      561      243      242
CQUAD4      417       1      135      562      558      134
CQUAD4      418       1      562      561      557      558
CQUAD4      419       1      136      244      562      135
CQUAD4      420       1      244      243      561      562
CQUAD4      421       1      563      565      509      508
CQUAD4      422       1      565      554      510      509
CQUAD4      423       1      564      566      565      563
CQUAD4      424       1      566      553      554      565
CQUAD4      425       1      556      555      566      564
CQUAD4      426       1      555      552      553      566
CQUAD4      427       1      132      567      506      131
CQUAD4      428       1      567      568      507      506
CQUAD4      429       1      568      563      508      507
CQUAD4      430       1      134      558      569      133
CQUAD4      431       1      133      569      567      132
CQUAD4      432       1      564      570      557      556
CQUAD4      433       1      570      569      558      557
CQUAD4      434       1      563      568      570      564
CQUAD4      435       1      568      567      569      570
CQUAD4      436       1      575      576      571      572
CQUAD4      437       1      576      424      423      571
```

```
CQUAD4      438       1      237      236      576      575
CQUAD4      439       1      236      235      424      576
CQUAD4      440       1      572      573      577      575
CQUAD4      441       1      575      577      238      237
CQUAD4      442       1      551      578      574      552
CQUAD4      443       1      578      577      573      574
CQUAD4      444       1      240      239      578      551
CQUAD4      445       1      239      238      577      578
CQUAD4      446       1      579      581      514      513
CQUAD4      447       1      581      421      420      514
CQUAD4      448       1      580      582      581      579
CQUAD4      449       1      582      422      421      581
CQUAD4      450       1      572      571      582      580
CQUAD4      451       1      571      423      422      582
CQUAD4      452       1      554      583      511      510
CQUAD4      453       1      583      584      512      511
CQUAD4      454       1      584      579      513      512
CQUAD4      455       1      552      574      585      553
CQUAD4      456       1      553      585      583      554
CQUAD4      457       1      580      586      573      572
CQUAD4      458       1      586      585      574      573
CQUAD4      459       1      579      584      586      580
CQUAD4      460       1      584      583      585      586
CQUAD4      461       1      632      633      628      629
CQUAD4      462       1      633      624      625      628
CQUAD4      463       1      617      618      633      632
CQUAD4      464       1      618      619      624      633
CQUAD4      465       1      629      630      634      632
CQUAD4      466       1      632      634      616      617
CQUAD4      467       1      590      635      631      589
CQUAD4      468       1      635      634      630      631
CQUAD4      469       1      591      615      635      590
CQUAD4      470       1      615      616      634      635
CQUAD4      471       1      636      638      172      173
CQUAD4      472       1      638      627      171      172
CQUAD4      473       1      637      639      638      636
CQUAD4      474       1      639      626      627      638
CQUAD4      475       1      629      628      639      637
CQUAD4      476       1      628      625      626      639
CQUAD4      477       1      587      640      175      176
CQUAD4      478       1      640      641      174      175
CQUAD4      479       1      641      636      173      174
CQUAD4      480       1      589      631      642      588
CQUAD4      481       1      588      642      640      587
CQUAD4      482       1      637      643      630      629
CQUAD4      483       1      643      642      631      630
CQUAD4      484       1      636      641      643      637
CQUAD4      485       1      641      640      642      643
CQUAD4      486       1      648      649      644      645
CQUAD4      487       1      649      210      209      644
CQUAD4      488       1      622      623      649      648
CQUAD4      489       1      623      211      210      649
CQUAD4      490       1      645      646      650      648
CQUAD4      491       1      648      650      621      622
CQUAD4      492       1      624      651      647      625
CQUAD4      493       1      651      650      646      647
CQUAD4      494       1      619      620      651      624
CQUAD4      495       1      620      621      650      651
CQUAD4      496       1      652      654      167      168
CQUAD4      497       1      654      207      166      167
CQUAD4      498       1      653      655      654      652
CQUAD4      499       1      655      208      207      654
CQUAD4      500       1      645      644      655      653
CQUAD4      501       1      644      209      208      655
CQUAD4      502       1      627      656      170      171
CQUAD4      503       1      656      657      169      170
CQUAD4      504       1      657      652      168      169
CQUAD4      505       1      625      647      658      626
CQUAD4      506       1      626      658      656      627
```

```
CQUAD4      507       1     653     659     646     645
CQUAD4      508       1     659     658     647     646
CQUAD4      509       1     652     657     659     653
CQUAD4      510       1     657     656     658     659
CQUAD4      511       1     668     669     664     665
CQUAD4      512       1     669     660     661     664
CQUAD4      513       1     608     609     669     668
CQUAD4      514       1     609     610     660     669
CQUAD4      515       1     665     666     670     668
CQUAD4      516       1     668     670     607     608
CQUAD4      517       1     595     671     667     594
CQUAD4      518       1     671     670     666     667
CQUAD4      519       1     596     606     671     595
CQUAD4      520       1     606     607     670     671
CQUAD4      521       1     672     674     618     617
CQUAD4      522       1     674     663     619     618
CQUAD4      523       1     673     675     674     672
CQUAD4      524       1     675     662     663     674
CQUAD4      525       1     665     664     675     673
CQUAD4      526       1     664     661     662     675
CQUAD4      527       1     592     676     615     591
CQUAD4      528       1     676     677     616     615
CQUAD4      529       1     677     672     617     616
CQUAD4      530       1     594     667     678     593
CQUAD4      531       1     593     678     676     592
CQUAD4      532       1     673     679     666     665
CQUAD4      533       1     679     678     667     666
CQUAD4      534       1     672     677     679     673
CQUAD4      535       1     677     676     678     679
CQUAD4      536       1     684     685     680     681
CQUAD4      537       1     685     215     214     680
CQUAD4      538       1     613     614     685     684
CQUAD4      539       1     614     216     215     685
CQUAD4      540       1     681     682     686     684
CQUAD4      541       1     684     686     612     613
CQUAD4      542       1     660     687     683     661
CQUAD4      543       1     687     686     682     683
CQUAD4      544       1     610     611     687     660
CQUAD4      545       1     611     612     686     687
CQUAD4      546       1     688     690     623     622
CQUAD4      547       1     690     212     211     623
CQUAD4      548       1     689     691     690     688
CQUAD4      549       1     691     213     212     690
CQUAD4      550       1     681     680     691     689
CQUAD4      551       1     680     214     213     691
CQUAD4      552       1     663     692     620     619
CQUAD4      553       1     692     693     621     620
CQUAD4      554       1     693     688     622     621
CQUAD4      555       1     661     683     694     662
CQUAD4      556       1     662     694     692     663
CQUAD4      557       1     689     695     682     681
CQUAD4      558       1     695     694     683     682
CQUAD4      559       1     688     693     695     689
CQUAD4      560       1     693     692     694     695
CQUAD4      561       1     713     714     709     710
CQUAD4      562       1     714     705     706     709
CQUAD4      563       1     698     699     714     713
CQUAD4      564       1     699     700     705     714
CQUAD4      565       1     710     711     715     713
CQUAD4      566       1     713     715     697     698
CQUAD4      567       1     600     716     712     599
CQUAD4      568       1     716     715     711     712
CQUAD4      569       1     601     696     716     600
CQUAD4      570       1     696     697     715     716
CQUAD4      571       1     717     719     609     608
CQUAD4      572       1     719     708     610     609
CQUAD4      573       1     718     720     719     717
CQUAD4      574       1     720     707     708     719
CQUAD4      575       1     710     709     720     718
```

```
CQUAD4        576       1     709     706     707     720
CQUAD4        577       1     597     721     606     596
CQUAD4        578       1     721     722     607     606
CQUAD4        579       1     722     717     608     607
CQUAD4        580       1     599     712     723     598
CQUAD4        581       1     598     723     721     597
CQUAD4        582       1     718     724     711     710
CQUAD4        583       1     724     723     712     711
CQUAD4        584       1     717     722     724     718
CQUAD4        585       1     722     721     723     724
CQUAD4        586       1     729     730     725     726
CQUAD4        587       1     730     220     219     725
CQUAD4        588       1     703     704     730     729
CQUAD4        589       1     704     221     220     730
CQUAD4        590       1     726     727     731     729
CQUAD4        591       1     729     731     702     703
CQUAD4        592       1     705     732     728     706
CQUAD4        593       1     732     731     727     728
CQUAD4        594       1     700     701     732     705
CQUAD4        595       1     701     702     731     732
CQUAD4        596       1     733     735     614     613
CQUAD4        597       1     735     217     216     614
CQUAD4        598       1     734     736     735     733
CQUAD4        599       1     736     218     217     735
CQUAD4        600       1     726     725     736     734
CQUAD4        601       1     725     219     218     736
CQUAD4        602       1     708     737     611     610
CQUAD4        603       1     737     738     612     611
CQUAD4        604       1     738     733     613     612
CQUAD4        605       1     706     728     739     707
CQUAD4        606       1     707     739     737     708
CQUAD4        607       1     734     740     727     726
CQUAD4        608       1     740     739     728     727
CQUAD4        609       1     733     738     740     734
CQUAD4        610       1     738     737     739     740
CQUAD4        611       1     749     750     745     746
CQUAD4        612       1     750     741     742     745
CQUAD4        613       1      99     100     750     749
CQUAD4        614       1     100     101     741     750
CQUAD4        615       1     746     747     751     749
CQUAD4        616       1     749     751      98      99
CQUAD4        617       1     605     752     748     604
CQUAD4        618       1     752     751     747     748
CQUAD4        619       1      96      97     752     605
CQUAD4        620       1      97      98     751     752
CQUAD4        621       1     753     755     699     698
CQUAD4        622       1     755     744     700     699
CQUAD4        623       1     754     756     755     753
CQUAD4        624       1     756     743     744     755
CQUAD4        625       1     746     745     756     754
CQUAD4        626       1     745     742     743     756
CQUAD4        627       1     602     757     696     601
CQUAD4        628       1     757     758     697     696
CQUAD4        629       1     758     753     698     697
CQUAD4        630       1     604     748     759     603
CQUAD4        631       1     603     759     757     602
CQUAD4        632       1     754     760     747     746
CQUAD4        633       1     760     759     748     747
CQUAD4        634       1     753     758     760     754
CQUAD4        635       1     758     757     759     760
CQUAD4        636       1     765     766     761     762
CQUAD4        637       1     766     225     224     761
CQUAD4        638       1     104     105     766     765
CQUAD4        639       1     105     106     225     766
CQUAD4        640       1     762     763     767     765
CQUAD4        641       1     765     767     103     104
CQUAD4        642       1     741     768     764     742
CQUAD4        643       1     768     767     763     764
CQUAD4        644       1     101     102     768     741
```

```
CQUAD4      645       1      102      103      767      768
CQUAD4      646       1      769      771      704      703
CQUAD4      647       1      771      222      221      704
CQUAD4      648       1      770      772      771      769
CQUAD4      649       1      772      223      222      771
CQUAD4      650       1      762      761      772      770
CQUAD4      651       1      761      224      223      772
CQUAD4      652       1      744      773      701      700
CQUAD4      653       1      773      774      702      701
CQUAD4      654       1      774      769      703      702
CQUAD4      655       1      742      764      775      743
CQUAD4      656       1      743      775      773      744
CQUAD4      657       1      770      776      763      762
CQUAD4      658       1      776      775      764      763
CQUAD4      659       1      769      774      776      770
CQUAD4      660       1      774      773      775      776
CQUAD4      661       1      804      805      800      801
CQUAD4      662       1      805      787      788      800
CQUAD4      663       1      779      780      805      804
CQUAD4      664       1      780      781      787      805
CQUAD4      665       1      801      802      806      804
CQUAD4      666       1      804      806      778      779
CQUAD4      667       1      196      807      803      195
CQUAD4      668       1      807      806      802      803
CQUAD4      669       1      197      777      807      196
CQUAD4      670       1      777      778      806      807
CQUAD4      671       1      808      810      796      797
CQUAD4      672       1      810      790      791      796
CQUAD4      673       1      809      811      810      808
CQUAD4      674       1      811      789      790      810
CQUAD4      675       1      801      800      811      809
CQUAD4      676       1      800      788      789      811
CQUAD4      677       1      193      812      799      192
CQUAD4      678       1      812      813      798      799
CQUAD4      679       1      813      808      797      798
CQUAD4      680       1      195      803      814      194
CQUAD4      681       1      194      814      812      193
CQUAD4      682       1      809      815      802      801
CQUAD4      683       1      815      814      803      802
CQUAD4      684       1      808      813      815      809
CQUAD4      685       1      813      812      814      815
CQUAD4      686       1      820      821      816      817
CQUAD4      687       1      821      792      793      816
CQUAD4      688       1      797      796      821      820
CQUAD4      689       1      796      791      792      821
CQUAD4      690       1      817      818      822      820
CQUAD4      691       1      820      822      798      797
CQUAD4      692       1      191      823      819      190
CQUAD4      693       1      823      822      818      819
CQUAD4      694       1      192      799      823      191
CQUAD4      695       1      799      798      822      823
CQUAD4      696       1      824      826      183      184
CQUAD4      697       1      826      795      182      183
CQUAD4      698       1      825      827      826      824
CQUAD4      699       1      827      794      795      826
CQUAD4      700       1      817      816      827      825
CQUAD4      701       1      816      793      794      827
CQUAD4      702       1      188      828      186      187
CQUAD4      703       1      828      829      185      186
CQUAD4      704       1      829      824      184      185
CQUAD4      705       1      190      819      830      189
CQUAD4      706       1      189      830      828      188
CQUAD4      707       1      825      831      818      817
CQUAD4      708       1      831      830      819      818
CQUAD4      709       1      824      829      831      825
CQUAD4      710       1      829      828      830      831
CQUAD4      711       1      838      841      843      837
CQUAD4      712       1      837      843      833      834
CQUAD4      713       1      592      844      842      593
```

```
CQUAD4      714       1     844     843     841     842
CQUAD4      715       1     591     832     844     592
CQUAD4      716       1     832     833     843     844
CQUAD4      717       1     839     845     841     838
CQUAD4      718       1     845     846     842     841
CQUAD4      719       1     846     594     593     842
CQUAD4      720       1     784     785     847     840
CQUAD4      721       1     840     847     845     839
CQUAD4      722       1     595     848     786     596
CQUAD4      723       1     848     847     785     786
CQUAD4      724       1     594     846     848     595
CQUAD4      725       1     846     845     847     848
CQUAD4      726       1     789     849     851     790
CQUAD4      727       1     790     851     836     791
CQUAD4      728       1     837     852     850     838
CQUAD4      729       1     852     851     849     850
CQUAD4      730       1     834     835     852     837
CQUAD4      731       1     835     836     851     852
CQUAD4      732       1     788     853     849     789
CQUAD4      733       1     853     854     850     849
CQUAD4      734       1     854     839     838     850
CQUAD4      735       1     781     782     855     787
CQUAD4      736       1     787     855     853     788
CQUAD4      737       1     840     856     783     784
CQUAD4      738       1     856     855     782     783
CQUAD4      739       1     839     854     856     840
CQUAD4      740       1     854     853     855     856
CQUAD4      741       1     858     861     863     857
CQUAD4      742       1     857     863     178     179
CQUAD4      743       1     587     864     862     588
CQUAD4      744       1     864     863     861     862
CQUAD4      745       1     176     177     864     587
CQUAD4      746       1     177     178     863     864
CQUAD4      747       1     859     865     861     858
CQUAD4      748       1     865     866     862     861
CQUAD4      749       1     866     589     588     862
CQUAD4      750       1     834     833     867     860
CQUAD4      751       1     860     867     865     859
CQUAD4      752       1     590     868     832     591
CQUAD4      753       1     868     867     833     832
CQUAD4      754       1     589     866     868     590
CQUAD4      755       1     866     865     867     868
CQUAD4      756       1     794     869     871     795
CQUAD4      757       1     795     871     181     182
CQUAD4      758       1     857     872     870     858
CQUAD4      759       1     872     871     869     870
CQUAD4      760       1     179     180     872     857
CQUAD4      761       1     180     181     871     872
CQUAD4      762       1     793     873     869     794
CQUAD4      763       1     873     874     870     869
CQUAD4      764       1     874     859     858     870
CQUAD4      765       1     791     836     875     792
CQUAD4      766       1     792     875     873     793
CQUAD4      767       1     860     876     835     834
CQUAD4      768       1     876     875     836     835
CQUAD4      769       1     859     874     876     860
CQUAD4      770       1     874     873     875     876
CQUAD4      771       1     894     895     890     891
CQUAD4      772       1     895     877     878     890
CQUAD4      773       1      88      89     895     894
CQUAD4      774       1      89      90     877     895
CQUAD4      775       1     891     892     896     894
CQUAD4      776       1     894     896      87      88
CQUAD4      777       1     206     897     893     205
CQUAD4      778       1     897     896     892     893
CQUAD4      779       1      85      86     897     206
CQUAD4      780       1      86      87     896     897
CQUAD4      781       1     898     900     886     887
CQUAD4      782       1     900     880     881     886
```

```
CQUAD4      783       1     899     901     900     898
CQUAD4      784       1     901     879     880     900
CQUAD4      785       1     891     890     901     899
CQUAD4      786       1     890     878     879     901
CQUAD4      787       1     203     902     889     202
CQUAD4      788       1     902     903     888     889
CQUAD4      789       1     903     898     887     888
CQUAD4      790       1     205     893     904     204
CQUAD4      791       1     204     904     902     203
CQUAD4      792       1     899     905     892     891
CQUAD4      793       1     905     904     893     892
CQUAD4      794       1     898     903     905     899
CQUAD4      795       1     903     902     904     905
CQUAD4      796       1     910     911     906     907
CQUAD4      797       1     911     882     883     906
CQUAD4      798       1     887     886     911     910
CQUAD4      799       1     886     881     882     911
CQUAD4      800       1     907     908     912     910
CQUAD4      801       1     910     912     888     887
CQUAD4      802       1     201     913     909     200
CQUAD4      803       1     913     912     908     909
CQUAD4      804       1     202     889     913     201
CQUAD4      805       1     889     888     912     913
CQUAD4      806       1     914     916     780     779
CQUAD4      807       1     916     885     781     780
CQUAD4      808       1     915     917     916     914
CQUAD4      809       1     917     884     885     916
CQUAD4      810       1     907     906     917     915
CQUAD4      811       1     906     883     884     917
CQUAD4      812       1     198     918     777     197
CQUAD4      813       1     918     919     778     777
CQUAD4      814       1     919     914     779     778
CQUAD4      815       1     200     909     920     199
CQUAD4      816       1     199     920     918     198
CQUAD4      817       1     915     921     908     907
CQUAD4      818       1     921     920     909     908
CQUAD4      819       1     914     919     921     915
CQUAD4      820       1     919     918     920     921
CQUAD4      821       1     928     931     933     927
CQUAD4      822       1     927     933     923     924
CQUAD4      823       1     602     934     932     603
CQUAD4      824       1     934     933     931     932
CQUAD4      825       1     601     922     934     602
CQUAD4      826       1     922     923     933     934
CQUAD4      827       1     929     935     931     928
CQUAD4      828       1     935     936     932     931
CQUAD4      829       1     936     604     603     932
CQUAD4      830       1      93      94     937     930
CQUAD4      831       1     930     937     935     929
CQUAD4      832       1     605     938      95      96
CQUAD4      833       1     938     937      94      95
CQUAD4      834       1     604     936     938     605
CQUAD4      835       1     936     935     937     938
CQUAD4      836       1     879     939     941     880
CQUAD4      837       1     880     941     926     881
CQUAD4      838       1     927     942     940     928
CQUAD4      839       1     942     941     939     940
CQUAD4      840       1     924     925     942     927
CQUAD4      841       1     925     926     941     942
CQUAD4      842       1     878     943     939     879
CQUAD4      843       1     943     944     940     939
CQUAD4      844       1     944     929     928     940
CQUAD4      845       1      90      91     945     877
CQUAD4      846       1     877     945     943     878
CQUAD4      847       1     930     946      92      93
CQUAD4      848       1     946     945      91      92
CQUAD4      849       1     929     944     946     930
CQUAD4      850       1     944     943     945     946
CQUAD4      851       1     948     951     953     947
```

```
CQUAD4       852       1     947     953     785     784
CQUAD4       853       1     597     954     952     598
CQUAD4       854       1     954     953     951     952
CQUAD4       855       1     596     786     954     597
CQUAD4       856       1     786     785     953     954
CQUAD4       857       1     949     955     951     948
CQUAD4       858       1     955     956     952     951
CQUAD4       859       1     956     599     598     952
CQUAD4       860       1     924     923     957     950
CQUAD4       861       1     950     957     955     949
CQUAD4       862       1     600     958     922     601
CQUAD4       863       1     958     957     923     922
CQUAD4       864       1     599     956     958     600
CQUAD4       865       1     956     955     957     958
CQUAD4       866       1     884     959     961     885
CQUAD4       867       1     885     961     782     781
CQUAD4       868       1     947     962     960     948
CQUAD4       869       1     962     961     959     960
CQUAD4       870       1     784     783     962     947
CQUAD4       871       1     783     782     961     962
CQUAD4       872       1     883     963     959     884
CQUAD4       873       1     963     964     960     959
CQUAD4       874       1     964     949     948     960
CQUAD4       875       1     881     926     965     882
CQUAD4       876       1     882     965     963     883
CQUAD4       877       1     950     966     925     924
CQUAD4       878       1     966     965     926     925
CQUAD4       879       1     949     964     966     950
CQUAD4       880       1     964     963     965     966
$
$HMMOVE        2
$             61THRU         880
$
$$
$$--------------------------------------------------------------------------------$
$$    HyperMesh name and color information for generic components               $
$$--------------------------------------------------------------------------------$
$HMNAME COMP                  1"Geometry"
$HWCOLOR COMP                 1       3
$
$HMNAME COMP                  2"ShellElements"        1 "Thickness" 4
$HWCOLOR COMP                 2       4
$
$
$
$$
$$  PSHELL Data
$$
$HMNAME PROP                  1"Thickness" 4
$HWCOLOR PROP                 1       5
PSHELL         1       11.62814        1               1        0.0
$$
$$  MAT1 Data
$$
$HMNAME MAT                   1"Aluminum" "MAT1"
$HWCOLOR MAT                  1      25
MAT1           169000.0         0.33    0.0027
$$
$$--------------------------------------------------------------------------------$
$$ HyperMesh Commands for loadcollectors name and color information
$$--------------------------------------------------------------------------------$
$HMNAME LOADCOL               2"Restraints"
$HWCOLOR LOADCOL              2       6
$$
$$
$$  SPC Data
$$
SPC            2      85  1234560.0
SPC            2      86  1234560.0
```

```
SPC             2      87  1234560.0
SPC             2      88  1234560.0
SPC             2      89  1234560.0
SPC             2      90  1234560.0
SPC             2      91  1234560.0
SPC             2      92  1234560.0
SPC             2      93  1234560.0
SPC             2      94  1234560.0
SPC             2      95  1234560.0
SPC             2      96  1234560.0
SPC             2      97  1234560.0
SPC             2      98  1234560.0
SPC             2      99  1234560.0
SPC             2     100  1234560.0
SPC             2     101  1234560.0
SPC             2     102  1234560.0
SPC             2     103  1234560.0
SPC             2     104  1234560.0
SPC             2     105  1234560.0
SPC             2     106  1234560.0
SPC             2     107  1234560.0
SPC             2     108  1234560.0
SPC             2     109  1234560.0
SPC             2     110  1234560.0
SPC             2     111  1234560.0
SPC             2     112  1234560.0
SPC             2     113  1234560.0
SPC             2     114  1234560.0
SPC             2     115  1234560.0
SPC             2     116  1234560.0
SPC             2     117  1234560.0
SPC             2     118  1234560.0
SPC             2     119  1234560.0
SPC             2     120  1234560.0
SPC             2     121  1234560.0
SPC             2     122  1234560.0
SPC             2     123  1234560.0
SPC             2     124  1234560.0
SPC             2     125  1234560.0
SPC             2     126  1234560.0
SPC             2     127  1234560.0
SPC             2     128  1234560.0
SPC             2     129  1234560.0
SPC             2     130  1234560.0
SPC             2     131  1234560.0
SPC             2     132  1234560.0
SPC             2     133  1234560.0
SPC             2     134  1234560.0
SPC             2     135  1234560.0
SPC             2     136  1234560.0
SPC             2     137  1234560.0
SPC             2     138  1234560.0
SPC             2     139  1234560.0
SPC             2     140  1234560.0
SPC             2     141  1234560.0
SPC             2     142  1234560.0
SPC             2     143  1234560.0
SPC             2     144  1234560.0
SPC             2     145  1234560.0
SPC             2     146  1234560.0
SPC             2     147  1234560.0
SPC             2     148  1234560.0
SPC             2     149  1234560.0
SPC             2     150  1234560.0
SPC             2     151  1234560.0
SPC             2     152  1234560.0
SPC             2     153  1234560.0
SPC             2     154  1234560.0
SPC             2     155  1234560.0
```

```
SPC            2     156  1234560.0
SPC            2     157  1234560.0
SPC            2     158  1234560.0
SPC            2     159  1234560.0
SPC            2     160  1234560.0
SPC            2     161  1234560.0
SPC            2     162  1234560.0
SPC            2     163  1234560.0
SPC            2     164  1234560.0
SPC            2     165  1234560.0
SPC            2     166  1234560.0
SPC            2     167  1234560.0
SPC            2     168  1234560.0
SPC            2     169  1234560.0
SPC            2     170  1234560.0
SPC            2     171  1234560.0
SPC            2     172  1234560.0
SPC            2     173  1234560.0
SPC            2     174  1234560.0
SPC            2     175  1234560.0
SPC            2     176  1234560.0
SPC            2     177  1234560.0
SPC            2     178  1234560.0
SPC            2     179  1234560.0
SPC            2     180  1234560.0
SPC            2     181  1234560.0
SPC            2     182  1234560.0
SPC            2     183  1234560.0
SPC            2     184  1234560.0
SPC            2     185  1234560.0
SPC            2     186  1234560.0
SPC            2     187  1234560.0
SPC            2     188  1234560.0
SPC            2     189  1234560.0
SPC            2     190  1234560.0
SPC            2     191  1234560.0
SPC            2     192  1234560.0
SPC            2     193  1234560.0
SPC            2     194  1234560.0
SPC            2     195  1234560.0
SPC            2     196  1234560.0
SPC            2     197  1234560.0
SPC            2     198  1234560.0
SPC            2     199  1234560.0
SPC            2     200  1234560.0
SPC            2     201  1234560.0
SPC            2     202  1234560.0
SPC            2     203  1234560.0
SPC            2     204  1234560.0
SPC            2     205  1234560.0
SPC            2     206  1234560.0
$$
$HMNAME LOADCOL               1"Gravity"
$HWCOLOR LOADCOL              1       8
$$
GRAV           1       00.00981 0.0     -1.0    0.0
$
$$
ENDDATA
$$
$$-------------------------------------------------------------------------------$$
$$        Data Definition for AutoDV                                             $$
$$-------------------------------------------------------------------------------$$
$$
$$-------------------------------------------------------------------------------$$
$$        Design Variables Card for Control Perturbations                        $$
$$-------------------------------------------------------------------------------$$
$
$-------------------------------------------------------------------------------$
```

```
$        Domain Element Definitions                                          $
$--------------------------------------------------------------------------$
$$
$$------------------------------------------------------------------------$$
$$            Nodeset Definitions                                          $$
$$------------------------------------------------------------------------$$
$$  Design domain node sets
$$
$$------------------------------------------------------------------------$$
$$            Control Perturbation                                         $$
$$------------------------------------------------------------------------$$
$$
$$
$$  CONTROL PERTURBATION Data
$$
```